LATE HOLOCENE COOL CLIMATE EPISODES, RECORDED IN LAKE BONNEY, AN ANTARCTIC AMPLIFIER LAKE

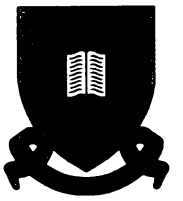

THE UNIVERSITY OF
WAIKATO
Te Whare Wānanga o Waikato

A thesis
submitted in partial fulfilment
of the requirements for the Degree
of
Master of Science in Chemistry
at the
University of Waikato
by

JACOB GRANT CROALL

University of Waikato
2005

ABSTRACT

Chemical, stable isotope and natural abundance radionuclide analysis of cores taken through sediments below Lake Bonney, Taylor Valley, Antarctica, show evidence of multiple episodes of flooding by meltwaters from Taylor Glacier and desiccation to brines sufficiently concentrated to produce ice free conditions. The last three identified desiccation events date 1550 ± 40, 800 ± 100 and 450 ± 160 yr B.P. and match the last three periods of sustained cooling identified by isotope changes in the Taylor Dome ice core. Similar cooling events have been identified by other authors elsewhere in Antarctica.

The desiccation events have produced dramatic changes in the sediment character of Lake Bonney East Lobe, but show little impact in the West Lobe. In East Lobe halite, hydrohalite, gypsum, and aragonite are precipitated and extreme isotopic enrichment of carbon (up to $\delta^{13}C$ of +12.0‰) occurred as aragonite was forced from solution by rapid freezing of the brine over winter. Reflooding events were often associated with algal blooms and resulted in radical changes in the $^{18}O/^{16}O$ ratio in the water column.

It is speculated that Taylor Glacier retreated to expose a 250 m deep subglacial depression during the last glacial maximum allowing Glacial Lake Washburn to extend westwards to perhaps Cavendish Rocks. The reduced Taylor Glacier enabled Taylor Dome to lower causing deposition of more ^{18}O enriched ice than would otherwise have been expected. Taylor Glacier and Taylor Dome have continued to advance throughout the Holocene.

ACKNOWLEDGEMENTS

I would like to thank Antarctica New Zealand for providing funding and logistical support for the project.

I wish to express my gratitude to the many people who have supported me over the past two years. Thanks to Annie Barker and Steve Cameron (ICP-OES and lab work), Helen Turner (SEM) and Steve Cook (isotope studies), thanks also to Dr Gideon Henderson who facilitated the U/Th dating. For field support I would like to thank Tom Whittaker, Amber Hawkins, Sean Birkel, and Aaron Schlosser, of the University of Maine, Mary-Anne DeMello, from Rockland Middle School and the TEA Program, and Sarah Milicich from the University of Waikato, all of whom made this the experience of a lifetime.

To Dr Megan Balks who assisted in draft revisions, time management and general support, I also wish to express my thanks, I always left your office feeling positive!

To Associate Professor Chris Hendy and Dr Brenda Hall I extend heartfelt thanks for the opportunity to undertake this project, and your continued support throughout.

Thanks also to my family for support and encouragement.

Finally, thanks to my wife Jo, whose immeasurable support and endless patience I am forever indebted to.

TABLE OF CONTENTS

Chapter 3 Methods

LIST OF TABLES

LIST OF FIGURES

Chapter 1:

Introduction

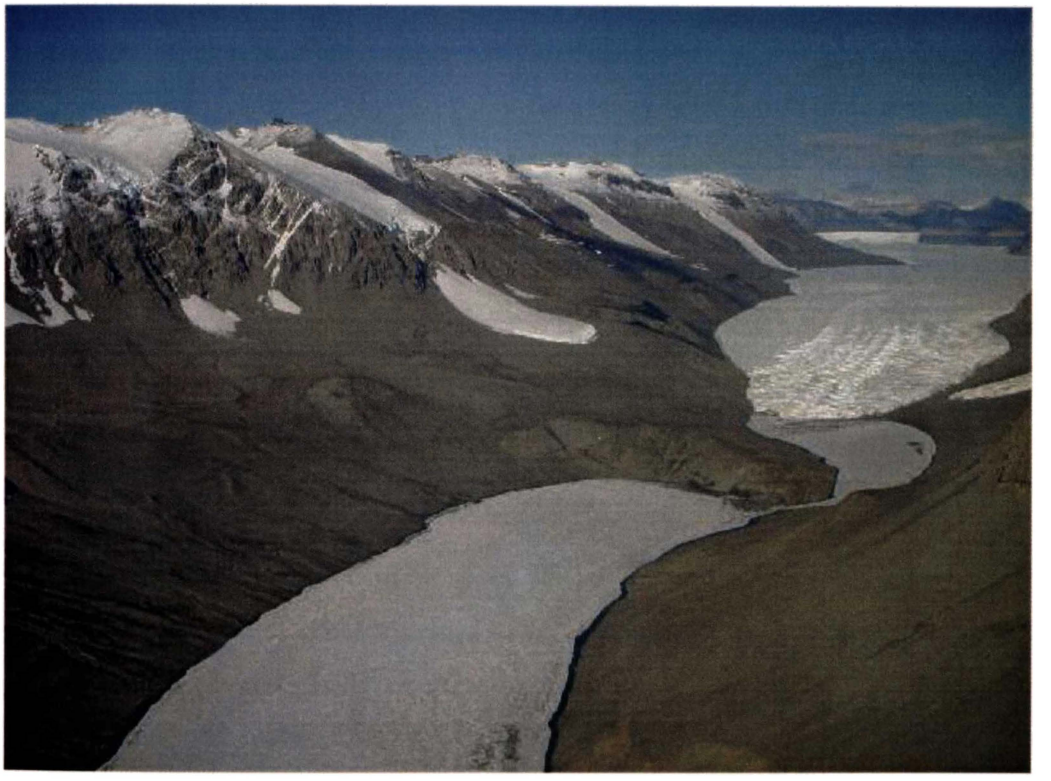

Lake Bonney and the Taylor Glacier, viewed west towards Beacon Heights. Taylor Glacier is currently advancing into the West Lobe of Lake Bonney. Bonney Reigel separates the East and West Lobes.

1.1 Background

Milankovitch suggested that seasonal insolation forcing defines the periodicity of ice ages in 1941, since then, millennial scale climatic events have been recorded by a number of proxy means (stable isotopes in ice cores and marine / freshwater sediments, aerosols in ice cores, pollen and other flora and fauna in sediments *etc*) in the Northern and Southern Hemispheres, and are well established in the literature. Key characteristics of the records are the apparent abrupt transition between glacial and interglacial conditions (referred to as terminations, the most recent being termination I) and events such as the Younder Dryas, and Bolling-Allerod. Comparison of the nature and timing of these events reveals discrepancies between the hemispheres over the last termination; Greenland ice cores show large abrupt changes at termination I, while Antarctic Plateau ice cores indicate a long, gradual warming leading Greenland by one to two thousand years. This raises questions regarding the means by which seasonal insolation change (suggested by Milankovitch), is propagated into global climate change. To determine whether the transferring mechanism is of global extent (synchronous change between hemispheres), or a chain reaction propagated by regional factors (asynchronous), investigation into the timing of paleoclimatic signals in the two hemispheres is critical. As yet no conclusion has been made regarding (a)synchrony.

The (a)synchrony question has been further complicated by the recent addition of ice sheet marginal cores taken at locations around Antarctica, these cores display the abrupt characteristics of the Greenland record, rather than the geographically closer plateau cores. Work at other Southern Hemisphere locations has also suggested an in-phase relationship with the Northern Hemisphere.

The importance of (a)synchrony and the nature of climate change, is best viewed in context of the recent "global warming" phenomenon. Understanding the mechanisms responsible for Holocene fluctuations in climate is vital when considering the potential changes brought about by anthropogenic influences.

Antarctica is central to this understanding as it controls the climate of the whole Southern Hemisphere (Hendy 2003).

This work sets out to identify the impact of decade – millennial climate changes on the hydrologic balance of Lake Bonney, an enclosed basin lake proglacial to the terminus of the Taylor Glacier, from the névé of which an ice core proxy record has recently been obtained.

1.2 Site Description

1.2.1 The McMurdo Dry Valleys

The McMurdo Dry Valleys Region, adjacent to McMurdo Sound at 76°30' to 78°30' S, 160° to 164°E (Figure 1), is the largest ice free region in Antarctica, at 4,800 km^2 and accounts for 2.4% of the Antarctic continent (Drewry *et al.* 1982).

The Western margin of M^{c}Murdo Sound in the Ross Sea embayment is separated from the East Antarctic Ice Sheet by the Trans-Antarctic mountain range, an impediment of ice flow to the sea. As a result, outlet glaciers have cut large valleys through the mountain range, of which a majority still occupy the valleys. However, the remaining valleys have insufficient ice entering to maintain ice flow to the sea. Two factors contribute to the ice free nature of the McMurdo Dry Valleys; the first is the barrier provided by the Trans-Antarctic Mountains, blocking the flow from the East Antarctic Ice Sheet to M^{c}Murdo Sound. The second is that ablation exceeds accumulation during all seasons (Clow *et al.* 1988), as adiabatic warming of air from the East Antarctic Ice Sheet causes extreme aridity, this characteristic affords the name, "Dry Valleys". (Chinn 1990; Fountain *et al.* 1999).

Figure 1: Antarctic continental outline. McMurdo sound region identified.
http://www.peakware.com/encyclopedia/ranges/maps/antarctica.htm

Landsat image of McMurdo Dry Valleys region.
http://earthobservatory.nasa.gov/Newsroom/NewImages/images.php3?img_id=7272

1.2.2 Climate

The M^{c}Murdo Dry Valleys are considered cold deserts, with low precipitation rates falling as snow. Annual precipitation, measured at Lake Vanda over three years, was variable, with an annual average of 6cm (water equivalent), an annual maximum of 10cm and annual minimum of 0.6cm (Bromley 1985). Precipitation occurs due to easterly winds associated with low pressure systems, passing over open water in the Ross Sea. As these systems move into the Dry Valleys, the air is forced to rise over the Trans-Antarctic Mountains, cools, and the moisture falls as snow (Bromley 1985). Thus precipitation decreases westward into the valleys, as the distance from the coast increases.

The valleys have a mean annual temperature of -20°C, with few summer temperatures rising above 0°C, winter extremes are below -60°C, low snowfall and very low relative humidity's give ice free conditions over most of the land surface (Hendy 2000; Thompson *et al.* 1971, Bull 1966 in Sadler 1989).

The floor of the Taylor Valley comprises multiple drift sheets, most of which are incorporated into deep permafrost (Chinn 1993). Bonney Drift was deposited during an expansion of the Taylor Glacier 90 – 105 kyr B.P. (Denton *et al.* 1989; Hall *et al.* 2000; Higgins *et al.* 2000), Ross Sea Drift was deposited during a glacial expansion and grounding of the Ross Sea Ice Sheet, which progressed up-valley, damming the seaward end of Taylor Valley between 25 and 7 kyr B.P (Denton *et al.* 1989; Hall 2000). The terrain is 'hummocky' and large expanses of bedrock are exposed on the valley walls. At least ten lakes containing salt brines and permanently liquid water, and a further ten lakes that are perennially frozen to their base, occupy the drainage basins of the Dry Valleys (Hendy 2000). A number of local alpine glaciers descend the valley walls.

1.2.3 Taylor Valley

Taylor Valley is 35km long and contains three major drainage basins, Bonney, Fryxell, and Hoare. Fryxell basin contains Lake Fryxell, Hoare basin contains lakes Hoare and Chad, and Bonney basin contains Lake Bonney, which is currently being displaced by the terminus of the Taylor glacier. During the austral summer, approximately 24 ephemeral streams flow from the glaciers to the lakes (Fountain et al. 1999) (Figure 2).

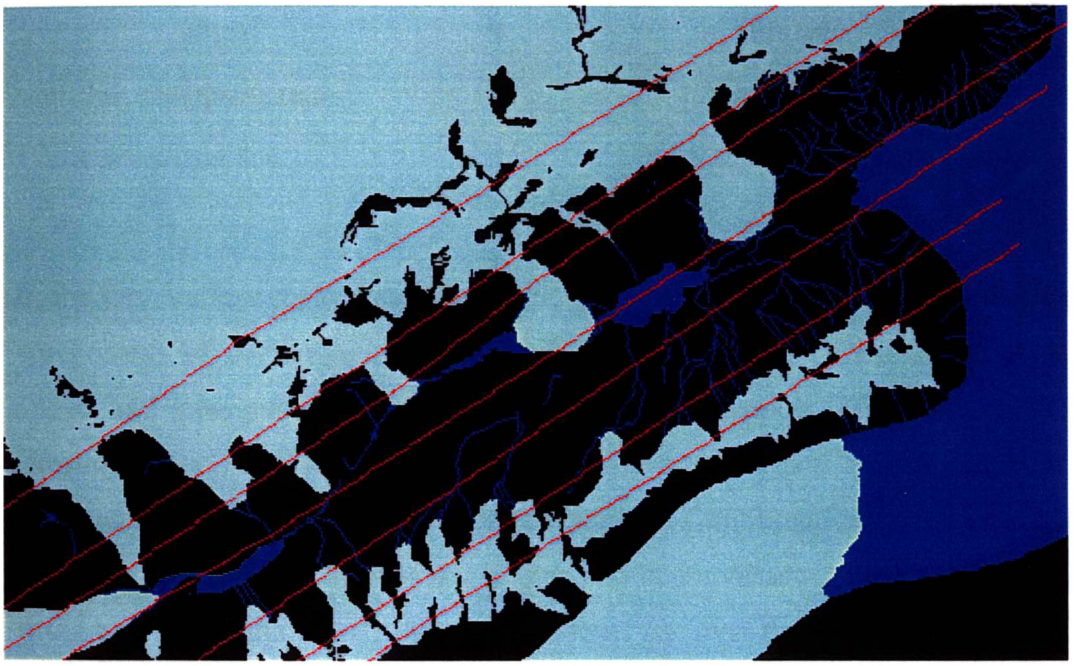

***Figure 2:** False colour image of the Taylor Valley showing lakes glaciers and ephemeral streams (white = glacier, blue = water, black = soil) (Long Term Ecological Research (LTER), 2004)*

1.2.4 Bonney Basin

Bonney basin, the largest enclosed drainage basin in the Taylor Valley has a catchment area of 370 km^2 feeding Lake Bonney, (77°55'S, 62°20'E) , which has a perennial ice cover over liquid water, and is 7 km x 1km divided into two lobes; These are separated by a submerged basement saddle (Bonney Reigel),

approximately 8m below the water surface (Hendy 2000). This study deals primarily with Lake Bonney and its lacustrine deposits.

1.3 Hydrology of Lake Bonney

Changes in lake levels occur as a result of changes to the hydrologic balance (input vs output ratio), and can act as a proxy recorder of climate in certain situations.

Input	**vs**	**Output**
Meltwater, direct precipitation, and groundwater flow.		Evaporation/sublimation, stream flow and groundwater flow

In the Dry Valleys region, the hydrologic budget can be simplified by removing components of negligible contribution. Groundwater flow, (Matsubaya et al., 1979) and precipitation are considered negligible inputs (Thompson 1973, (Bromley 1985). The closed basin lakes have no stream output, therefore, meltwater is the principal input, and evaporation / sublimation is the principal output (Hendy 2000). Glacier flow is known to be important in Lake Bonney, and is the only Dry Valley lake to show a lake level rise over the winter season (as the glacier advances into the lake).

Meltwater input to Dry Valley lakes is highly variable (Chinn 1993), only occurring during the summer season, and depends on the balance between; temperature, cloud free days, precipitation and albedo (Denton et al. 1989). Lake Bonney has a large potential source of meltwater from the terminus of Taylor Glacier (accommodated by the West Lobe) and this is the principal input into the lake. Ephemeral streams from local alpine glaciers also contribute a small amount of water during the summer months. Lake level changes can be interpreted as a response to conditions favourable to increased meltwater production (warm / wet), or the reverse (cold / dry). The result is that small changes in runoff can create large changes in volume, and therefore lake level.

Lakes of this characteristic are called amplifier lakes (Street-Perrot and Harrsion, 1985) because they magnify even minor climate signals. This aspect makes these lakes among the most sensitive recorders of climatic variability. Subsequent discussions on lake level changes will however be restricted to changes in the paleohydrology, rather than direct inferences on climate change, which will be addressed in later chapters of this thesis.

1.4 Previous work

Previous studies have indicated a considerable deposit of evaporites at the bottom of Lake Bonney, but their origin and history are uncertain. Fluctuations of high lake levels have been discovered and investigated with over 150 AMS radiocarbon dates of deltaic and shoreline algae of the enclosed drainage basin lakes within the Dry Valley region (Denton et al. 1985, Hall et al 2000, 2001) revealing that the lakes occupying the Dry Valleys were much larger during the late Pleistocene and early Holocene (Péwé 1960; Stuvier et al. 1981; Hall 2001), and fluctuated enormously over short time scales. This record is discontinuous, and is restricted to upper lake levels giving information of periods of positive water balance (increased flow). Almost all of these high lake levels were due to a large lake proglacial to the now absent Ross Sea Ice Sheet, which occupied McMurdo Sound until early Holocene times. To complete the record by obtaining information about negative water balance, (aridity) it is necessary to look below present lake level. Concentration of the dissolved salts contained in the water column during negative water balance results in the deposition of salts such as sodium chloride and calcium carbonates in the lacustrine sediments, allowing numerical dating via the Uranium / Thorium disequilibrium technique (U/Th) (reservoir effects limit the C^{14} dating potential of the carbonate sediments), and the history of the lake's response to regional climate change quantifiable.

There has been considerable speculation surrounding the origin and history of the massive quantities of sodium chloride contained in the East Lobe. Lake Bonney contains more salt than any other lake in the Taylor or adjacent valleys:

- 11 million tonnes of salt in solution

- 36 million tonnes in the sediment (at least) (Hendy et al 1977).

Water column diffusion gradients of ^{18}O, and Cl^- have been used to identify the timing of dilute influx into a concentrated brine (Wilson 1964; Hendy *et al.* 1977).

1.5 Aims and Objectives

The Aim of this study is to interpret Holocene evaporation and flooding of Lake Bonney and resultant lacustrine sedimentation (containing precipitate minerals) in terms of the climate and glacial history as experienced in the sensitive Dry Valley Region compared, to other proxy records:

- In the same region; The oxygen isotope and gas temperature record from the nearby Taylor Dome core (at odds with the ice cores from the centre of the East Antarctic Ice Sheet).
- Worldwide.

This work is an extension of long standing studies of climate change recorded in the sediments, geomorphology and ice core chemistry in the Dry Valleys region (Hendy 2003).

Therefore the objectives of this study are: To:

1. Recover and describe the stratigraphy of Lake Bonney sediments.
2. Analyse the sediments for trace element content and $\delta^{18}O$ to determine the origin of the evaporite deposits.

3. Construct a comprehensive lake level reconstruction for the past 2000 years.

4. Determine the timing of low lake stands by dating precipitate minerals contained in the sediment via the U/Th disequilibrium technique.

5. Relate these findings to local and regional proxy records adding to the existing body of research towards understanding climate change in the Ross sea region of Antarctica.

Chapter 2:

Literature Review

AA Road sign, Ross Island, Antarctica (2002).

2.1 Introduction

The purpose of this chapter is to describe the climate history (and the means of its measurement) of the McMurdo Oasis, especially the Taylor Valley, to provide a framework for the interpretation of the work to follow. Particular attention will be focused on the glacial history and the occupation of Taylor Valley by lakes. Lake Bonney will be discussed comprehensively.

2.2 Antarctic Paleoclimate

2.2.1 Ice core records

Ice core records yield a high resolution record of paleoclimate, acting as "paleo weather stations" (Steig *et al.* 2000), preserving information on a number of atmospheric conditions present at the time the ice was formed, including;

-Atmospheric aerosols	- Atmospheric circulation patterns. Increased continental aerosols indicates aridity.
-Methane, CO2 -Ammonia	- Mixing of air masses between hemispheres -Biomass burning
-Beryllium-10	- Snow accumulation rate
-$\delta^{18}O$ and δD	- Temperature

Data collected from ice core records are only proxies, each reflecting the conditions at their unique location over meso and synoptic scales. To illustrate Antarctic climate completely, it is therefore essential to gain a number of records over the continent, and correlate common features. The comparison of ice core records and terrestrial proxy records (glacial geomorphology, lake level history, etc) can aid reconstruction of regional climate change, and its effect on terrestrial environments and ecosystems.

Greenland ice cores were the first to be drilled, and include; the Greenland Ice Core Project (GRIP), and the Greenland Ice Sheet Project 2 (GISP2). Antarctic ice cores at; Vostok, Dome B, Byrd, Plateau Remote, Komsomolskaia, Dome C, Taylor Dome (formerly McMurdo Dome), Dominion Range, D47, KM105, Siple Dome, Dome Fuji and Law Dome (and others), have also been collected (Figure 3).

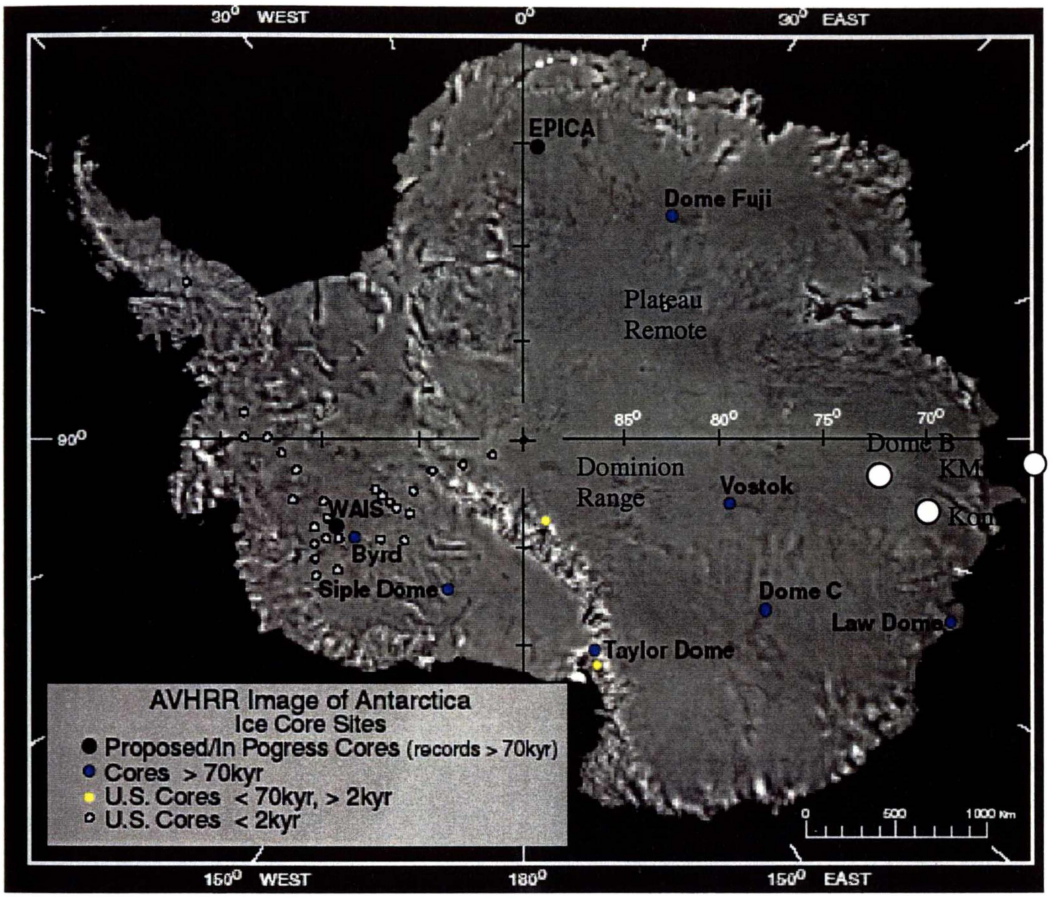

Figure 3: Map of Antarctica showing the locations of ice core drilling sites (group 2003)

2.2.2 Synchrony Vs Asynchrony of hemispherical climate change.

Temperature changes inferred from GISP2 ^{18}O record show abrupt warming and slow gradual cooling over the last termination (Mayewski *et al.* 1995). In contrast the Antarctic deglaciation, recorded in the Byrd ice core, is characterised by a long gradual warming rather than abrupt change. In addition Antarctica may have lead the Northern Hemisphere by several thousand years at termination I, and greater amounts at the termination of previous glaciations, establishing an anti-phase relationship (Broecker and Henderson, 1998; Jouzel, 1998). Complications

resolving the timescale of the Vostok core have made it unable to support either hypothesis.

Ice core interpretation is subject to a number of inconsistencies and problems related to correlation between sites, including:

- Low accumulation rates complicate time scales.
- Trapped gases are younger than the ice that contains them (Δ age).
- Elevation changes of the ice accumulation surface superimpose a signal on the ^{18}O used to infer paleotemperature.

To investigate the validity of the problematic Antarctic ice core records, which differ in deglacial character regionally, and from the northern hemisphere, mid latitude southern hemisphere climate proxies were sought. South American (Lowell *et al.* 1995; Ariztegui *et al.* 1997; Moreno and León 2003), African (Abell and Plug 2000) and New Zealand (Denton and Hendy 1994; Newnham *et al.* 1998; Newnham and Lowe 2000) work suggest an in-phase relationship with Northern Hemisphere climate over the last termination.

If the timing of climate change is synchronous, global forcing is implied, (probably through the atmosphere), asynchrony implies regional forcing. Broecker and Denton, (1989) and Denton, (1988) hypothesised that regional climate affected the production of North Atlantic Deep Water (NADW), by changing the amount of low salinity meltwater from large North Atlantic ice sheets, this then propagated globally via the global ocean conveyer, *ie* an asynchronous signal of climate change between hemispheres.

2.2.3 Taylor Dome

The Taylor Dome ice core record is the closest to the field site for this research (Lake Bonney). Discussion will be limited to the last Glacial – Interglacial cycle, allowing for comparison between the preserved moraines, paleo lake strandlines,

lacustrine deltas, and lake level changes which make up the climate history of Taylor Valley over this period. This will provide a framework for comparison to achieve the aim of the work undertaken in this thesis, to contribute to the late Holocene climate record of Taylor Valley. Other ice cores will only be mentioned insofar as to briefly discuss large scale regional climate.

Taylor Dome is located 150 km from the western edge of the Ross Sea, Southern Victoria Land, Antarctica (Figure 4). It is a local snow accumulation site supplying ice to Taylor Glacier (to the east), and to Skelton Névé and the Portal (to the South).

The Taylor Dome record does not show the gradual warming seen in other Antarctic cores between 20 and 15 ka (the LGM – Holocene transition), but corresponds with deglacial warming (Bolling Allerod, younger Dryas) events recorded in Northern Hemisphere ice cores (GRIP and GISP2) to within 500 years (Steig *et al.* 2000) (Figure 5). Interstadials during MOIS 4 and 3 are very pronounced at Taylor Dome, this broadly corresponds to Dansgaard Oeschger events in Greenland cores (Grootes *et al.* 1993; Mulvaney et al., 2000), but are not at present at Vostok or Byrd, however, this is approached with caution and suggested that this may have been an artifact of very low accumulation rates. Despite this, Allerod and Younger Dryas transitions appear synchronous.

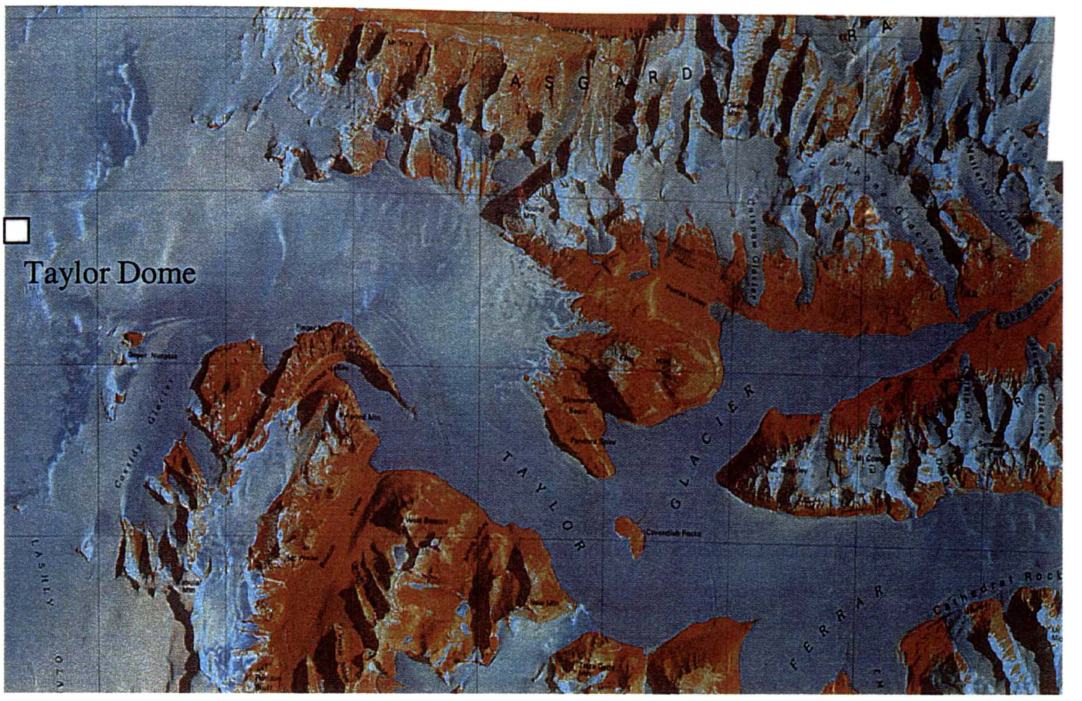

Figure 4: Location map showing the Taylor Dome, Taylor Glacier and the Ferrar Glacier.

2.2.4 Prominent features of Taylor Dome ice core record (Figure 5).

The following is a synopsis of climatic events recorded at Taylor Dome, inferred from the $\delta^{18}O$ record (Figure 5).

- More positive $\delta^{18}O$ than Holocene in Isotope stage 5e (last interglacial), while parts of stage 5a and c are even more negative than parts of stage 3. This is a common feature of all ice cores.
- Large scale oscillations during isotope stage 3, with progressive decrease in $\delta^{18}O$ to end of stage 2.
- Abrupt increase of $\delta^{18}O$ at 15 ka, marking the end of the last glacial and the transition into Holocene.
- A prominent reversal in $\delta^{18}O$ (cold period) between 13 and 12 ka. This is interpreted as being correlative with the Younger Dryas in the Northern Hemisphere.
- A peak in $\delta^{18}O$ in the early Holocene optimum 11.5 ka and 9 ka (Masson *et al.* 2000)
- Progressive decrease in $\delta^{18}O$ between ~9.5 and ~6.5 ka.

- A general decrease through the late Holocene (Steig *et al.* 2000).

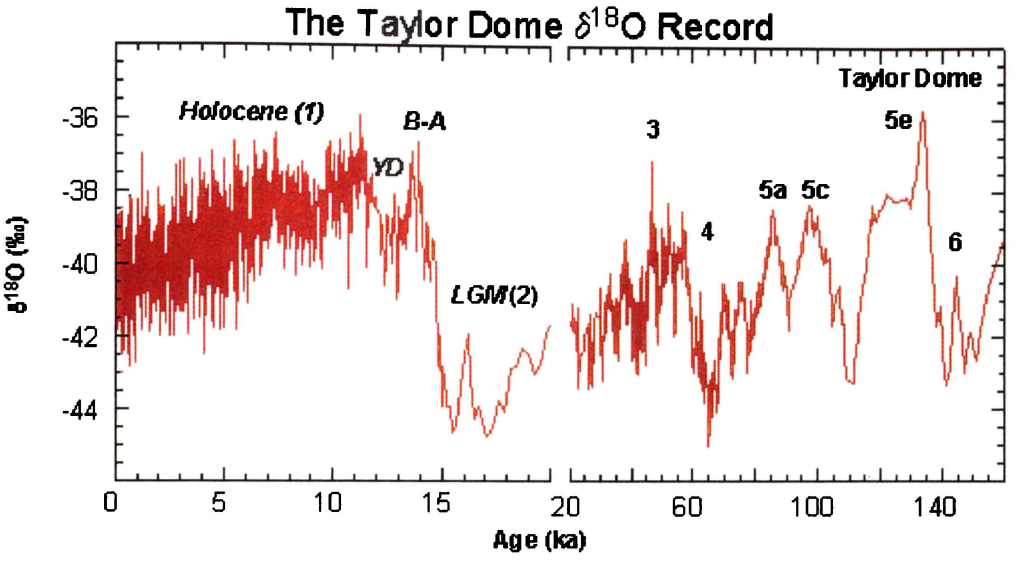

Figure 5: The Taylor Dome $\delta^{18}O$ record for the past 150 ka showing large scale climate change. Isotope stages are identified, as are the Last Glacial Maximum (LGM), Bolling – Allerod (B-A) warming events and the Younger Dryas (YD) cooling event. (Less negative = warm) (after Figure 6 steig et al 2000).

Although the $\delta^{18}O$ records have generally been interpreted as a temperature record, they are also responsive to ice thickness change at the site. The progressive shift of almost 2.5‰ during the Holocene in the Taylor Dome ice $\delta^{18}O$ record is likely the result of a gradually rising dome altitude as Taylor Glacier advanced down the Taylor Valley following the draining of Glacial Lake Washburn. If altitude increases, $\delta^{18}O$ decreases and vice versa. During MOI stage 5, the dome was likely higher than at present, which would have resulted in more negative $\delta^{18}O$ values than would be expected during MOI stage 2 (and possibly 3), the dome was likely much lower and would have resulted in more positive $\delta^{18}O$ values than would have been expected. A 2.5‰ change is equivalent to an altitude change of ~ 300m (dry adiabatic lapse rate).

Study of drift beyond the present Taylor Glacier have led Higgins *et al.* (2000) to suggest that Taylor Glacier advanced down Taylor Valley during MOI stage 5. During MOI stage 2, Taylor Glacier was absent from much of the Taylor Valley, it's place being taken by Glacial Lake Washburn, an ice damned lake proglacial to the Ross Sea ice sheet. Changes of up to 50% in the length of Taylor Glacier are

likely to significantly impact on the altitude of the névé (Taylor Dome) supported by the glacier.

2.2.5 Late Holocene from Taylor Dome

During the recent past (6000 years), terrestrial records are scarce and not well constrained. This is where lake level reconstruction could improve the understanding of regional climate, as correlation with the ice core record over this period helps to add confidence to the accuracy of the proxy records. Quantifying widespread natural climate oscillations analogous to the 20th century "greenhouse warming" can be used to test the importance of natural versus anthropogenic forcing, and the global properties of climate change (Cook *et al.* 2002), and adding to the synchrony argument by correlating smaller events, at higher resolution.

Two significant correlateable climate periods during the late Holocene have been identified in the literature. 1- The Medieval Warm Period (MWP) and 2- The "Little Ice Age" (LIA). The Medieval Warm Period's occurrence in the Southern Hemisphere is largely uncertain due to the lack of well-dated high resolution records covering the past 1000 years (Cook *et al.* 2002), but Soon and Baliunas (2003) report a worldwide imprint. The LIA, however, has been well documented everywhere on Earth where ice-covered mountains are present (with the exception of Antarctica), as glacier advance and subsequent retreat after the 1860 maximum. There is no doubt that the Little Ice Age and the post-1860 warming was global in extent (Broecker 2001).

The timing of the MWP and LIA are subject to debate in the literature, in part due to the geographical distribution and diversity of proxy records, it is generally accepted that these events are highly variable and not strongly synchronous (Hughes and Diaz 1994; Cook *et al.* 2002). Therefore I will adopt the broad definition of Soon (2003), that the LIA and MWP were anomalously cool and warm periods lasting at least 50yr, between 700 and 100 yr BP and between 1200 and 700 yr BP respectively. The question can then be posed: Do anomalies

consistent with the LIA and MWP exist in the Taylor Dome ice core record? (Figure 6).

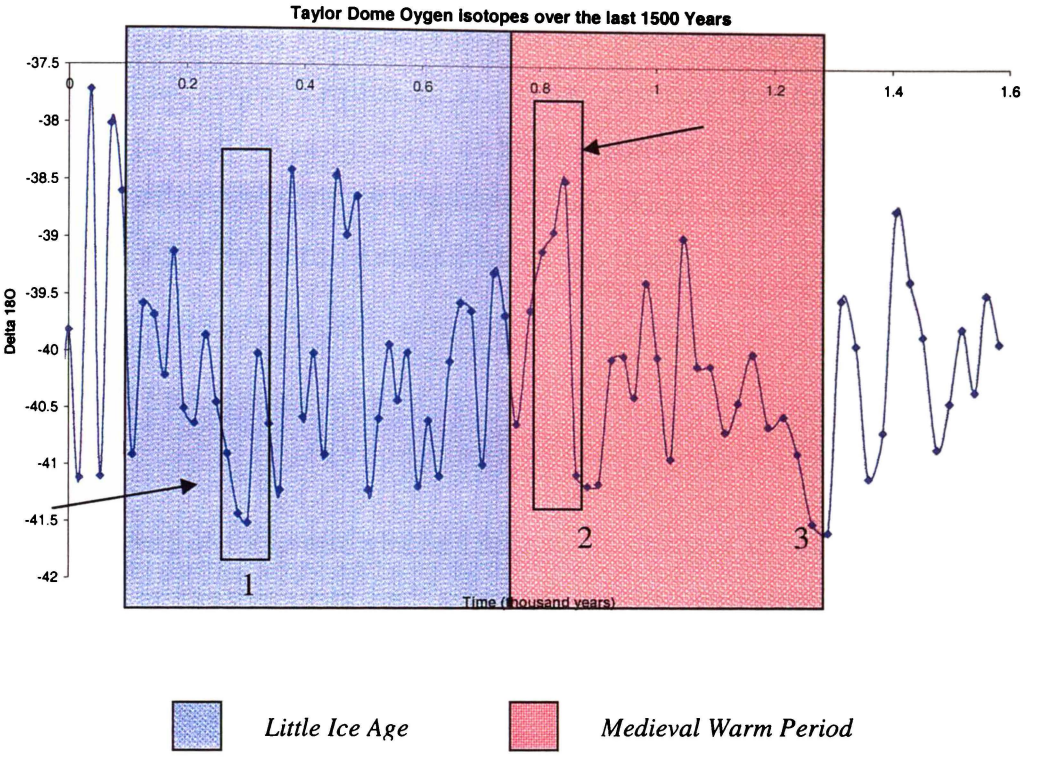

Figure 6: Oxygen isotopes used to infer paleotemperature over the period 1.6 ka to present (Steig 1999; 2000[1]). Periods corresponding to the Little Ice Age (LIA, the Medieval Warm Period (MWP) and prolonged cold periods are indicated.

The Taylor Dome $\delta^{18}O$ record has two events which fall into the broad definition of the LIA and the MWP respectively, and are identified in Figure 6. The cold period identified here at approximately 300 years B.P. has been also identified in other cores around Antarctica, (Masson *et al.* 2000) who termed it event D. Three prolonged cold periods are also recorded at Taylor Dome, indicated as 1, 2 and 3 (Figure 6), which may be significant.

Recent work using Antarctic lakes as proxy recorders of climate, indicates similar features to the ice core record; (Bjorck *et al.* 1996) found climate warming at 1200yr B.P. on James Ross Island, (Webster *et al.* 1996), found that Lake Wilson desiccated to low volume ~1000yr B.P, and (Bronge 1992) reported brief but pronounced cold periods between 1300-1100 yr B.P., and 400-250yr B.P. from lake sediments in the Vestfold Hills.

[1] St9810 timescale (Steig *et. al.* 1998;2000), smoothed data.

2.3 Glacial History of the Valleys.

The Ross Drainage System encompasses approximately a quarter of the surface area of the East Antarctic Ice Sheet. Changes associated with the extent of outlet glaciers and the Ross Ice Shelf dominate the glacial history of the Dry Valleys (Denton *et al.* 1989). Denton *et. al.* (1989) postulate that following global sea level lowering, an advanced Ross Ice Shelf grounded in Ross Sea, and converted from a floating ice shelf to a grounded ice sheet, which then thickened and backed-up along the Trans-Antarctic Mountain front.

2.3.1 Drift Sheets (Figure 7)

As the extent of the outlet glaciers respond to changes in local climate, drift is deposited at the terminus and sides of the ice, providing a history of ice movement. The McMurdo Oasis contains numerous drift sheets, of which the most prominent are:

"Ross Sea Drift" - The youngest drift sheet represents the infilling of McMurdo Sound by a west flowing grounded ice sheet, blocking the entrance to Taylor Valley, transporting material into the valley, (Stuvier *et al.* 1981; Denton *et al.* 1989), which reached a maximum altitude of 350m at the Hjorth Hill moraine, at the mouth of the Taylor Valley (Hall *et al.* 2000).

"Bonney Drift" - Occurs on the floor of the Taylor Valley, as far east as the western edge of Lake Fryxell, andrepresents the penultimate advance of the Taylor Glacier. It is contemporaneous with advances of local alpine glaciers, but out of phase with ice sheet grounding (Denton *et al.* 1989). Bonney drift is intermediate in age between Ross Sea Drift and Marshall Drift, indicating the advance of the Taylor Glacier is out of phase with the ice sheet groundings.

"Marshall Drift" - (best exposed in Marshall Valley) Represents the previous infilling of the Sound by a similar grounded ice sheet.

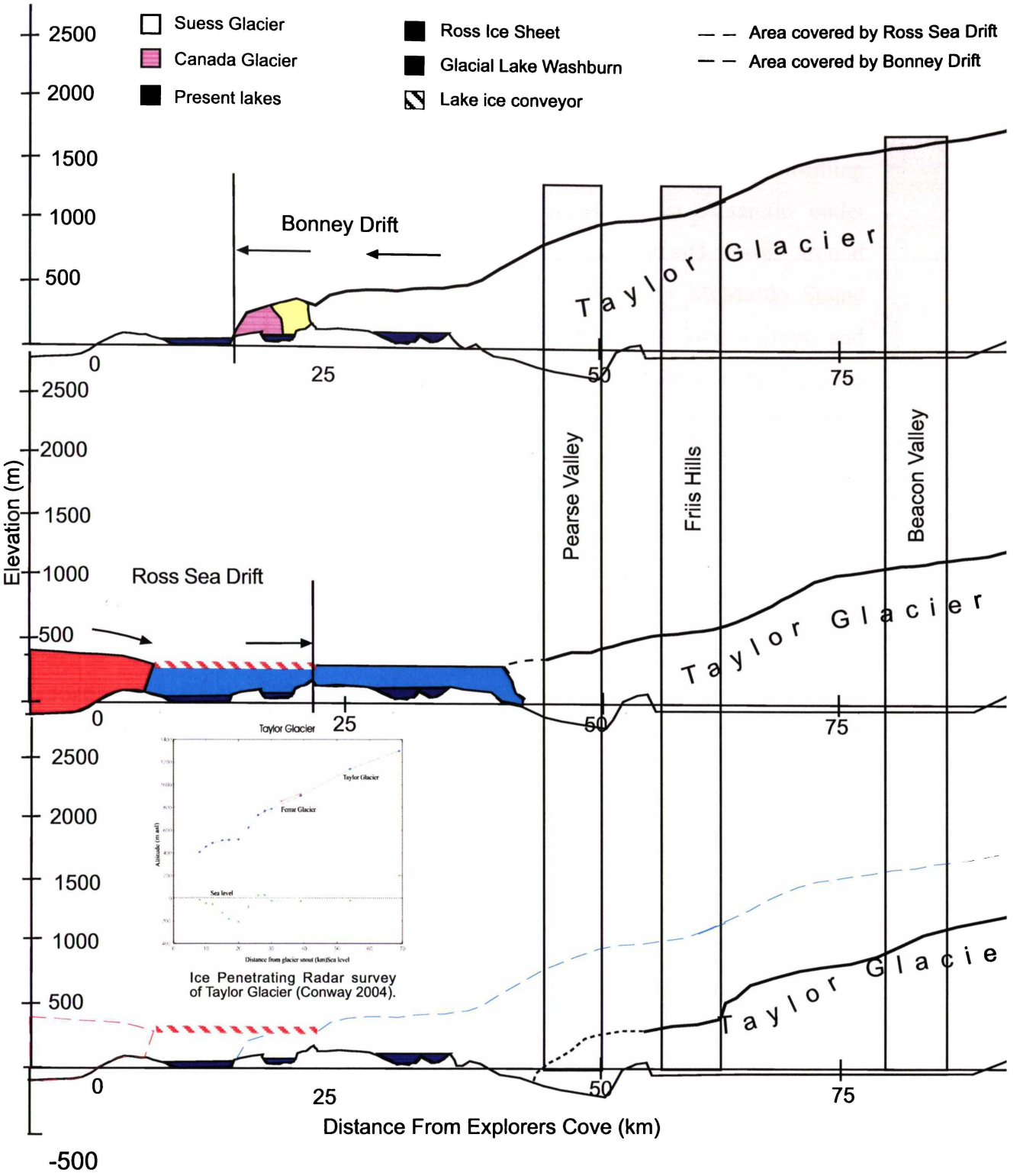

Figure 7a: The Taylor Glacier advanced eastward down the Valley (the Suess and Canada glaciers, also advancing at this time, adjoin with the Taylor), and deposited Bonney Drift, not quite reaching the western edge of Lake Fryxell.

Figure 7b: A lobe of Ross sea ice dams the entrance to Taylor Valley, occupying Explorers cove. Conditions favorable to meltwater production result in the formation of a large lake, proglacial to the lobe of the Ross Sea known as "Glacial Lake Washburn" (Pewe 1960). This lake is responsible for the deposition of Ross Sea Drift.

Figure 7c: Taylor Glacier retreated an unknown extent, before advancing to its current position. A sub-glacialdepression extends to 200m below sea level, this could have been inundated with sea water at this time.

At present, the Taylor Glacier is advancing into Lake Bonney, occupying its most advanced position since the Bonney II advance.

Figure adapted from Denton *et. al.* (1989)

Denton *et al.* (1989), infer that the Ross Sea Drift and Marshall Drifts, "represent regional ice sheet grounding, with ice flow from the eastern Ross Sea in-filling McMurdo Sound in the absence of through-flowing East Antarctic outlet glaciers". The ice entered the Sound from the Southeast and flowed around Minna Bluff, reaching a maximum thickness of 1325m in McMurdo Sound (Stuvier *et al.* 1981). This ice reached the mouths of the Dry Valleys, and tongues/lobes extended westward into the valleys. The presence of the large ice sheet dammed the valley mouths, and supplied vast amounts of meltwater, which formed lakes proglacial to the lobe of Ross Sea Ice Sheet. The history of Taylor Valley is presented in Figure 7, adapted from (Denton *et al.* 1989).

2.3.2 Sub-glacial profile of the Taylor Glacier

Figure 7 shows the glacial history of the Taylor Valley, adapted from Higgins (2000), with one important difference, the inclusion of the sub-glacial profile performed by Howard Conway in 2003. The Sub glacial profile shows a depression almost 500m below sea level, reference to the sub-glacial profile will be made later in this thesis.

2.4 Lakes in the Taylor Valley

The occupation of Taylor Valley drainage basins by lakes leaves distinctive lacustrine deposits. Strandlines and perched deltas left by previous higher lake levels often contain algae suitable for carbon dating, providing an age for the high lake water levels. Lacustrine carbonates formed in the sediments of these lakes also yield valuable information, as they can be analysed for stable isotopes of oxygen and carbon, identifying the source of the water, as well as a date of formation, using the Uranium / Thorium disequilibrium technique. These carbonates may be in-situ or contained within glacial drift deposits, giving secondary information about the age of the drift, helping to constrain the timing of ice movements.

2.4.1 Timing of occupation of Taylor Valley drainage basins by paleo lakes

The following is a synopsis of lake presence dating from approximately 300 000 years B.P., to the LGM. The transition from the LGM to the Holocene will be discussed in greater detail subsequently.

-Lacustrine carbonate sediments dating 300 000 ± 40 000 years have been found in the Taylor Valley, their isotopic signature indicates they originated from a lake proglacial to Taylor Glacier (Hendy *et al.* 1979). At this time Taylor glacier advanced into Eastern Taylor Valley (seaward), and deposited approximately 70m of sediments up to Lake Hoare (Powell 1981).

-Extensive lacustrine sedimentation occurred around 220 000 ± 50 000 years ago, depositing algal limestones whose isotopic signature indicates they were formed from local alpine glacial meltwater (except for those formed adjacent to Taylor glacier). The clasts of light oxygen isotopic signature did not leave the Bonney basin, indicating that this advance of the Taylor Glacier was not as extensive as the Bonney II glaciation, in isotope stage 5 (Hendy 2000).

-Between 87 000 and 100 000 years BP, an extensive lake filled the Bonney Basin, overflowing into the Fryxell Basin (Hendy *et al.* 1979; Higgins *et al.* 2000). Hendy *et al.* (1979) concluded from oxygen isotope data, that the depositing lake was proglacial to Taylor during the Taylor II advance. The advance of the Taylor Glacier continued, and with the adjoining of alpine glaciers Suess and Canada, did not quite reach the western edge of Lake Fryxell (where the Canada Glacier is currently) at about 70 - 100,000 yr B.P. (Hendy *et al.* 1979), the limit of "Bonney Drift".

2.4.2 Lakes over the LGM to Holocene transition in Taylor Valley (Fig 7)

By 23 800 ^{14}C yr B.P[2] the Ross Sea ice sheet occupying McMurdo sound, had advanced westward and grounded in Explorers Cove, sending ice to over 350m above sea level (Hall *et al.* 2000), at this time. The Taylor Glacier had retreated and a lobe of the Ross Sea Ice Sheet extended to approximately Lake Fryxell

[2] Beyond range of radiocarbon calibration program

(Denton *et al.* 1989), damming the entrance to Taylor Valley, enabling the creation of a large proglacial lake, "Glacial Lake Washburn" (Péwé 1960) (Figure 7), which, fed by meltwater, developed west into the valley. This lake was in existence until 8 700 cal yr B.P., (Stuvier *et al.* 1993) and relict shorelines indicate it reached at least 336m above sea level in the Taylor valley (Stuvier *et al.* 1981; Hall 2000), lakes in adjacent valleys reached similar elevations (566m in Wright Valley (Hall and Denton 1995) and 252 in Marshall Valley (Judd 1986)).

The formation mechanisms of these high level lakes are not well understood (Hendy 2000; Hall *et al.* 2001), but may relate to increased meltwater production resulting from a climate regime of cool, clear, dry conditions enabling higher absorption of solar radiation (Hall *et al.* 2001), and large extent of "blue ice" contributing occasional summer meltwater from a huge catchment area (Hendy pers. com).

Ross Sea Drift shows evidence the Ross Sea lobe had retreated from the crest of Explorers Cove by 13,040 yr B.P. and from the seaward slope by 11,370yr B.P. Glacial Lake Washburn persisted above the mid valley threshold (into Bonney Basin) until 13,300 yr B.P. (Hall pers. com; www.ume.maine.edu). In Fryxell Basin, it persisted until at least 8700± 65 yr B.P., (Stuvier *et al.* 1981; Hall *et al.* 2000). Grounded Ross Sea Ice had cleared Explorers Cove between 8,340 and 6,670 yr B.P. (Denton et al. 1989).

2.4.3 Glacial Lake Washburn level changes

Hall (2000) has presented sets of ^{14}C dates from relict shorelines of Dry Valley lakes, and concluded that lake levels have fluctuated hundreds of metres over the last 25, 000 years due to changes in the ratio of inflow vs outflow caused by climate changes (Figure 8).

Glacial Lake Washburn lake levels persisted, (although apparently oscillating, Figure 8) until the LGM / Holocene transition, (from 23 800 and 12 450 yr BP

and possibly as late as 11 820 BP (Denton *et al.* 1989; Hall and Denton 2000), consistent with the recession of the Ross Sea ice lobe occupying Explorers Cove. The lake was then separated into the two basins (Bonney and Fryxell) by Nussbaum Riegel at 200m elevation, the lake in Bonney basin receded, and very little evidence is available for the lake after this time (Hendy 2000). The lake occupying the Fryxell Basin however, persisted until as late as 9200 BP (Stuvier *et al.* 1981), fed by overflow from a lake still trapped against the receding Ross Ice Sheet in Explorers Cove (Chinn 1993).

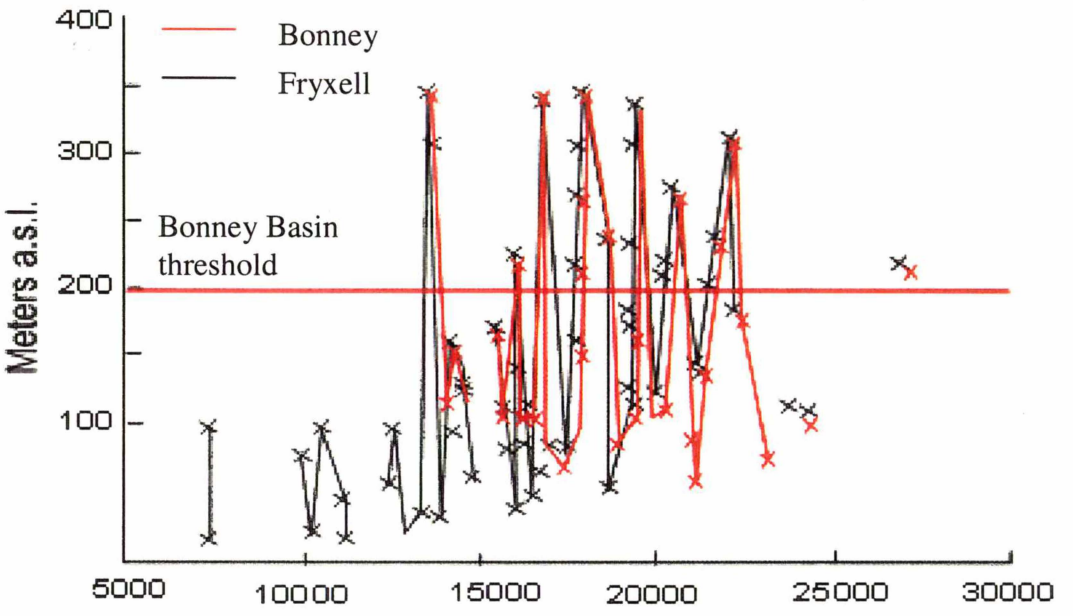

Figure 8: Lake level reconstruction of Lakes Bonney and fryxell from ^{14}C dated algae in perched deltas and paleostrandlines. (Hall unpublished) Any level above the Bonney Basin threshold indicates a large connected lake, levels lower indicate separate lakes.

At approximately 13, 040 yr B.P., ice core records place the beginning of the climatic warming (the same time as the grounded ice sheet begins reducing in its extent). Isotope records from Vostok and Dome Circe ice cores show a 9 - 10° C warming, coupled with a doubling of snow accumulation rate across the full transition from the LGM (Isotope Stage II) to the Holocene (Jouzel *et al.* 1989). This is however, not analogous with the glacial evidence from the valleys, which shows little to no change of height of the inland plateau, which would also be expected to reduce in extent (Denton et al. 1989), implying that the isotopic change across the transition is not a result of massive lowering of the East

Antarctic plateau, but instead widespread climate change (Denton et al. 1989). Denton *et al.,* (1989) suggested this resulted in increased accumulation in the valleys and on the plateau, as the Ross Sea ice receded, with the barrier to storm tracks is removed and the precipitation increases allowing the glacier to advance.

To recap; lakes of the region, extensive during the LGM, decreased during the LGM / Holocene transition and were succeeded by much smaller lakes, even smaller than those present today. Hendy (2000) reported that between 14 000 and 8 000 yr BP these large lakes evaporated to low volume depositing insoluble carbonates and sulfates. Why would lakes decrease in area and volume if the climate was warmer and wetter? Denton *et al.* (1989) offer three possible explanations; 1. The loss of the extensive meltwater input from the Ross Sea Ice lobe, 2. Lake level variations only reflect the effect of summer temperatures on glacier melt and hence lake level, or 3. Recession of ice shelf and decreasing aridity through the transition, created a situation where the barrier to storm events was removed and snowfall increased the albedo, reducing the length of the melt season, coupled with the removal of melt water.

2.4.4 Summary of Lake Persistence in Taylor Valley (Table 1)

Lakes occupying the Basins in the Taylor Valley have varied in their extent according to local ice and climate conditions. These changes have been recorded by lacustrine carbonate deposits, algal mats in perched deltas and paleo strandlines on the valley walls, as well as by geochemical and observational means (Table 1)

Table 1: Summary of lake level changes in the Taylor Valley (Hendy 2000).

	Years BP	Age Basis	Lake or region	Change Observed	Evidence
MID PLEISTOCENE	300 000 ± 25 000	$^{230}Th/^{234}U$	Taylor Valley	Taylor Glacier meltwaters extend to fryxell basin	Algal limestones in drift in DVDP #12 core (Hendy *et al.* 1979; Higgins *et al.* 2000)
	~ 250 000	$^{230}Th/^{234}U$	Lower Taylor Valley	Ross sea or alpine glaciers form lake(s) in the lower Taylor Valley	Algal limestones in drift in DVDP #12 core
	190 000	$^{230}Th/^{234}U$	Bonney	Taylor Glacier	Algal limestones in

	– 210 000		Basin	meltwater fill Bonney basin	drift (Hendy 1979; Hendy *et al.* 1979; Higgins *et al.* 2000)
	145 000 ± 10 000	$^{230}Th/^{234}U$	Taylor Valley	McMurdo ice sheet meltwaters create a proglacial lake	Algal limestones buried in till (Judd 1986)
	87 000 – 120 000	$^{230}Th/^{234}U$	Taylor Valley	Taylor Glacier meltwaters fill Bonney, Frxyell and Hoare basins	Algal limestones on valley floor and drift sheets(Hendy 1979; Higgins *et al.* 2000)
LATE GLACIAL	26 000	^{14}C	Taylor Valley	Ross sea ice meltwaters enter valley	Algae in perched deltas, algal limestones of valley floors (Hall and Denton 2000)
	16 000 - 18000	^{14}C, $^{230}Th/^{234}U$	Taylor Valley	Lake levels ~ 340m above sea level	Algae in perched deltas, algal limestones of valley floors (Hall and Denton 2000)
HOLOCENE	1000	Chemistry	Bonney	East lobe evaporated to low volume	Dating of evaporite salts (Hendy 1979)
	>250	Chemistry	Bonney	West Lobe overflowed into East Lobe	Solving the diffusion equation for the salt gradient in East Lobe (Hendy *et al.* 1977)
	90	Historical records	Bonney	Rose by 3-4m between 1903 and 1911	Width measurements made by Scott (1905), and Taylor (1922)
	AD 1960 – 1990	Historical records	Lakes; Vida, Vanda, Joyce, Bonney, Hoare, Fryxell.	All lake levels rising ~ 6m	Leveling from benchmarks twice annually

Lake level reconstructions after the full recession of the Ross Sea Ice Sheet are unavailable by exposed remnants, as the desiccation to low volume lakes (smaller than those of today (Denton *et al.* 1989) means the associated strandlines and deltas are beneath the current lake level. To reconstruct the lake levels, and thus the hydrologic balance from this period, it is necessary to study the record contained in the lake sediments and diffusion gradients of the water column, and correlate these to other local proxy records.

2.5 Lake Bonney (present) and its evolution

2.5.1 Present Lake Bonney Bathymetry

A bathymetric survey (Hendy *et al.* 1977, surveyed by Hendy 1975 (Antarctic report #4)), using holes augured through the ice, and leadline measurements to the lake floor, found a flat bottomed lake 32-33m deep (from water line) (Figure 9a). This contrast with a second survey (Golder Associates, 1995) using ice penetrating radar (Figure 9b) showed uneven bottom topography, of depths less than 30m to greater than 38m depth. The discrepancy between the two surveys, and the admission in the report that elongate bubbles within the ice on Lake Bonney caused extreme scattering of the radar signal, casts doubt on the second survey. As a result the Hendy *et. al.* (1977) survey has been used to describe Lake Bonney bathymetry. Since these measurements were made, lake levels have continued to rise.

The two lobes of Lake Bonney are separated by Bonney Reigel (currently about 9m depth). The lake appears to be rising since first explored by Scott (1905) (Scott 1905; Chinn 1993; Bomblies *et al.* 2001), Golder associates LTER report (1995) estimates approximately 12 m rise since the depth measurements made in 1964.

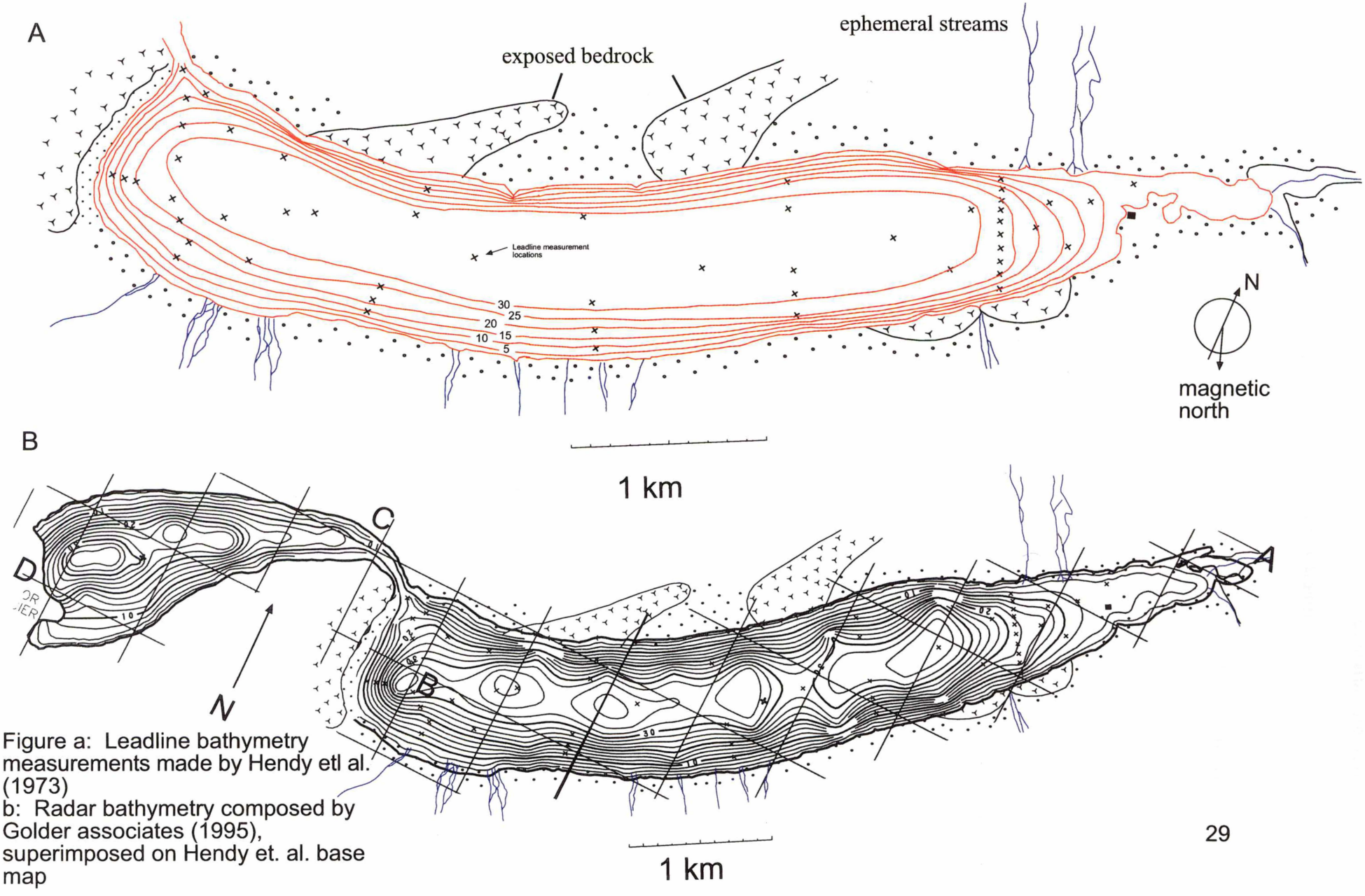

Figure a: Leadline bathymetry measurements made by Hendy etl al. (1973)
b: Radar bathymetry composed by Golder associates (1995), superimposed on Hendy et. al. base map

2.5.2 Isotopic and major ion characteristics of Bonney Basin.

Lake Bonney, the largest enclosed drainage basin in the Taylor Valley contains more salts than any other lake in the Dry Valleys. The majority of the salt is contained in the East lobe, where 11 million tonnes of NaCl are in solution, and at least 36 million tonnes are contained in the sediments (Hendy *et al.* 1977). The East has a flat bottom, shown to be a mirror like surface of halite with an unknown thickness of hydrohalite underneath (Hendy *et al.* 1977).

Since Lake Bonney's discovery, much attention has focused on its history (Angino and Armitage 1963; Angino *et al.* 1964; House *et al.* 1966). Subsequently, much contention surrounded the source of the salts in Lake Bonney, with debate focusing on groundwater contributions (Weand *et al.* 1975), chemical weathering from the catchment (Lyons *et al.* 2000), Aerosol deposition (House *et al.* 1966) and trapped seawater (Angino *et al.* 1964; Hendy *et al.* 1977), or a combination (Hendy *et al.* 1977; Takamatsu *et al.* 1998).

Prior analysis of sediments show the presence of evaporite salts, halite, hydrohalite, aragonite and gypsum in East Lobe (Wilson *et al.* 1974), and gypsum overlying sub-aerially weathered sands in West Lobe (Gumbley 1975). Analysis of the lake water column shows a similarity to sea water, but with substantial depletions in HCO_3, SO_4 and Ca^{2+} (Angino *et al.* 1964; Matsubaya *et al.* 1979), so that the most significant salts to be deposited on evaporative concentration will be minor calcite/aragonite and gypsum, and mostly halite at temperatures above -0.1°C, hydrohalite at temperatures below -0.1°C (Hendy pers. comm).

^{18}O from Taylor Glacier is the dominant source of water for Lake Bonney, the 15000 year reservoir effect age of the HCO_3 in the water body suggests that most of the inflowing Dissolved Inorganic Carbon (DIC) has also come from Taylor Glacier. Neuman *et al.*(unpublished) tentatively suggest –0.78‰ ^{13}C for waters entering Lake Bonney, but highlight the paucity of data, stating; "it is extremely difficult to actually estimate the average $\delta^{13}C$ entering Lake Bonney".

East Lobe water column

The East Lobe bottom waters are of near uniform composition before an abrupt diffusion gradient at 13-20m depth (Figure 10a). Below 35m NaCl is supersaturated, and below 25 m supersaturated with respect to $CaCO_3$, $CaSO_4$ (Neumann *et al.* unpublished). The East Lobe waters are enriched in ^{18}O and D (compared to the West Lobe) and show the same gradient seen in the major ions (Figure 10b; Figure 11a and b) but above 13-20m match those of West Lobe at 9.5m (Figure 10b).

The concentration gradients measured in the water column strongly suggest the presence of a diffusion gradient, likely the result of a mixing of freshwater over a concentrated brine or salt playa (Hendy *et al.* 1977).

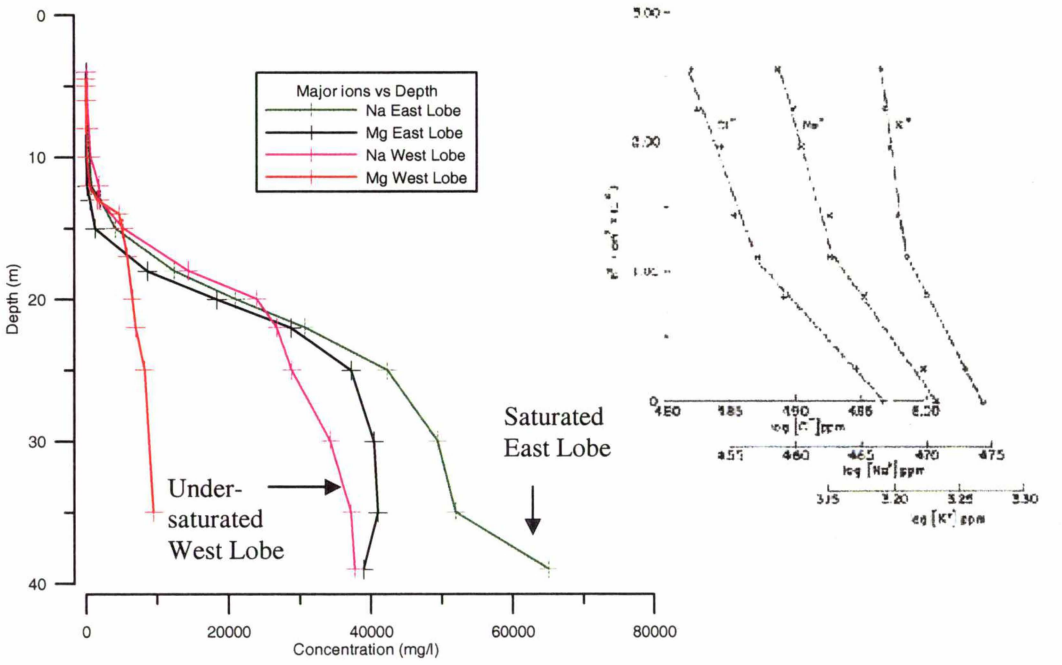

Figure 10a: : Major ions vs depth. The disturbed profile of West Lobe is also shown.

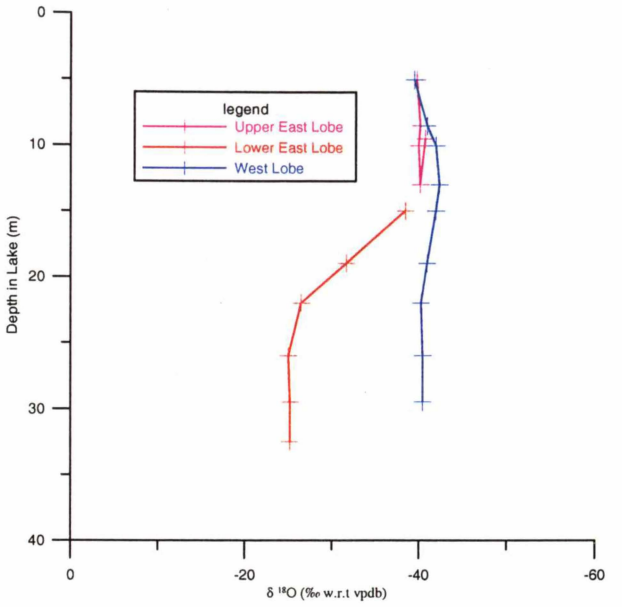

Figure 10b: $\delta^{18}O$ vs depth

West Lobe water column

West Lobe remained undersaturated with respect to calcite at all depths and became supersaturated with respect to gypsum below 17 m, the major ions show a gradient, not originating from a saturated brine (Figure 10a), which has been disturbed by the advance of Taylor Glacier into the lake (Figure 10a) (Hendy *et al.* 1977).

Seasonal changes

The upper 10 m of the water column of both lobes were 2 to 5 times supersaturated with respect to calcite at the beginning of the summer season and became under-saturated as the summer progressed. Neumann *et al.*(unpublished) hypothesise that, during the course of the winter, the formation of new lake ice "freezes-out" salts, and algal productivity in the summer season releases inorganic carbon via respiration, causing the increase of Ca^{2+}, HCO^{3-}, and CO_3^{2-} concentrations in the upper 12 m.

In the epilimnion, the preferential uptake of ^{12}C by planktonic algae and cyanobacteria create a profile of enriched $\delta^{13}C$ with depth (Quay *et al.* 1986)

(Figure 11a and b), reaching a maximum at the respective depths of maximum primary productivity. Photosynthetic assimilation of carbon fractionates the isotopes of carbon, leaving organic matter depleted, and water enriched in ^{13}C (Quay *et al.* 1986). In the east lobe, the $\delta^{13}C$ values decreased below the chemocline at 10 m, to the lowest value of 0.47‰ at 22 m depth corresponding to the depth at which respiration ceases entirely (Priscu, 1992), below this, the $\delta^{13}C$ values increased reaching 5.34‰ at 37 m depth (Figure 13 a) . The increase with depth is likely due to diffusion caused by resolution of sediments into the water column.

A continuous preferential removal of ^{12}C will increase the $\delta^{13}C$ during the season (Figure 11). The maximum $\delta^{13}C$ values in Lake Bonney were 4.52‰ (West Lobe) and 5.02‰ (East Lobe), in late November 1996 (Figure 13a and b).

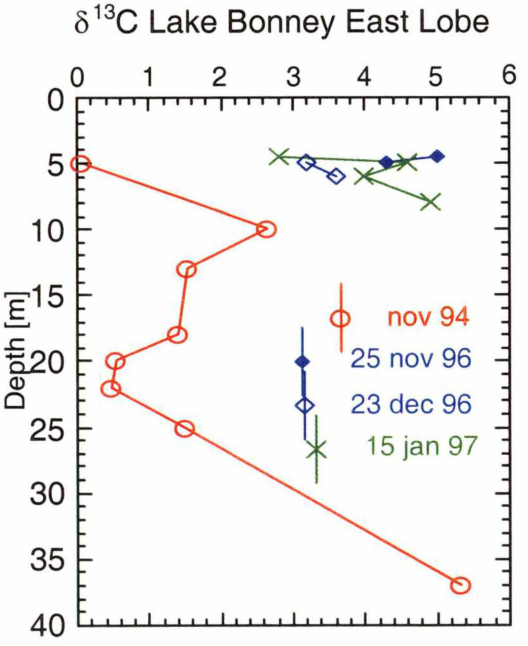

Figure 11 a: Carbon – 13 changes with depth in the East and West Lobe of Lake Bonney (Neumann et al. unpublished).

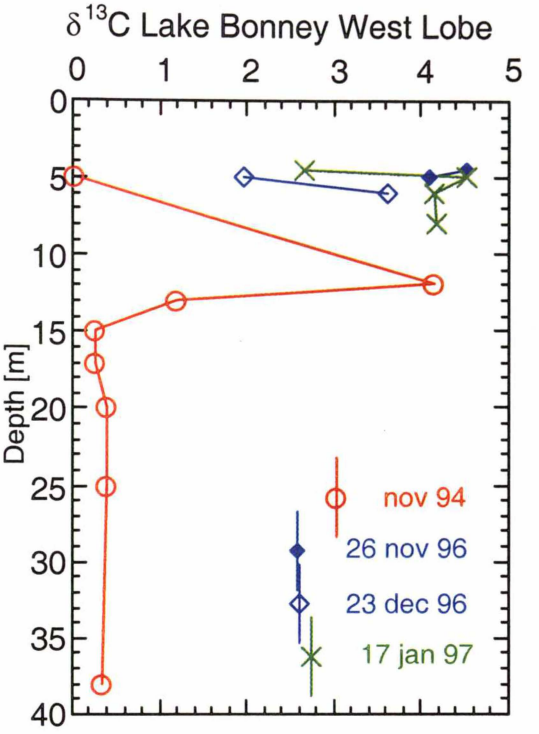

Figure b: Carbon – 13 changes with depth in the East and West Lobe of Lake Bonney (Neumann et al. unpublished).

The cyanobacteria *Lyngbia martensiana* reported to be found in benthic mats of lakes Fryxell, Hoare, and Bonney, is orders of magnitudes higher than the abundance in the water column, the mats can be expected to play a major, yet unquantified role in both calcium and carbonate removal from the lakes (Craig *et al.* 1974; Neumann *et al.* unpublished)

2.6 Principles of Lake Bonney (amplifier lake) as a climate recorder

The basic hydrological principles governing lake level, explained throughout this literature review become particularly valuable when the period of negative water balance is sufficient to cause the lake to desiccate to a very small volume. This is for two reasons. 1. The content of the lake is concentrated, increasing the salinity of the remaining water, whereby a point is reached that maintenance of an ice

(which results in enrichment of ^{18}O and D) and exchange of CO_2 with atmospheric carbon dioxide. 2. Subsequent infilling of the lake develops a diffusion profile, as salts mix.

Decreasing lake volume caused by a negative water balance causes the minerals to approach saturation and begin to precipitate. There is a substantial body of literature concerning the formation of evaporites from seawater, dependent on temperature, producing a sequence of mineral precipitation that determines the evolution of the resulting solution. At low temperature, the general sequence is calcite, gypsum at about 0°C, then mirabilite at about -6°, with halite/hydrohalite down to -22°C. Magnesium chloride brines result (ie Lake Bonney).

2.6.1 Diffusion Ages

Modeling of the diffusion profile for ^{18}O and Cl^- (solution of the diffusion equation), has enabled the time since the filling event occurred to be estimated at approximately 1200 yr BP in Lake Vanda (Wilson 1964; Matsubaya *et al.* 1979), and ~250 yr B.P. in the East Lobe of Lake Bonney, (Hendy *et al.* 1977) and between 650 and 1250 in Lake Fryxell (Lawrence and Hendy 1985), although subsequent Lake Fryxell studies failed to support a complete desiccation, Lyons *et al.* (1998) suggest a minimum depth of no less than 7m, and (Whittaker 2004) could not find evidence of evaporites in the sediments to support such a drying.

Solution of the diffusion equation of West Lobe gives an age of about 6000 years, and ^{14}C dating of the Dissolved Inorganic Carbon (DIC) gives an impossibly old age of 11 000 years (Hendy *et al.* 1977). This suggests that ancient CO_2 is being introduced directly from the Taylor Glacier and a continuous ice cover has prevented exchange in West Lobe. This conclusion is supported by an equally impossible age of 10^6 years required to gain the ^4He measured in the West Lobe (Poreda *et al.* 2004). There is likely a sub glacial evaporite deposit contributing to the lake, supported by the anomalous ^4He quantity, (Poreda *et al.* 2004) the Blood Falls discharge (Black *et al.* 1965), the low ^{36}Cl:^{35}Cl ratio of both lobes, which the

authors (Lyons *et al.* 1998) suggest is the result of a slightly modified source of seawater.

The current water structure of Lake Bonney has been interpreted as the result of West Lobe overflow into East Lobe sometime between 5000 and 1800 yr B.P. (Hendy *et al.* 1977; Hendy 2000; Neumann *et al.* unpublished)The lobes were again isolated, and the East Lobe evaporated to a depth of about 17m, at which time it became too saline to support an ice cover (Matsubaya *et al.* 1979). Hydrohalite, halite, gypsum and calcite precipitate as water vapour is lost by evaporation, causing enrichment in D/H and $^{18}O/^{16}O$, and loss of inherited ^{4}He. Subsequently West Lobe again overflowed re-flooding East Lobe, resetting the ^{4}He "clock" when the ice cover returned, and establishing a new diffusion gradient ~ 250 yr B.P. This process is summarised in Figure 12 a,b and c.

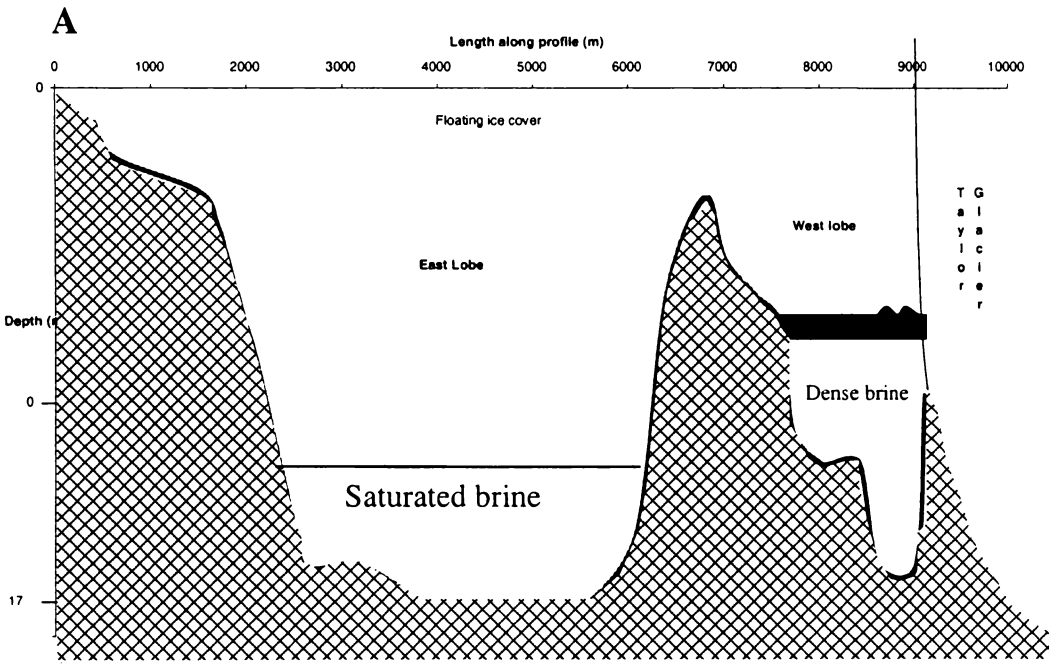

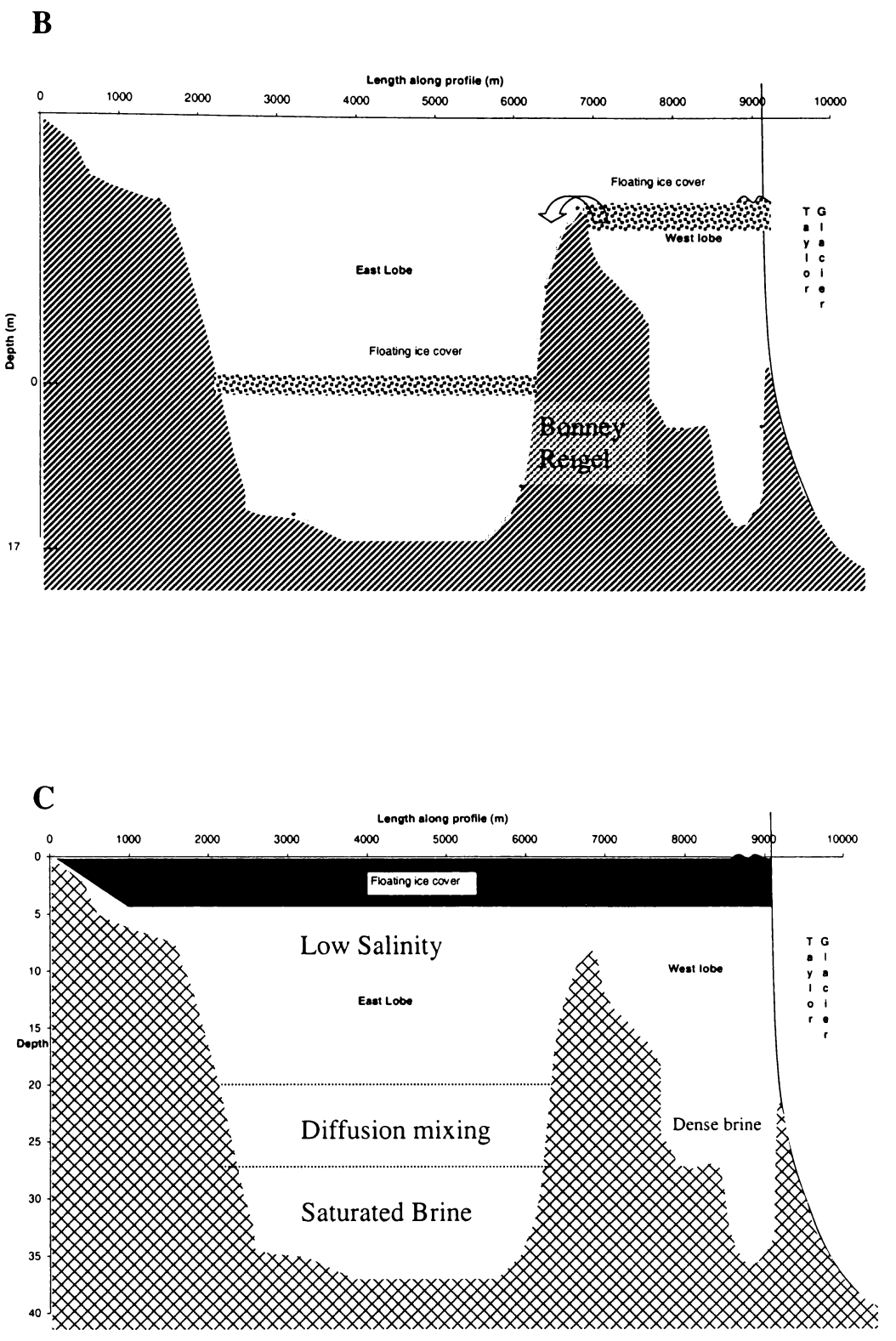

Figure 12 a: Longitudinal bathymetric cross section of Lake Bonney along Transect A-B-C-D, showing the East Lobe desiccation approximately 1200 years B.P. b: Overflow of West Lobe into East Lobe, ending approximately 250 years B.P.. c: Present lake level.

2.6.1 Stumbling blocks for a seawater origin

The salts, whatever their origin, have been modified by precipitation and re-solution. If seawater was the origin, oxygen isotopes show all the original water has been lost and replaced by Taylor Glacier meltwater (Hendy *et al.* 1977; Hendy *et al.* 1977). In addition most of the sulphate and much of the calcium has also been lost.

A number of authors have speculated on mechanisms to produce such a composition from sea water. The common stumbling blocks are:

1. The lack of evidence of a marine incursion into Taylor Valley within a reasonably recent time. This is particularly pertinent in the Taylor Valley has experienced multiple occupations by the Taylor Glacier, extending beyond the coast, and multiple occupations by very large proglacial lakes.

2. The lack of evidence of a any deposits of the salts which would have to be removed from sea water to produce the current composition of Lake Bonney water.

2.7 Geochemical relationships

Data have been collected to trace the evolution of the source waters. Analyses include determining the concentrations of trace elements (Sr, Mg, Ba, Fe, S, Na, K, Br), bromine to chlorine ratio, and Na to Mg ratio, sulphur, and oxygen and carbon isotope ratios (Schreiber and El Tabakh 2000).

2.7.1 Bromine

Bromine fractionation between the evaporating solution and the precipitate is conservative, and the partition function follows a predictable pattern not significantly affected by temperature (Schreiber and El Tabakh 2000). Bromine in a Halite precipitate can be used to estimate the concentration in the precipitating brine, and thus the extent of concentration.

2.7.2 Magnesium

The most accurate indicator of brine concentration was found to be Mg as it is conserved during brine evolution, all other major ions eventually become depleted with respect to Mg (Matsubaya *et al.* 1979).

2.7.3 Isotopic variation

The isotopic composition of evaporites is a direct reflection of the isotopic composition of the waters of formation (Schreiber and El Tabakh 2000; Neumann *et al.* unpublished). The major factors governing the isotopic composition of the brine are; 1) initial isotopic composition, and 2) amount of dissolution of older evaporites, which would be expected in Lake Bonney given the diffusion profile.

Oxygen – 18 (^{18}O)

As water evaporates, while an ice cover remains, little fractionation of oxygen isotopes occurs, so that the remaining solution is not significantly enriched in ^{18}O When the ice cover is lost, and evaporation from an open water source occurs, ^{16}O is selectively removed, carbonates formed during this type of evaporation should show a signal of increasing $\delta^{18}O$ as evaporation continues (the evaporative enrichment precludes the carbonates from being used in paleotemperature reconstruction). Changes in ^{18}O provide information on rates of meltwater input and evaporation, as an input of water more depleted in ^{18}O will mix with the enriched waters, lowering the overall ^{18}O value, carbonates formed after a freshwater input will have ^{18}O values lower than previous carbonate (Bird *et al.* 1991).

The oxygen isotopes yield a bonus which is unique to these lakes, the ice cover excludes exchange with the atmosphere (as previously mentioned), and therefore, any evaporative enrichment will be slow until such a time as the ice cover is lost due to the resultant high salinity. If the ice cover is lost, the waters will exchange with atmospheric oxygen rapidly, and any carbonates precipitated at this time

would record an oxygen isotope signature much enriched in ^{18}O compared to previous evaporites formed with an ice cover. The loss of ice cover could only occur as the result of climate change, either a warm period, or a cold period concentrating the waters until salinity precludes the maintenance of the ice.

Carbon – 13 (^{13}C)

The ^{13}C composition of carbonate in hypersaline lakes provides a record of changes in paleoproductivity (Bird *et al.* 1991), the removal of inorganic carbon by algal mats would increase the ratio of ^{12}C to ^{13}C, since the lighter ^{12}C is preferentially assimilated (Des Marais 1995).

Calcite precipitated during the freezing of water can also create very enriched isotopic compositions. The only known mechanism is fractionation via freezing of a saturated solution. Freeze concentration drives the remaining brine to saturation, whereby carbonate is precipitates, forcing the carbon isotopes to fractionate between HCO_3 and $CO_{2\,(gas)}$. Calcite has been recorded to precipitate as a cryptocrystalline powder within the ice under such conditions (Clark and Lauriol 1992), this is then deposited upon melting of the ice (equilibrium fractionation at 0°C between $CaCO_3$ and HCO_3 is 10.3‰) (Clark and Lauriol 1992), repetitive freeze concentration can progressively enrich the $\delta^{13}C$ of $CaCO_3$ up to a maximum value of +14.3‰ (Clark and Lauriol 1992). Isotopically enriched carbonate crusts (up to 18‰) have been observed along the shorelines of Lake Vanda (Nakai 1974) (exceeding the maximum theoretical value of +14.3‰). These higher values could be produced by non-equilibrium fractionation, or by first removing ^{12}C through photosynthesis, then freezing of the remaining solution (Hendy pers comm.).

The relationship between $\delta^{13}C$ and $\delta^{18}O$ in a closed basin lake is a function of hydrological change, vapour exchange and lake productivity (Bird *et al.* 1991).

2.7.4 Isotope covariance

Perhaps the most important information is the co-variance of $\delta^{13}C$ and $\delta^{18}O$ (enrichment or depletion) resulting from rapid increase or decrease in lake volume, with rapid decrease giving enriched, and rapid increase giving depleted, isotopic values. A stable lake will give relatively poor isotopic co-variance (Li and Ku 1997).

2.8 Summary

Taylor Valley was occupied by the Taylor Glacier in previous interglacials, when the warmer wetter environment facilitated the advance of the glacier down valley. The advancing glacier would likely have stripped the valley floor of soluble salts and unfrozen sediments.

During the last glacial period, a Lobe of Ross Sea Ice damned the Taylor Valley mouth in Explorers Cove, sending ice to 320m above sea level along the Trans-Antarctic Mountain front in McMurdo Sound. The massive quantity of ice provided a source of meltwater which created Glacial Lake Washburn. Glacial Lake Washburn was in existence from the LGM to about 9000 years B.P. extending into the Bonney Basin, and fluctuated enormously for reasons unknown, but thought to be the result of climate changes affecting hydrological balance.

The lakes of the Dry Valleys are perennially ice covered, and contained in enclosed drainage basins with delicate hydrological balances governing lake level. The term "amplifier lakes" (Street-Perrot and Harrsion, 1985) has been coined, as lake level changes are significantly more dramatic than the causal climate change.

Large changes in lake level concentrate or dilute the water column. Large enough periods of concentration (inferred as cold / dry climate) would be recorded as precipitate salts in the sediments, of which gypsum carbonate and halite are

known to be present in Lake Bonney. These sediments can be analysed for trace elements and isotopes to infer the composition of the water at the time of precipitation, and carbonate can be dated via U/Th providing a timescale.

Bathymetry studies show the East Lobe has very steep sides, and is dominated by a flat mirror like surface of NaCl (halite) at 38m depth (currently), and the West Lobe is an ellipsoidal basin, deepest just in front of the Taylor Glacier snout.

The large amounts of salts reported in the sediments of Lake Bonney have been the subject of much contention in the literature, as much less salt is found in basins eastward and westward of Bonney Basin. The salt must be the result of something only affecting the Bonney Basin otherwise similar amounts would be found elsewhere.

The source of the salts is thought to be a marine incursion, which has been altered by evaporation and dissolution in antiquity, but no evidence has been found to support this, as there is no evidence of an incursion from the seaward end of the valley, and the glacier currently occupies the area which would contain further evidence westward. Uncertainty surrounds how far the glacier retreated during the last glacial, this evidence is also covered by the advancing glacier. It has been speculated that another lobe of Lake Bonney (~1km from the current terminus of the Taylor Glacier), containing evaporite salts has been overridden (Keys 1979; Keys 1981), transporting evaporite salts into West Lobe in the basal till and Blood Falls. Howard Conway *et. al.* (2003) confirmed the presence of a sub-glacial depression with the results of an ice penetrating radar survey of the glacier in 2003. The depression is massive (~250m below sea level), but occurs approximately 10km further up valley than expected (Figure 7).

Changes in $\delta^{18}O$ from an ice core extracted from the Taylor Dome (the source of the Taylor Glacier) are the result of changing temperature of the atmosphere when the ice is deposited. The Taylor dome ^{18}O record over the late Holocene shows a warm and a cold period falling into the broad definition of the Medieval Warm

Period and the Little Ice Age respectively, and also shows a number of prolonged cold periods, which could possibly be reflected in lake sediments.

Chapter 3:

Methods

Field transportation in Antarctica

3.1 Introduction

The measures and procedures taken to collect and analyse the samples used in this thesis are described in the following chapter. Throughout this chapter I will also outline the considerable process of method development, both in field technique and laboratory work as this has been an important aspect.

3.2 Sample locations

This thesis is based on the sediment collected from four locations within Lake Bonney, three from the hypersaline East Lobe, and one from the West Lobe (Figure 13). Although a total of ten cores were attempted, not all were successful, or analysed (Appendix 1 contains the location and details of all cores, Appendix 2 contains the descriptions of all cores not analysed). The cores which have been used are described separately in chapter 4.

3.3 Field Methods

Collecting sediment cores from Antarctic perennially ice covered lakes is not an easy process. The ice cover, freezing temperatures, wind chill and difficulty transporting equipment complicate the process.

In order to gain access to the sediments, it is first necessary to penetrate the 5 metre floating ice cover of the lake. To do this we had two options available to us, The S.I.P.R.E auger and the Jiffy® drill.

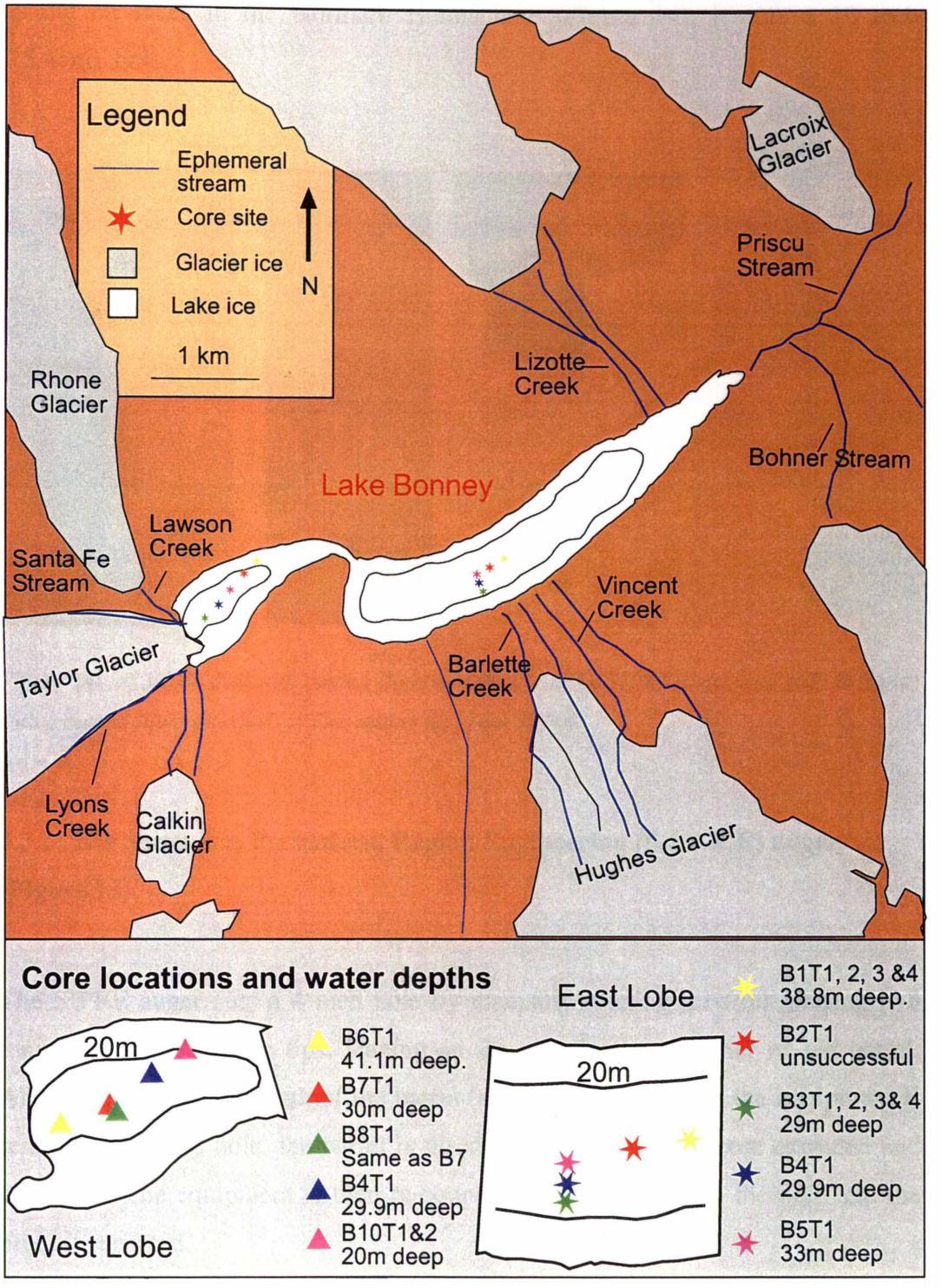

Figure 13: Core locations on Lake Bonney

3.3.1 The Jiffy® Drill

The Jiffy® drill is a three horse power, two stroke ice drill commonly used for ice fishing on lakes in the Northern Hemisphere (Figure 14), it cuts a 10 inch (25.4cm) hole.

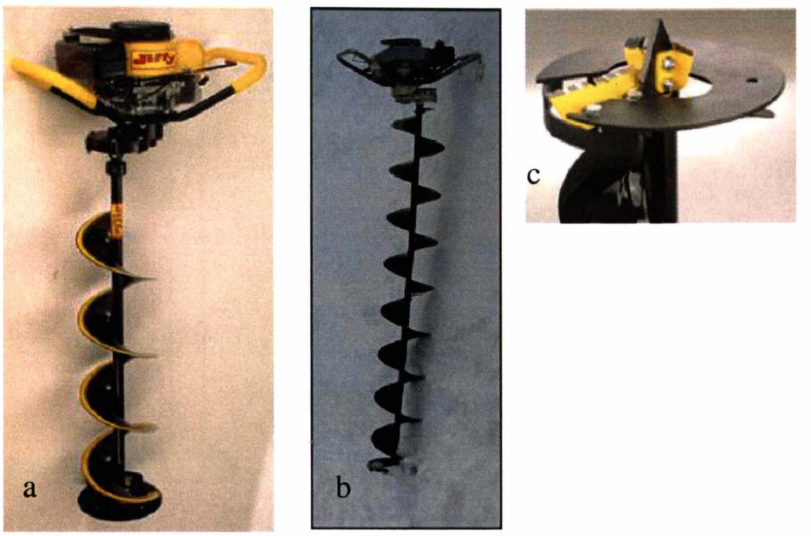

Figure 14: a) Jiffy® drill with cutting flight attached. b) The SIPRE (left), and Jiffy ® (right) with a second flight attached. c) The cutting tip of the Jiffy®.

3.3.2 The Snow, Ice, Permafrost Region Engineering (S.I.P.R.E) auger (Figure 15).

The SIPRE auger cuts a 4 inch hole by manually rotating a barrel housing two tungsten-carbide cutting tips, leaving an ice core in the chamber of the barrel. After descending the length of the barrel (approximately 85cm), the equipment is removed from the hole, the barrel is disconnected and the ice core extruded and discarded. The equipment is then re-connected and put back in the hole and the process repeated.

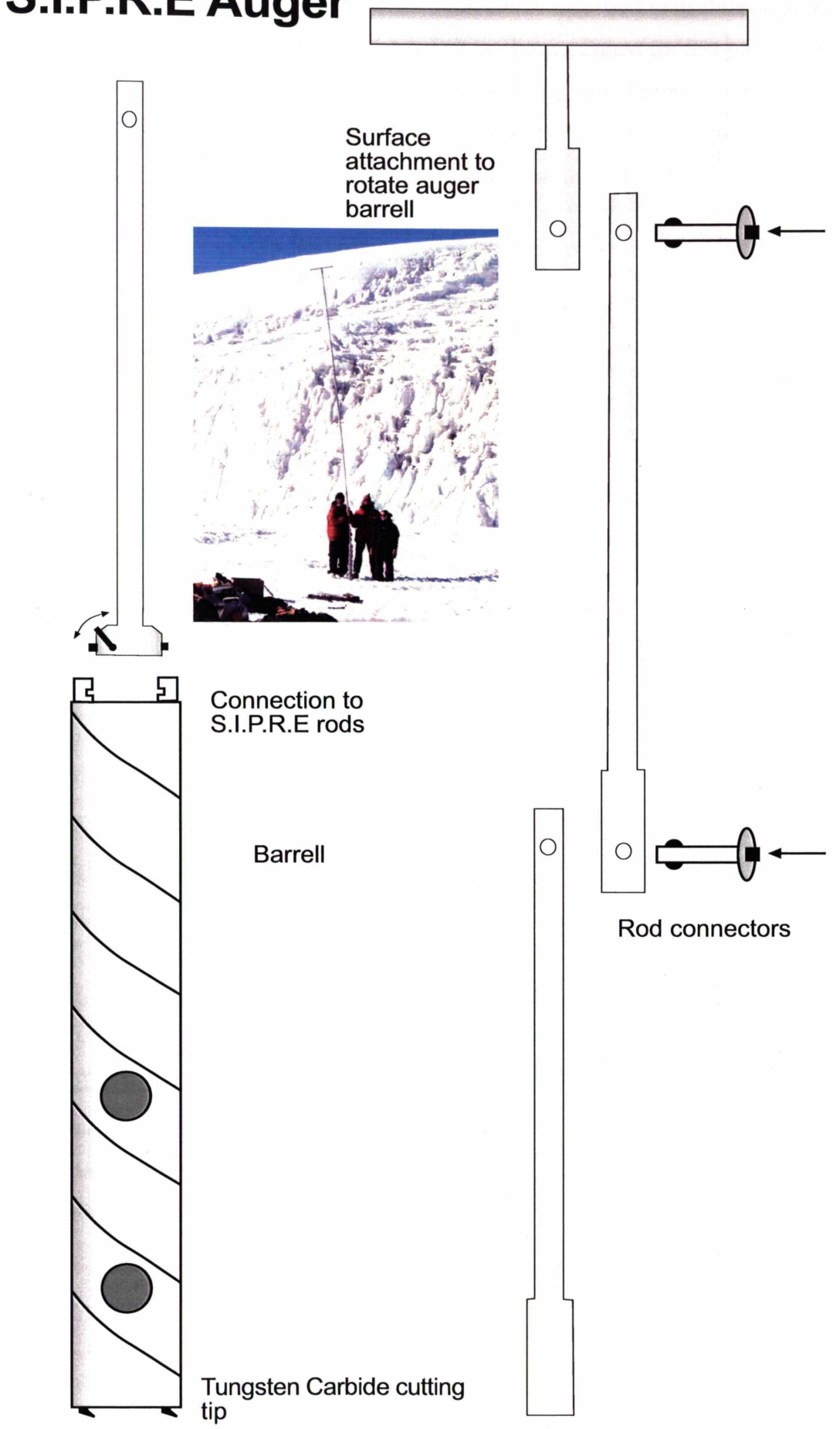

Figure 15: S.I.P.R.E auger equipment used to bore through the floating ice cover

It is worthy of note that this type of drill is not commonly used to drill through the 5m of ice common to the Dry Valley lakes, it has been adapted for this purpose by the addition of further, thirty-six inch (91.5cm) corkscrew "flights" (Figure 14b) to the cutting flight, extending the penetratable distance. The limiting factor of this method is the ability to lift the flights and the engine out of the hole, the five or so meters is very heavy.

When drilling using the Jiffy® at least three people are required. Two people hold the drill straight as it cuts, the third clears the slush carried to the surface by the corkscrew. As the drill descends, and the engine approaches the ice surface, it is necessary to add the next flight, this is done by securing the flight in the hole with a SIPRE rod and removing the engine, the next flight is added, followed by the engine. Cutting continues.

Each method had its pros and cons. The Jiffy® was the preferred method, as the larger diameter hole provided more flexibility when retrieving the equipment through the ice (often the coring process would bend and bow the joints, making it impossible to remove on one occasion, and very difficult on others). Also, the SIPRE required tungsten carbide cutting tips which proved to be very brittle and required replacing often. The SIPRE was also very susceptible to cold temperatures, the moving parts required for connection (Figure 15) would freeze and need to be thawed. Despite the SIPRE corers drawbacks, it required less team members to operate, and in the interest of efficiency, the majority of holes were SIPRE augered. The first hole each day would be drilled by the whole team, with the Jiffy®, followed by the erection of the tripod and set-up of coring equipment, then the "boring" team (as they affectionately called themselves) would continue to the next site and drill.

3.3.3 Coring procedure

When the ice has been penetrated, a weight secured to a measuring tape was used to measure depth, which was recorded along with the GPS coordinates. A five meter tripod was then erected with the apex directly above the hole (Figure 16).

Two ropes (braided not twisted, the strain on the ropes can stretch them causing twisted ropes to tangle easily) and a wire are threaded from reels, through pulleys at the apex of the tripod and connected to the coring equipment.

The coring equipment, an adaptation of a Livingston corer (Livingston 1965; Wright 1967) was assembled according to Figure 16 with the oblong rod extended and contained in the blind channel (A decision was made regarding core retention, section 3.3.4). The equipment was suspended by the rope attached to the guide rod, from the apex of the tripod and lowered into the hole via a team member who secures the rope under foot, allowing it to slip gradually (Figure 17).

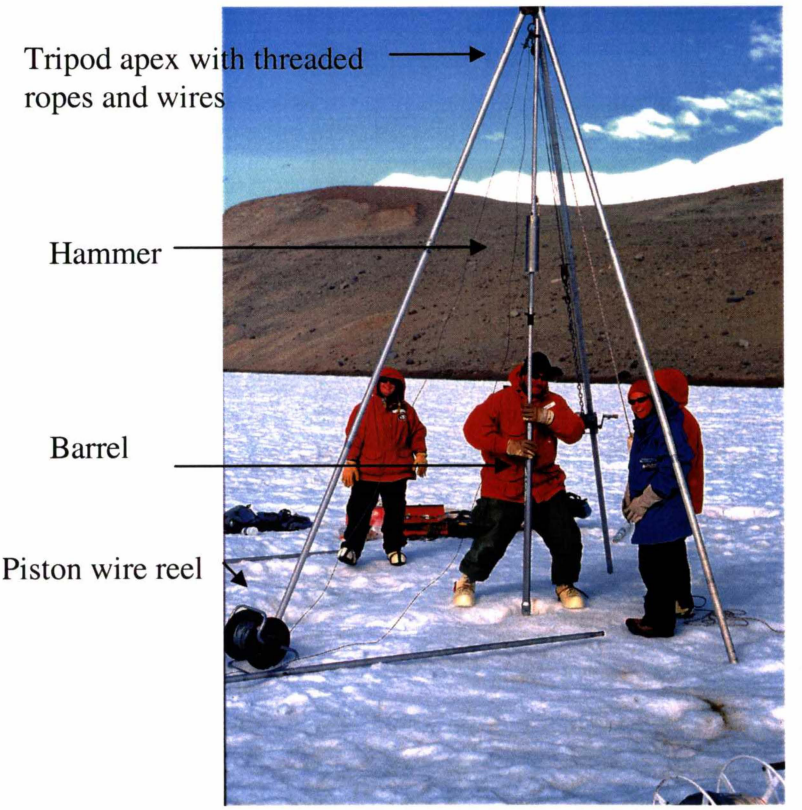

Figure 17: Assembled coring equipment about to be lowered into the lake.

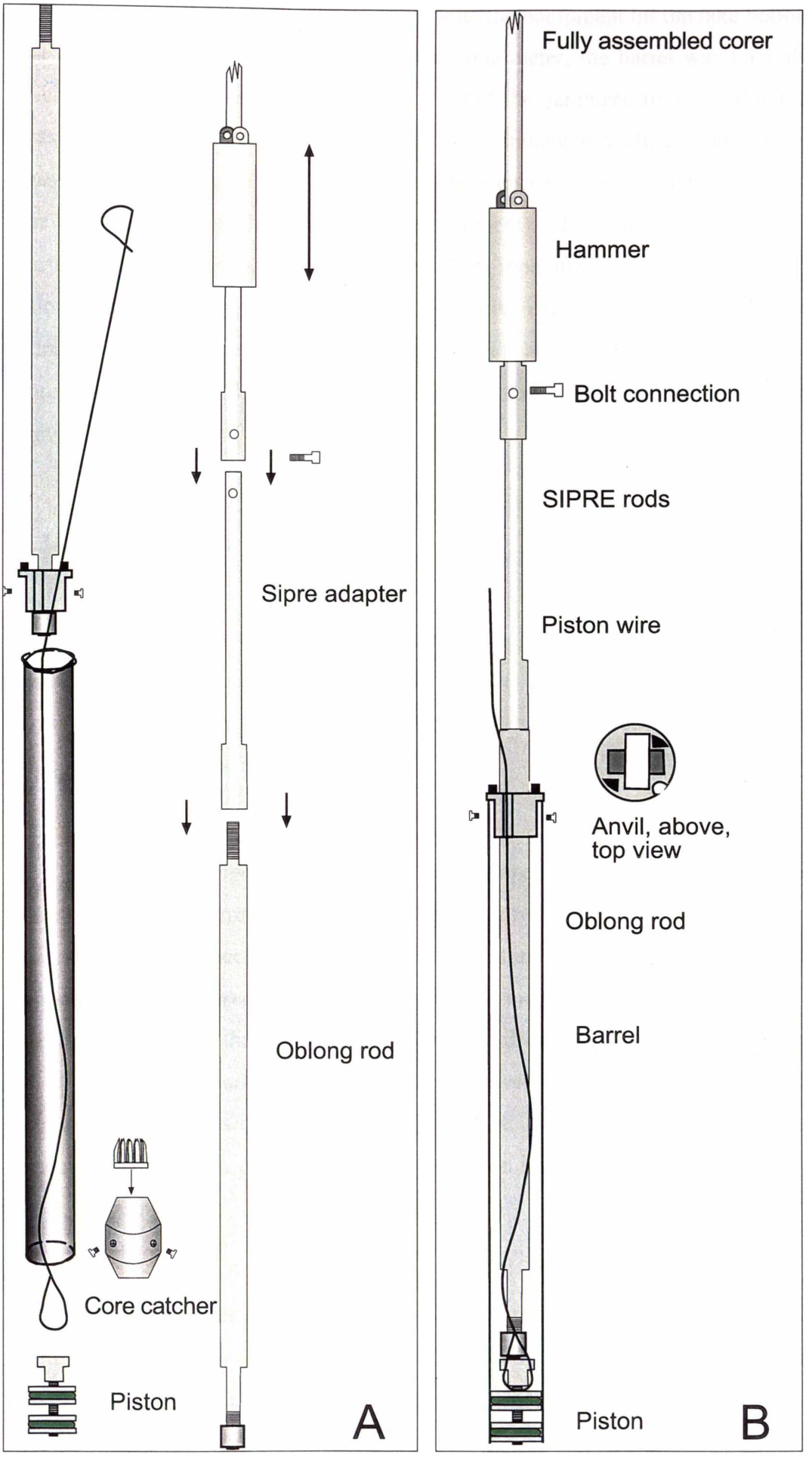

Figure 16a: Complete coring equipment; the constituent parts and how they are connected.
b: The set-up for taking a 2nd metre of core

When the person lowering the equipment "felt" the equipment hit the lake bottom, the 20kg hammer was raised approximately one meter, the barrel was then also slightly raised (without supporting the weight of the hammer); re-lowered until it was just above the bottom (this ensures the equipment is vertical) and the rope was secured under foot (note was taken of a reference marker on the rope to assess the distance the corer has gone into the sediment). The hammer was raised a further meter, and dropped onto the anvil. The rope attached to the guide rod is allowed to slip under foot, and the barrel is driven into the sediment with each hammer impact (Figure 18). The hammer is repeatedly dropped onto the anvil forcing the barrel further into the sediment until the 1.2m barrel length has been travelled.

3.3.4 Core retention

The retention of the sediment in the core poses a significant challenge, well sorted sands fall out easily, and a number of core attempts were made before a successful core was retrieved (Appendix 1 details the methods for each core). Two methods of core retention were available;

1. Piston (Figure 16). A wire trace, looped at both ends, was threaded through the core barrel and a notch cut in the anvil (Figure 16), the piston was connected to the trace and inserted into the bottom end of the barrel, while the opposing end was shackled to the wire reel (this method requires an extra wire to the bottom). When the equipment is about to be driven, the piston wire is secured to a leg of the tripod with a chain clamp, therefore when driving, the piston remains stationary as the barrel moves beyond it. The piston therefore creates a vacuum in the barrel, once the corer is withdrawn from the lake bottom, aiding in core retention.

2. Core catcher (Figure 16). The core catcher is a device mounted on the cutting end of the barrel. As the sediment passes into the barrel the "fingers" are forced apart, when the core is extracted from the sediment, the fingers close due to the downward force, retaining the material. Lake Bonney sediments proved very

difficult to recover. The halite and sands ripped the fingers off, the core catchers, and the piston was unsuccessful, so two team members created a more sturdy core catcher from olive tins at Bonney Hut (Figure 18).

Figure 18a: Team members Aaron and Amber making core catchers, b. the result

The nature of the sediment determined the method of core retention, the piston method is best used with soft sediments as it reduced core disruption and preserved the stratigraphy, while the core catcher was suited to well sorted sands.

3.3.5 Core extraction from sediment

- A wire from the winch secured to a leg of the tripod, was also threaded through a pulley at the apex of the tripod, a hook on the end of the wire was lowered as far as it could extend.

- A Figure eight knot was tied in the rope attached to the coring equipment, creating a loop over the hook from the winch

- The winch was wound in, extracting the corer from the sediment. When the corer was free from the sediment the equipment was pulled to the surface manually.

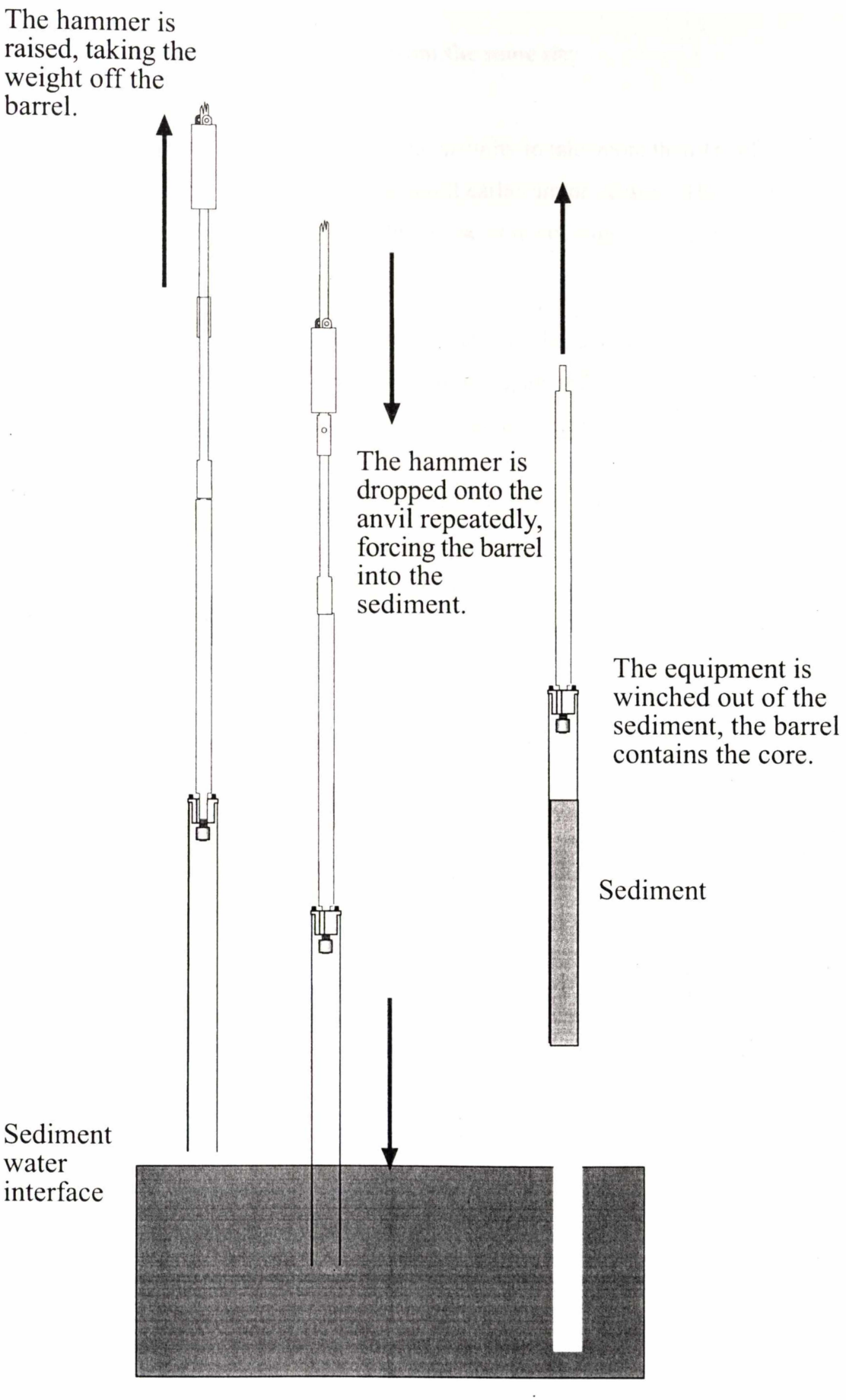

Figure 19: Steps in the coring process

3.3.6 Taking a second meter of core from the same site

The main limitation of the equipment is the inability to take more than 1m of core, as the only 3m barrel was lost in Lake Fryxell earlier in the season. The corer we took was designed to overcome this with the use of the oblong rod (Figure 16b).

The oblong rod slides through the sleeve in the corer head, and can be contained within the barrel, butting up against the piston (Figure 16B). When driving with the equipment set up in this way, no material can enter the barrel, as the piston is forced to remain at the end. When the desired depth has been reached, coring begins by first raising the oblong rod, and twisting it 90° to the right, allowing it to slide into another, blind, oblong slot. The oblong rod is no longer in the barrel and the piston is free to move. The piston wire is secured to the tripod, and further driving continues.

Lake Bonney could not be cored by this method, as it requires a rod connection to the surface in order to rotate the oblong rod, Lake Bonney is too deep and was cored remotely using the rope method.

We were however, enslaved to the oblong rod set-up, as the connection of the barrel to the SIPRE rods required the oblong rod, no connection could be made without it, providing the main weakness of the technique. The oblong rod; thin and able to be easily bent, but indispensable. After several times straightening the oblong rod, it was decided we required its removal, so we contacted McMurdo station with the approximate measurements of a bolt which could replace the oblong rod, and thread into the SIPRE adapter (Figure 16). A number of bolts were dispatched by helicopter, and the replacement made. The improvement was immediate; driving from a lower position reduced the potential for bending equipment.

Taking a second meter of core at Lake Bonney required the re-entry of the hole made by the first core, which was attempted a number of times with limited success (Appendix 1).

3.3.7 Core extrusion packaging and labelling

When the equipment was returned to the surface, the barrel was disconnected and laid on a tarpaulin. If used, the core catcher was removed. The piston was always set at the top of the barrel to push the core out, and a 2m SIPRE rod butted against it in the top of the barrel (Figure 19). A "Prussic Loop" was tied around the barrel and a come-along winch hooked to the top of the SIPRE rod, and to the end of the Prussic Loop. The winch was wound in, effectively pulling the barrel towards the SIPRE rod, forcing the core out the bottom (Figure 19).

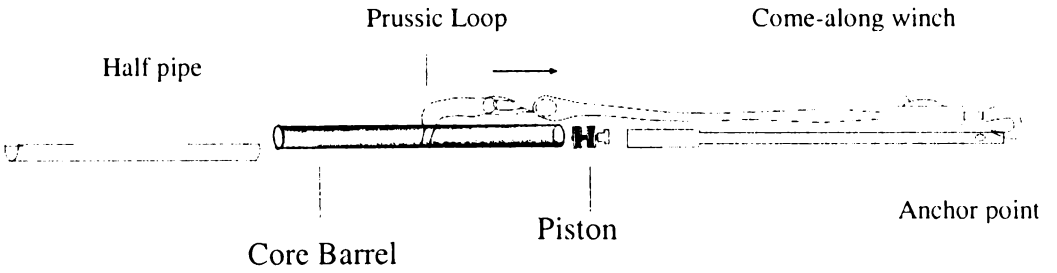

Figure 20: Core extrusion equipment

The core was caught in a PVC pipe that has been split in two lengthwise. When fully extruded the other half of the PVC pipe was placed on top and a piano wire dragged from end to end, cutting the core in half, it was then opened and split along the cut, leaving half the core in each pipe. A polystyrene bung was placed in each end and the core was photographed and described immediately, wrapped twice with plastic wrap, taped, capped and inserted into a plastic sleeve, to prevent dehydration. The core labelling code was:

- Season (0203)
- Hole - B #
- Thrust -T #

e.g. B4 = hole 4, T2 = 2nd thrust

3.4 Laboratory analysis

3.4.1 Equipment Preparation

3.4.1.1 Acid washing

All vials, bottles, ICP tubes and volumetric flasks to contain samples were first acid washed by the following procedure.

Acid strength

-1429 ml of 70% nitric acid was added to 8571.43 ml of distilled water to create 10 litres of 10% nitric acid.

Procedure

- The containers were fully immersed and left to soak in this acid at least overnight.
- The following day, the items were removed from the acid using rubber gloves, and placed into a distilled water bath. The items were removed and rinsed six times each with distilled water, before being left to dry (all items other than volumetric flasks were dried in a 40°C oven).

3.4.1.2 Weighing

All samples were weighed on the same Metler Toledo™ four place balance, F.3.12 analytical chemistry lab at Waikato University, and recorded to 4dp.

3.4.1.3 Dilution

Equipment

Eppendorf ™ autopipette. Volumetric flasks. Distilled water. Balance. Pipette tips.

Calibration

The autopipette was calibrated with distilled water on a two place balance. The desired volume was dialled on the pipette, this volume was then dispensed into a beaker on the two place balance. The dial was adjusted according to the result until the desired volume reproduced 5 times sequentially. A new tip was used for each sample.

The sample was dispensed directly into a volumetric flask which was filled to the mark.

3.4.2 Core sampling

The cores were each unwrapped (with only half being unwrapped fully), and laid on the bench. A tape measure was laid next to the core and photographs taken. Full descriptions of the samples are provided in Appendix 3.

3.4.2.1 Uranium – Thorium Sampling

These samples were taken first.

-The core was examined visually for carbonate plates or units. These were removed and placed into acid washed, labelled vials (core number and depth). Samples from evaporite sequences were taken at the top middle and bottom.

The samples were then sent to Oxford University England for analysis on a Nu-Plasma multi collector ICP-MS. Preparation of the samples was carried out by Dr Brenda Hall (University of Maine) and Dr Gideon Henderson (Oxford University).

3.4.2.2 Chemistry sampling

Sampling for the chemistry was initially done the same as for uranium-thorium dating, however it was later realized that the entire core had a carbonate coating, after I performed an "acid test" on some sand from a core. Further sampling was carried out by taking a sample of the sand as well as taking the carbonate plates. The vials were labelled with the core # and depth the sample came from.

The aim of this research was to trace the effect of changing climate on the hydrologic balance of the lake. Cold, dry climate results in ablation exceeding inflow, and a net loss to the lake, concentrating the waters. The changes in carbonate chemistry were expected to yield information on the evolution of the precipitating solution.

3.4.3 Sample Processing

3.4.3.1 Soluble sample extraction

In order to investigate the chemistry of the samples, it was first necessary to dissolve the carbonate. The carbonate samples are impure, and therefore cannot be simply weighed, dissolved and the chemistry reported as mg/g of the material dissolved[1].

The carbonate was dried, weighed, dissolved, filtered, and the remainder on the filter paper re-dried and re-weighed. The difference between the original dry weight and the remainder, is the amount of carbonate dissolved. The following details the process.

- The sample was placed into a labelled aluminium foil tray and dried at 60°C.

[1] The material analysed is therefore anything soluble in water or acid.

- A separate foil container for each sample, containing a Glass Fibre C (GFC) filter paper was also dried at 60°C.

- An amount of sample was weighed directly into a dry, acid washed 50ml volumetric flask, the weight is recorded to 4 decimal places. The dry GFC filters and foil trays are also weighed to 4 d.p., and recorded on the same line in the results sheet.

The first samples taken were only carbonate plates, therefore these plates are weighed. Later samples were divided into a sand fraction and a carbonate fraction from the same depth (if carbonate plates were large enough to be sampled separately), these samples were labelled, A-carbonate and B- sand.

- 5ml of 1M glacial acetic acid was added to each flask to dissolve the carbonate, the reaction was monitored, if fizzing stopped and carbonate was still visible, a further 2ml of acid was added. The reaction rate was increased for hard samples, by placing the flask into a beaker of tap water stirring on a hot plate. When the reaction was complete, and the carbonate sample has dissolved completely, the flask was filled to the 50ml mark.

3.4.3.2 Filtration

Equipment

Due to the accuracy required for the determination of the weight of carbonate dissolved from the complex sample matrix, I designed a specialized vacuum filtration unit which was created by the Waikato University engineering shop (Figure 21).

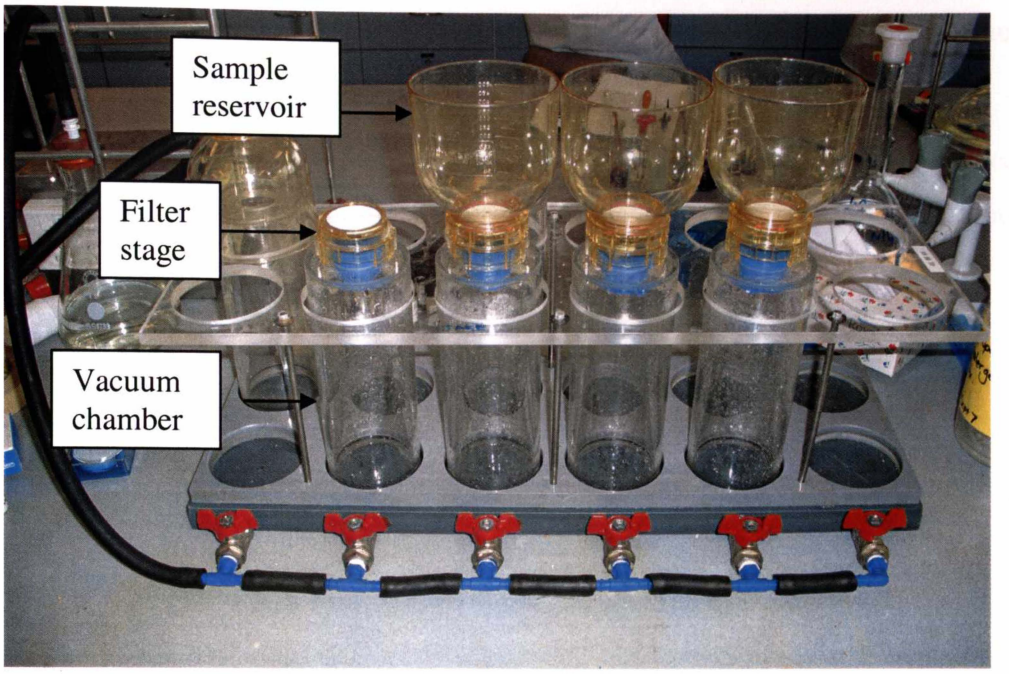

Figure 21: Vacuum filtration unit purpose built for this research.

Filtration Procedure (Instructional)

- Place a labelled, acid washed PVC sample bottle directly beneath the filter stage's spout in the vacuum chamber.
- Place a 0.45µm cellulose acetate filter on the filter stage, place the dried GFC on top, and secure the reservoir in position.
- Pour the sample into the reservoir and apply the vacuum.
- When the sample has finished filtering, rinse the volumetric flask with distilled water to ensure there are no particles left behind, and pour into the reservoir. Rinse the reservoir with distilled water to ensure that there are no particles stuck on the edge.
- Turn off the vacuum and remove the reservoir. Release the vacuum in the chamber by lifting the edge of the filter paper gently with tweezers. Separate the GFC and the membrane filter, return the GFC to the foil container it came from, and place in the 60°C oven.
- Remove the sample bottle from the vacuum chamber and cap.
- Two blanks are done for each run of samples to account for any loss from the filter paper. Also A Quality Control (AQC) samples is weighed. The

AQC revealed that less than 1% of the average sample was lost due to the filtration procedure (Appendix 4).

- When dry, the filter and tray are re-weighed, the difference between the original weight and that remaining on the filter paper is the amount of carbonate dissolved.

Weight of dissolved material = Weight of dry sample – Weight recovered

3.5 Analysis

3.5.1 $\delta^{13}C$ and $\delta^{18}O$

Isotope analysis requires the sample to be in the gas phase in order to be analysed by the Mass Spectrometer. The carbonate was reacted with 100% phosphoric acid, and the gas evolved collected and purified by the following procedure.

3.5.1.1 100% Phosphoric acid preparation.

It is necessary to produce CO_2 from carbonate without exchanging oxygen isotopes with the acid and without volatilising the acid. The only acid that can do this is 100% is phosphoric acid (H_3PO_4). It is made by evaporating the water contained in the acid by the following procedure.

This procedure was carried out in a fume cupboard using a rotary evaporator (Figure 22).

- Approximately 400ml of 70% H_3PO_4 is added to a rotary evaporator round bottom flask and lowered into the water bath.
- Water is flowed through the condenser, and the water bath set to 100°C with a constant supply of water. The rotary evaporator has a vacuum

applied, with a liquid nitrogen water trap between the pump and the rotary evaporator.

This process takes up to three weeks to complete, it is necessary to empty the water trap every day when the evaporation is started, and maintain liquid nitrogen in the trap for at least 10 days.

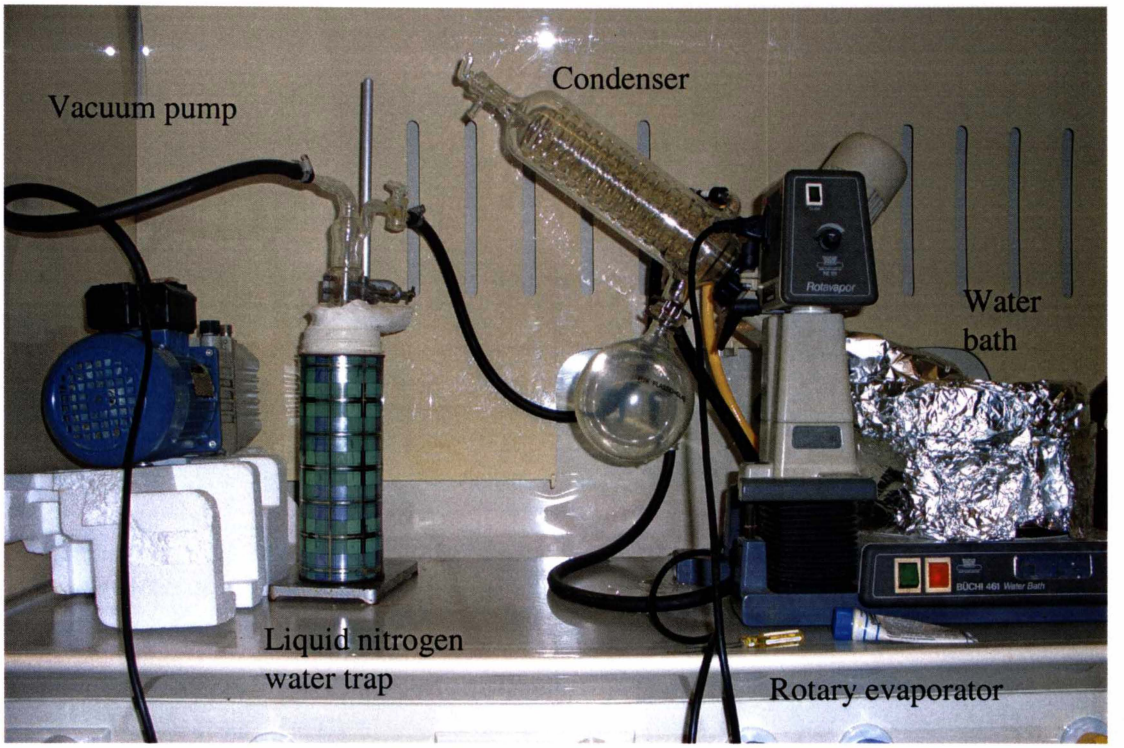

Figure 22: 100% phosphoric acid apparatus.

3.5.1.2 Off-line sample preparation.

This preparation was necessary due to a broken sample doser, rendering the on-line reaction process unavailable for quite some time. Later samples were done "on-line", the difference between the two techniques was investigated by selecting 7 samples analysed off-line, and repeating them on-line, the results indicate the on-line technique results in $\delta^{13}C$ values slightly lower than the on-line technique, and $\delta^{18}O$ values very similar. The results are reported in Appendix 4.

- A small amount of sample is added to a Rittenberg tube (Figure 21). A ml or so of 100% phosphoric acid is then placed into the arm of the Rittenberg tube using a special curved pipette.
- The tube is then greased and placed on a vacuum manifold to pump down, this is usually done overnight.

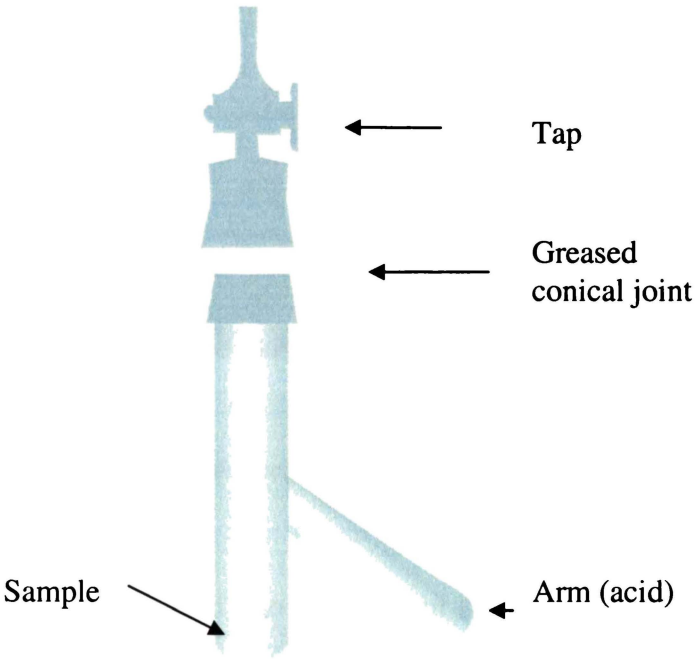

Figure 23: Rittenberg tube.

- The sample and acid are isolated by closing the tap.
- The tube is placed in a 70°C oven for 20 minutes, at which time the acid is introduced to the sample by tipping the tube, beginning the reaction.
- The tube is left for at least 30 minutes for the reaction to complete.

The Rittenberg tube is then connected to a vacuum line (Figure 22) to isolate the CO_2 evolved from the reaction.

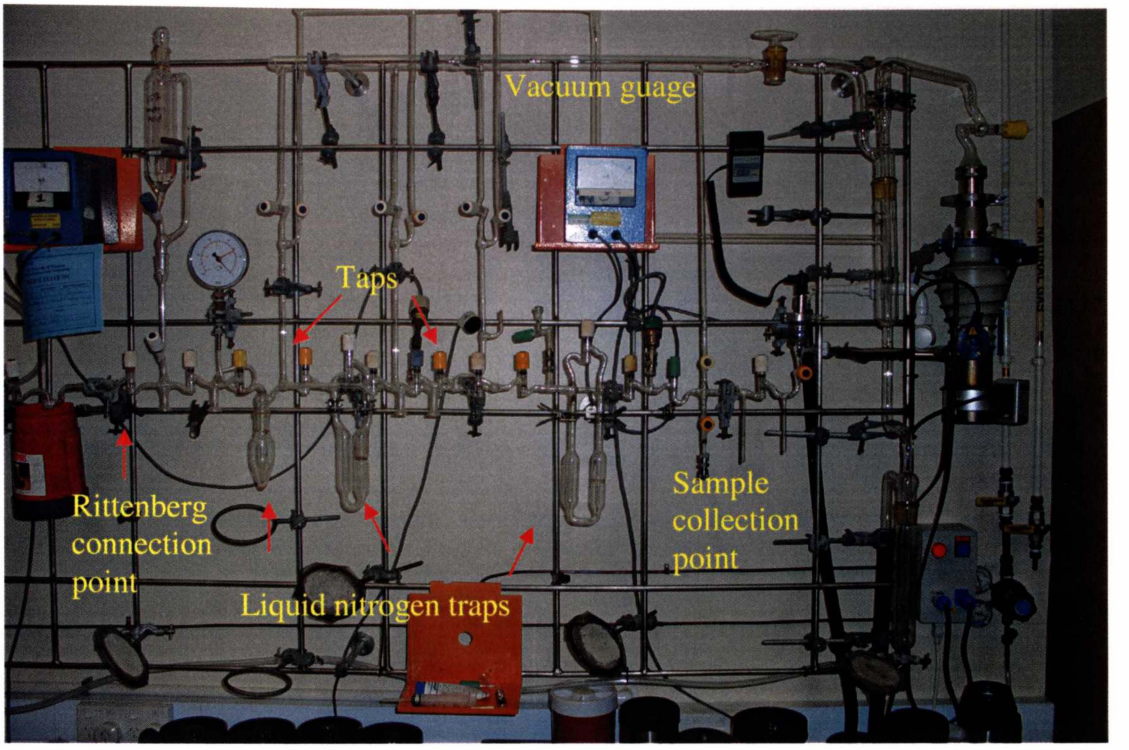

Figure 24: Vacuum line for the isolation of carbon dioxide.

The sample is introduced into the vacuum line, and the CO_2 gas is frozen in the liquid nitrogen traps. The sample is remobilized by replacing the liquid nitrogen with a mix of isopropyl alcohol and liquid nitrogen, which is at a lower temperature causing the CO_2 gas to sublime. The trap is still cold enough that any water vapour that may be present remains frozen. This process is repeated twice, and the gas is frozen into a labelled sample tube, ready for analysis. The exact procedure for vacuum line operation is outlined in Appendix 5.

3.5.1.3 "On Line" Technique

Samples are reacted in the Europa CAPS (Carbonate Automatic Preparation System) using the individual acid dosing or 'drip' method, in which a small amount of acid is allowed to drip onto the sample.

The samples are loaded into individual reaction vessels, which in turn are placed in a 24-position carousel. Each sample is analysed sequentially. The vessel is

evacuated and a predetermined dose of orthophosphoric (100%) acid is dispensed. While the sample reacts the evolved CO_2 is frozen onto a dedicated cold finger, positioned close to the mass spectrometer inlet, to minimise sample transfer time. Water is removed during the reaction by passing the CO_2 through a loop that is maintained at -90°C.

3.5.1.4 Mass Spectrometer conditions for Oxygen 18 and Carbon 13.

After the reaction is completed, the sample CO_2 is introduced to the Europa Geo 20-20 (directly for the on line technique, and via a manifold for the off line prepared samples), where gas pressures are balanced, and the sample gas run against an internal reference gas. This reference gas is calibrated daily by running an internal standard, WCS against it. WCS was calibrated against NBS-19, and cross-checked against NBS-20. External precision for replicate analyses of WCS is better than 0.05‰ for both carbon and oxygen.

Carbon 13 and oxygen 18 isotope values are presented in the delta (δ) notation, normalised, and expressed in per mille (‰), relative to Vienna Peedee belemnite, VPDB (Coplen 1988; Coplen 1994).

It was discovered that the mass spectrometer conditions would deteriorate when samples from lower in the core were analysed, yielding an unreliable result. After discussion, we concluded that NaCl contamination within the samples caused the evolution of HCl vapour, upon reaction with 100% orthophosphoric acid. All subsequent samples were pretreated via the following method.

3.5.1.5 Sample pre-treatment for isotope analysis

The sample is added to a 10ml centrifuge tube, crushed, and washed with distilled water. The sample is then filtered (Figure 19), dried at 60°C, and transferred to a labelled vial for analysis.

3.5.2 Atomic Absorption Spectroscopy (AAS) (Ca, Mg, Na, K)

3.5.2.1 Principle

Absorption mode (Ca, Mg, Na) Samples were aspirated directly into an air acetylene flame. A hollow cathode lamp individual to each element, provides a light source, which is passed through the flame, to a monochromator and finally to a detector. Each element absorbs, at specific wavelengths, the amount of light absorbed in the flame by the target element is proportional to the concentration of the target element in the sample. An expected concentration range was selected, and the corresponding wavelength for the target element was selected in the AAS software (Refer Appendix 6 for the specific instrument conditions for elements read).

Emission mode (K) Samples are aspirated in the flame, the element's energy state is elevated by the high flame temperature, and emits a wavelength of light following the return to ground state energy level. The concentration range available for emission mode is limited, but can be extended by optimising the burner angle, this was necessary to prevent time consuming and error introducing dilutions. The burner head was rotated ~ 20°.

3.5.2.2 Calibration curve

Calibration standards are made by dilution of a 1000ppm stock solution, and a calibration curve of the target element is constructed and used as a reference to determine the concentration in the sample.

3.5.2.3 Optimisation

The AAS must first be optimized for the target element before reading any samples. Optimisation was carried out in the following way (instructional)

- Light the machine and allow 10 minutes to stabilize.
- The flame must be approximately that required for the target element, and is either fuel lean, stoichiometric or fuel rich. Adjust the fuel to that required, and ensure the nebuliser is screwed all the way in.
- Select the element and wavelength to be read.
- Open the "FLAME" window in the software, and click "OPTIMIZE", an analogue gauge is displayed, and several options are available on the right.
- Introduce a distilled water "blank" to the nebuliser, click "PERFORM INSTRUMENT ZERO".
- Introduce the highest standard that will be used for calibration, view the analogue needle's response. If the absorbance is greater than two, the sample is too concentrated, and a new calibration range required, or a new wavelength should be selected (an ideal absorbance is one).
- Begin unscrewing the nebuliser while watching the analogue needle, there are two absorbance peaks affected by flow rate, stop unscrewing when the best absorbance is reached.
- Adjust the burner height and position. While viewing the analogue needle, move the burner in the X plane (forward and back), until the needle peaks. Repeat for the Y plane (up and down), again until it peaks. (ensure that when moving in the Y plane, the burner does not intersect the light path, this will give an erroneous peak).

At this point the AAS is optimized.

Enter the sample labels into the AAS software. Every 20 samples, the calibration standards are re-read as samples, this is to quantify instrument drift.

3.5.3 Inductively Coupled Plasma - Optical Emission Spectroscopy (ICP-OES) (Ca, Mg, Ba, Fe, Mn, U, Sr, S)

3.5.3.1 Principle

The excitation of the outer electron of a ground-state atom occurs as the sample travels through the different heating zones of the Argon plasma. When it arrives at the analytical zone of the plasma, at approximately 6000–7000 K, it exists as excited atoms and ions, representing the elemental composition of the sample. This excitation produces wavelength-specific photons of light, which are detected; their intensity is proportional to the amount of the element in the sample.

3.5.3.2 Optimisation

The 1000ppm stock standards were diluted to create calibration standards within the expected sample range. A number of wavelengths or "lines" are available for each element, having different sensitivity, and therefore range. Each high standard is run through the machine for a number of different lines, and the response is monitored on the trace, the ideal trace is a well defined peak that is not saturated (flat at the top) or base saturated (high signal to noise ratio). The line is selected (Appendix 6).

3.5.3.3 Calibration

The machine is calibrated by the same method as for AAS, by determining the instrument response for a known concentration of the target element. Standards are made by diluting a 1000ppm stock "soup" to the appropriate concentration.

3.5.4 Ion Specific Electrodes (Cl- and Br-)

3.5.4.1 Principle

Ion Selective Electrodes work on the basic principle of the galvanic cell (Meyerhoff and Opdycke). Measuring the electric potential generated across a membrane by "selected" ions, compared it to a reference electrode, the net charge is determined. The strength of this charge is directly proportional to the concentration of the selected ion.

The preferred techniques (AAS or ICP-OES), are unable to measure Cl^- and Br^- (bromine is too far in the ultra violet and requires a special filter attachment to the ICP, which we do not have), and so ion specific electrodes were chosen, as the alternative methods (mohr titration-Cl^- and bromine precipitation –Br^-) are destructive and require pH control.

3.5.4.2 Equipment required

100ml measuring cylinder. 2X 120ml Plastic beaker. 1ml & 10ml volumetric pipettes. Distilled water supply. Magnetic stirring plate and magnetic flea. 1000ppm Cl^- and Br^- solutions (Supplied by manufacturer of electrode). 1.3M KNO_3 ionic strength adjustment buffer. Cl- and Br- (Orion 94-35) electrodes and filling solutions. Orion 520A pH/mv meter. Vortex mixer.

3.5.4.3 Slope calculation

The electrode is prepared according to the manufacturers instructions prior to the first use(Thermo 2003). It is essential that the electrode response is determined prior to any analysis.

- Connect electrode to meter, set to read mv.
- Measure 100ml distilled water and pour into 120ml beaker.
- Place the beaker on the stirring plate and add the stirring flea, set stirring gently.
- Place the electrode in the distilled water so it is approximately half way.
- Add 2ml $NaNO_3$ leave to stir for a few seconds.
- Pipette 1ml of 1000ppm Cl^- into the beaker, allow the meter to stabilise and record value (mv).
- Pipette 10ml of 1000ppm Cl- solution into beaker, record value.

Calculate the electrode slope by subtracting the 1ml value from the 10ml value. This value must be 56±2mv for correct electrode operation. See electrode manufacturers troubleshooting guide if slope is outside the range.

3.5.4.4 Sample measurement

Place the electrode into the sample bottles, ensuring the tip is covered. To stir, place the sample bottle (with electrode inserted) onto a gently rotating vortex mixer. When the reading stabilises, indicated by a "beep" and the display reading "READ", record the value in millivolts (mv).

3.5.4.5 Calibration curve

Dilute the 1000ppm manufacturers Cl- stock solutions with 1.3mol/l KNO_3 to:

Cl^- -500ppm, 250ppm, 100ppm, 50ppm and 25ppm

Dilute the 1000ppm manufacturers Br- stock by 4 sequentially

Br^- - 62.5, 15.63, 3.93, 0.4885

Place these solutions into labelled, acid washed polythene sample bottles. Read each standard according to the process above.

The data are plotted on a logarithmic scale, and the equation of the line of best fit is used to calculate the sample concentrations.

The calibration curve is repeated every 15 samples to assess electrode drift, and the slope measurement is repeated at the end of the run, to determine if the electrode has behaved acceptably throughout the analysis.

It was discovered that the chloride electrode drifted substantially, and the slope was not acceptable at the end of a run, particularly after samples of high concentration (>250ppm) were analysed, these results were discarded. Upon investigation, a black precipitate had formed on the electrode surface. The electrode was treated with 10% Nitric acid for half an hour, polished with the supplied polishing strip, and the slope calculation repeated, this yielded an acceptable result.

The samples of high concentration were diluted by four times with 1.3M KNO_3, and repeated.

The precipitation on the surface of the chloride electrode continued, and the drift was severe at times. To assess this method, a comparison was made between data obtained via the electrode, and data from a Mohr titration (Eaton *et al.* 1995). The electrode differed substantially across a series of 10 samples. After discussion with my professor I concluded that interference existed in the samples that could not be overcome. I could not make comparison tests for the bromine analysis. For these reasons, the decision was made to discontinue the ion specific electrode studies.

3.5.5 Scanning electron microscope (SEM)

3.5.5.1 Principle

Electrons are scanned across the target and reflect onto a fluorescent screen where the image is captured by a camera and enlarged. Because electrons are much smaller than atoms, a scanning electron microscope creates an extremely sharp image of the target. The picture however, has no true colours, just black and white. The electron beam of the SEM causes atoms in the field of view to emit x-rays, the energy of which is characteristic of the emitting element. These x-rays can be detected using the, "energy dispersive X-ray microanalysis" (EDX) detector to identify the target composition. This facility can be used to qualitatively identify a wide range of elements.

3.5.5.2 Equipment

The Electron Microscope Facility is a Hitachi S-4100 Field Emission Scanning Electron Microscope with X-ray analyser. It is used for investigating structure at high magnifications and determining elemental composition of small samples.

3.5.5.3 Sample selection

Samples of the carbonate were selected for SEM analysis based on their position in the core, texture and size. The evaporite sequence in B4T1 was chosen to investigate changing crystal growth conditions through this major event.

3.5.5.4 Sample preparation

A small mounting stub was first covered with double sided tape, and a representative portion of the sample placed on top. The stub is then placed in a Hitachi Sputter (Platinum) Coater. The chamber is pumped to high vacuum and a

potential applied between a platinum plate and a cathode. This strips platinum from the plate, coating the sample, providing the conductive surface required for the analysis.

The sample stub is then screwed onto the mounting plate, and introduced into the sample chamber where it can be navigated by moving the sample stage in the X plane, changing which part of the sample is in the electron beam.

Images were taken by slowing the image capture rate of the machine, and synchronously pressing the capture buttons on the capture computer and export computer. EDX traces (elemental composition) were captured using a separate computer and taken of areas of interest in the sample.

3.5.6 X-Ray crystallography

During sample processing of B5T1 crystals were found, much the same as the algae was found in B7T1. The crystal, whatever it was, must have been growing at the same time the carbonate was forming.

The unidentified crystal was sent to Dr. T. Groutso and Professor G. Clark, at the University of Auckland, for X-ray data collection.

Data were collected on a Siemens SMART CCD diffractometer using standard procedures and software (Smart and Saint 1996). Empirical absorption corrections were applied(Blessing 1995). Structures were solved by direct methods and developed and refined on F^2 routinely using the SHELX programmes (Sheldrick 1997). All non-hydrogen atoms were refined anisotropically, while H atoms were located and refined with isotropic temperature factors.

3.6 Result manipulation, quality control and error quantification

The results provided by the AAS and ICP were scrutinized for reproducibility and instrument drift.

3.6.1 AAS – Drift

Calibration standards were run as samples approximately every 10^{th} sample (or as required).

The result file was exported from the instrument as a text file, and imported into Microsoft Excel ™. In Excel, the initial calibration data were plotted, and the R^2 and equation displayed on the chart. On the same graph, the successive calibration standards (run as samples) were also plotted, if the change was substantial (an obvious deviation, line not straight), the data following, and the data immediately preceding (up to the last acceptable calibration) were discarded and the samples were repeated.

Instrument drift was generally attributed to flow changes in the sample introduction tube and nebuliser. An unidentified white "cotton like" substance was found in some of the samples, I later discovered that a fungus was known to grow in dilute acetic acid as it aged, SEM confirmed the presence of fungal hyphae. The samples containing the blockage causing fungus were centrifuged to remove it, this was unsuccessful as the density was not sufficient to separate it from the sample. A plastic Pasteur pipette was used to suck the material out of the sample. The West Lobe gypsum samples (1^{st} 20cm) also proved difficult to analyse, colloidal gypsum was present which crystallized in the jaws of the burner altering flow rate. To overcome this, the samples were diluted, however, the dilution factor required to remove the colloidal gypsum exceeded the lower instrumental limits for Na and K, and these were unable to be analysed.

If the successive calibration standards were within an acceptable deviation, indicating the instrument response was not affected by sample injection changes, the equation was used to re-calculate the sample concentration, and accepted as the most accurate concentration (Appendix 4)

A reproducibility error of ~2% was determined.

3.6.2 Quality Assurance

As the process of data collection continued, and ICP instrument failures (blocked nebuliser, blank and standard contamination etc) wasted sample, it became important to conserve the remaining sample. Ca and Mg data were outstanding for a number of cores, but insufficient sample remained to run undiluted through the ICP. It was decided to dilute by a factor of 100 (to within the AAS operating range) and run the samples on the AAS. To account for any difference between the two techniques, samples successfully analysed on the ICP were selected to be re-run by AAS (Appendix 4).

A maximum discrepancy of ~5% was found between the two techniques.

External reference standards were run as samples as (Leng and Marshall 2004)a quality assurance measure.

A 1000ppm stock "soup" was diluted to within the operating range of the element being analysed and measured on both the ICP and the AA (Appendix 4).

Chapter 4

Results

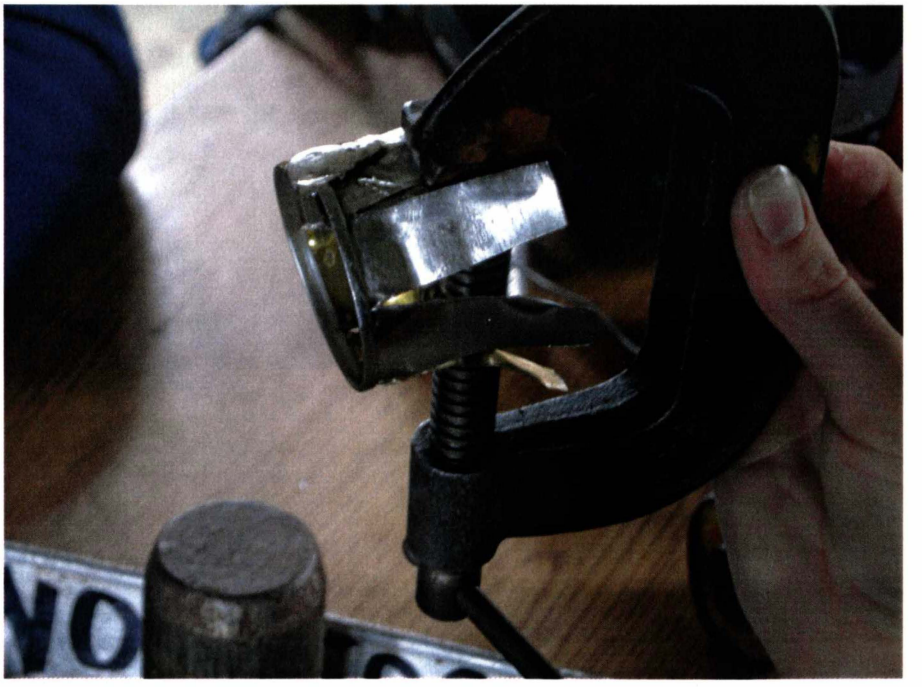

Making replacement "core catchers" from olive tins, at Bonney Hut, Taylor Valley, Antarctica.

4.1 Introduction

Sediment cores were taken from Lake Bonney in order to determine depositional responses to lake volume, caused by local climate change. Lake Bonney was known to contain evaporite minerals in the sediment (Craig *et al.* 1974; Nakai 1974; Hendy *et al.* 1977; Matsubaya *et al.* 1979) and was speculated to contain further preserved evaporite minerals. These sediments would contribute to the history of the lake by providing inferences to climate, affecting lake water balance.

The cores were first examined visually and described, then sub-sampled for carbonate. Samples were selected for SEM analysis based on their perceived importance; evaporite sequences, large plates, potentially correlateable features, odd colours *etc,* and all were analysed for isotope ratios of oxygen and carbon and their chemistry. Core B4T1's evaporite sequence was also photographed by light microscope as it was the most well preserved.

This chapter is set out as follows.

-Coring results

-Visual properties and descriptions (microscope) followed directly by the chemistry and isotope data of each core.

The data will be discussed in the following chapter. See Appendix 6 for full descriptions of samples taken for analysis.

4.2 Coring results

Appendix 1 details the coring method adopted for each core.

4.2.1 East Lobe

We began coring in the middle of the East Lobe, at what we believed to be the deepest point, recorded the depth as 38.8m, and used the piston method to core to 1m (B1T4). The first 3 thrusts were unsuccessful; we were unable to recover the sediment, as it was very sandy and was not held in by the piston vacuum, also something hard stopped the barrel damaging the end, we decided to switch to the core catcher as well as the piston, and recovered a successful core (Figure 25). Only ~30cm (Figure 25) of sediment was recovered, also we hit something hard at 1m depth during the coring and bent the core barrel.

We tracked westward on the lake, and drilled another hole through the ice (B2T1), at this site we lowered the hammer to the bottom first, raising and lowering it to smash the halite playa to make it easier to core through, this proved unsuccessful, and we were unable to recover any material. The halite player was destroying the core catchers, by ripping off the fingers as it was forced into the barrel. Two team members went back to Bonney Hut to manufacture new core catchers using empty olive cans (Figure 18).

The third hole (B3T1) was closer to the shore on the Bonney Hut side of the Lake, to get above the halite playa causing us problems, this core was 29m deep, and was successful. At this site we attempted to take a second meter of core by re-locating the hole (as set out in methods chapter), we appeared to drive 1.2m, but recovered very little material (B3T2). A second attempt was made to core deeper, failing also, before a successful third attempt recovered 47cm of sediment (B3T3). This core appeared disturbed and I noted that the previous attempts may have disturbed the hole. We attempted to gain a third meter of core, and recovered 45cm of visibly disturbed

material (B3T4).

After B3, we tracked towards the middle of the lake on a line perpendicular to the shore, and drilled a fourth hole. B4T1 had 29.9m of water depth, and we recovered 77cm of core, the best core up to that point. An attempt to get a second meter of core was unsuccessful, and we recovered minimal material. I noted that we may have penetrated a layer of hydrohalite, similar to that seen in B1T4, as the core "ran out".

Continuing the transect to the middle of the lake, we drilled a fifth hole (B5T1). At 33m this was the deepest successful core, recovering 88cm of sediment in the barrel, however, the core was running out, exaggerating the amount we recovered. I estimate that this core may only represent ~ 50cm.

4.2.2 West Lobe

We were due to relocate camp to the West Lobe, but were held up because of a helicopter crash down valley. We traversed our gear to the new camp site at the foot of the Taylor Glacier using a six-wheel All Terrain Vehicle, a snowmobile and two sledges.

Coring began in the middle of the lobe, at 41.1m water depth (B6T1), and recovered 43 cm of sediment, and a dented core catcher. We traversed a line from the snout of the glacier towards the shore near the neck of the lake (Figure 13).

B7T1 and B8T1 were at the site of a previous Polar Haven (structure) on the lake. Two holes were drilled at this site because we destroyed the first hole attempting to take a second metre of core.

B9T1 and B10T1 were shallower cores towards the neck between the two lobes.

The decision was made to analyse only B7T1, due to the lack of datable material in the cores and the perceived inability of the sediments to contribute to the climate history of the lake.

4.3 Core results

4.3.1 B1T4

We found approximately 20cm of Halite, followed directly by ~ 7cm of hydrohalite, which re-crystallised in front of us.

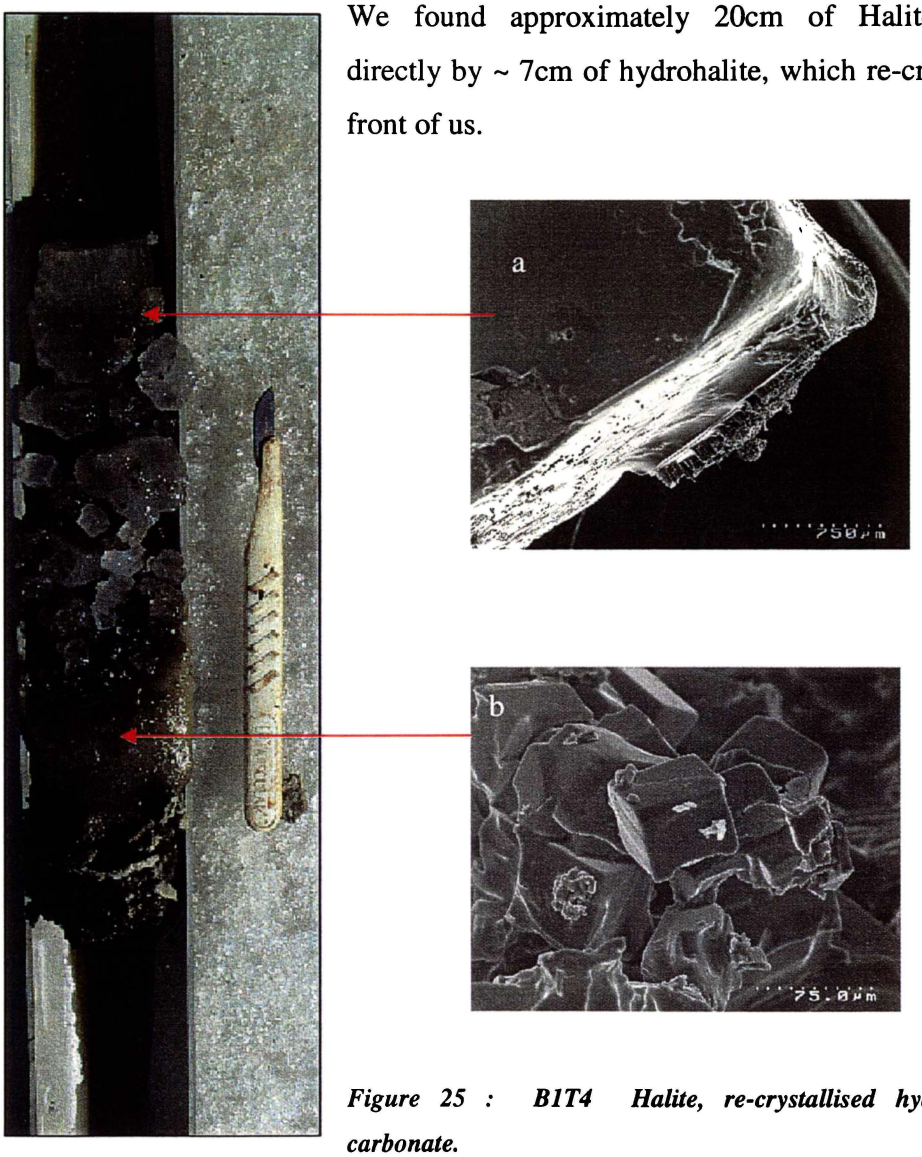

Figure 25 : B1T4 Halite, re-crystallised hydrohalite and carbonate.

The hydrohalite had been identified previously by (Craig *et al.* 1974).

4.3.2 B3T1 Stratigraphy and description

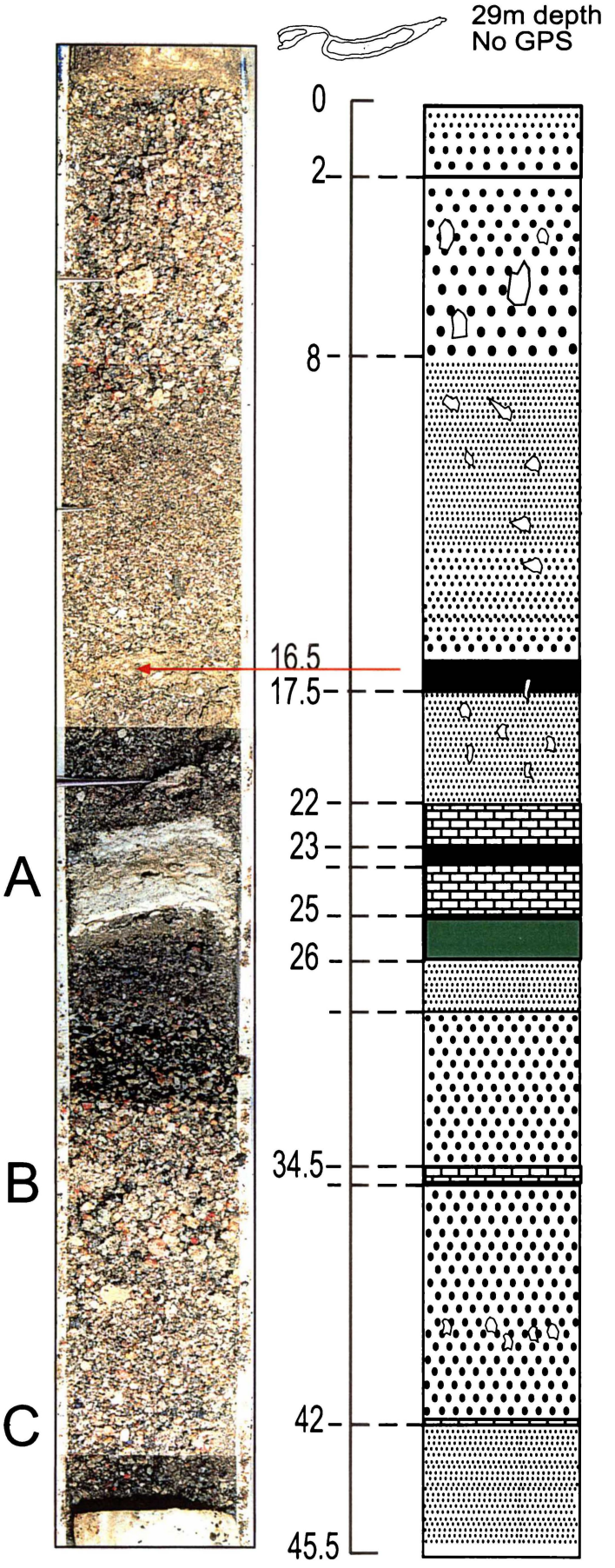

0-2cm	Sandy material grading into coarser sand
2-8cm	Grading to Coarser sand, containing few large carbonate plates.
8-14.5cm	Well defined boundary into fine sand containing small carbonate plates.
14.5-16.5cm	Grades to a coarser sand.
16.5-17.5cm	Soft, greeny material with what appears to be carbonate laminae
17.5-22cm	Fine sand containing carbonate biscuits (Small)
22-23cm	Carbonate layer, some laminations
23- 23.5cm	Soft green material
23.5- 26cm	Carbonate layer, parts very pure (white) and clean.
25- 26cm	Soft greeny material (gypsum)
26-28.5cm	Fine sand, distinct transition to coarser sand.
28.5-34.5cm	Coarse unsorted sand.
34.5- 35cm	Chunky carbonate layer
35-42cm	Coarse sand, carbonate
42.5cm	Carbonatae layer (thin).
42.5-45cm	Fine sand

Figure 26: B3T1. East Lobe. Visual core stratigraphy and description.

4.3.2 B3T1 Chemistry

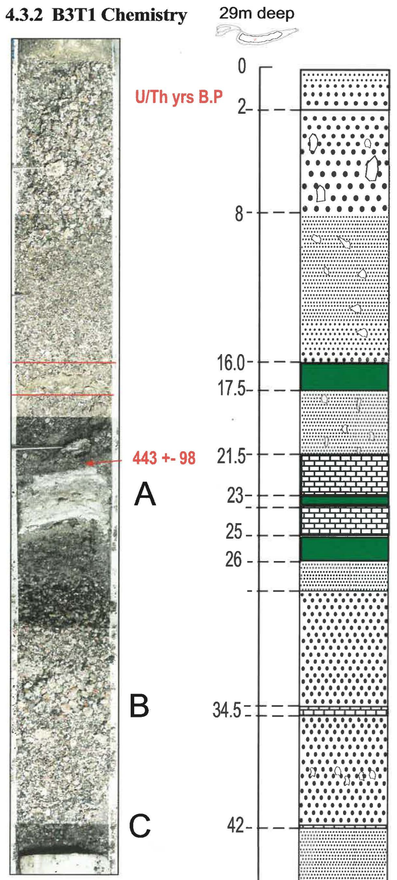

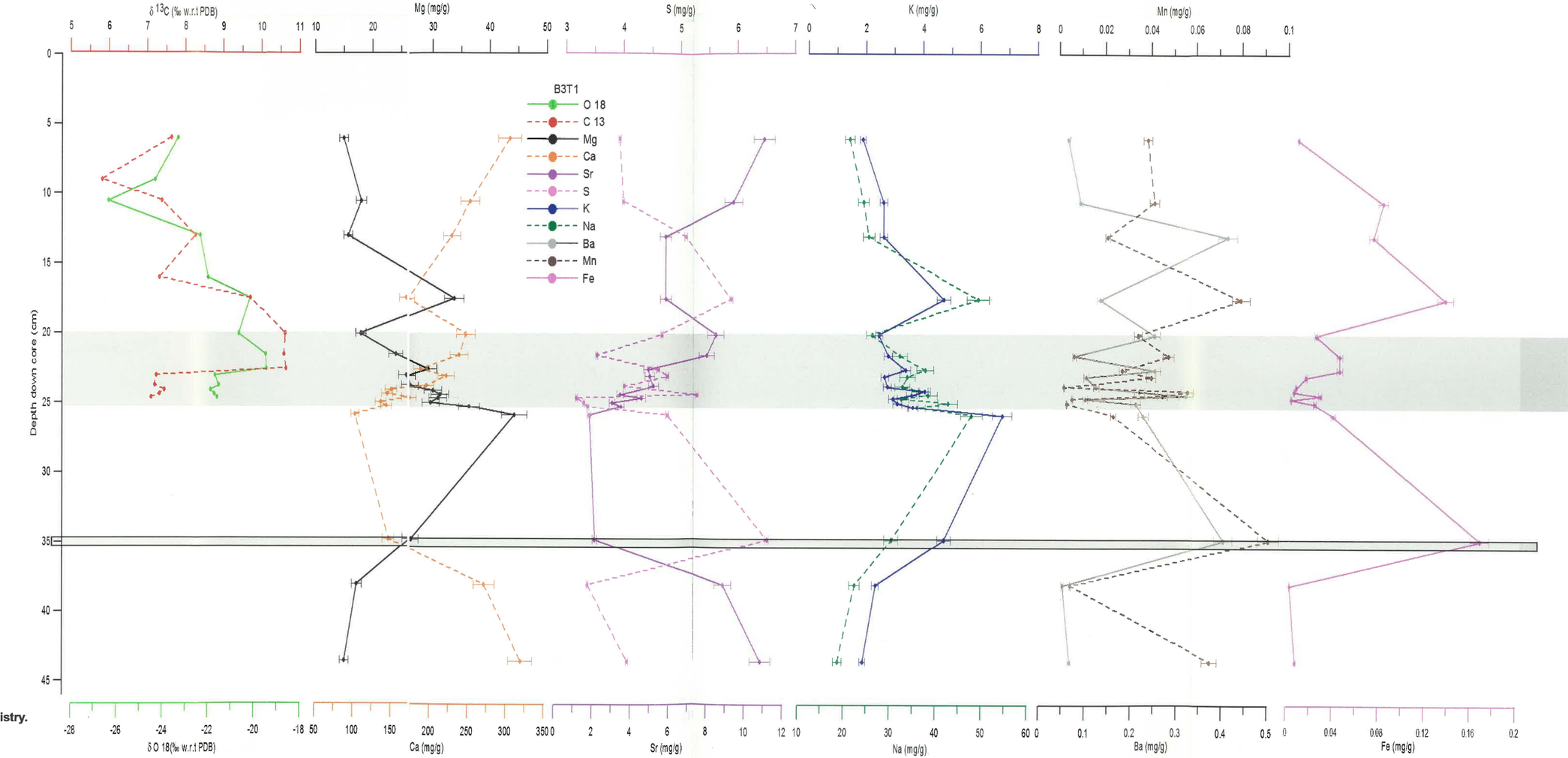

Figure 27: B3T1. East Lobe, 29m, Isotopes and chemistry.

4.3.3 B3T1 (Figure 26 and 27) Summary of core characteristics

B3T1 has three distinct carbonate units A, B and C.

Unit A is:

- Located between 21.5 and 25.5cm
- Thick (~5cm)
- Soft
- Pure and highly laminated
- U/Th dated at 443±98 yr B.P.
- Is flanked by biological material (above and below)

Unit A (from bottom to top) is initially characterised by:

- Enriched ^{18}O and ^{13}C
- A concurrent $\delta^{18}O$ (2‰) and $\delta^{13}C$ (~5‰) shift coincident with, or just after a thin layer of biological material in the unit
- Initially low but rising Fe and Mn
- Moderate falling Ba, Na
- Rapidly falling Mg in the beginning stages of the unit, and rising after
- Low S
- Rising Ca, Sr
- Coherency between; Mg, Na and K, Ca and Sr, Fe and Mn, Ba and S

Above unit A the isotopes of C and O co-vary becoming depleted. Na, K, Mg, S, Mn and Fe all peak coincident with a layer of biological material, and reduce coherently after.

Between unit B and C, there was insufficient carbonate for all analysis, isotopes were given priority, however NaCl contamination in the samples lead to the formation of HCl gas during the off-line preparation, inhibiting analysis by mass spectrometry, hence the lack of data below unit A.

Unit B is:

- Located between 34.5 and 35cm
- Thin ½ cm
- Chunky
- Hard
- As yet undated (Appendix)

Unit B is characterised by

- High Fe, Ba, Mn and S
- Coherency between Fe, Ba, Mn and S

Unit C is:

- Located between 41.5-42cm
- Thin ½ cm
- Chunky
- Hard

4.3.3 B3T3 core stratigraphy and description

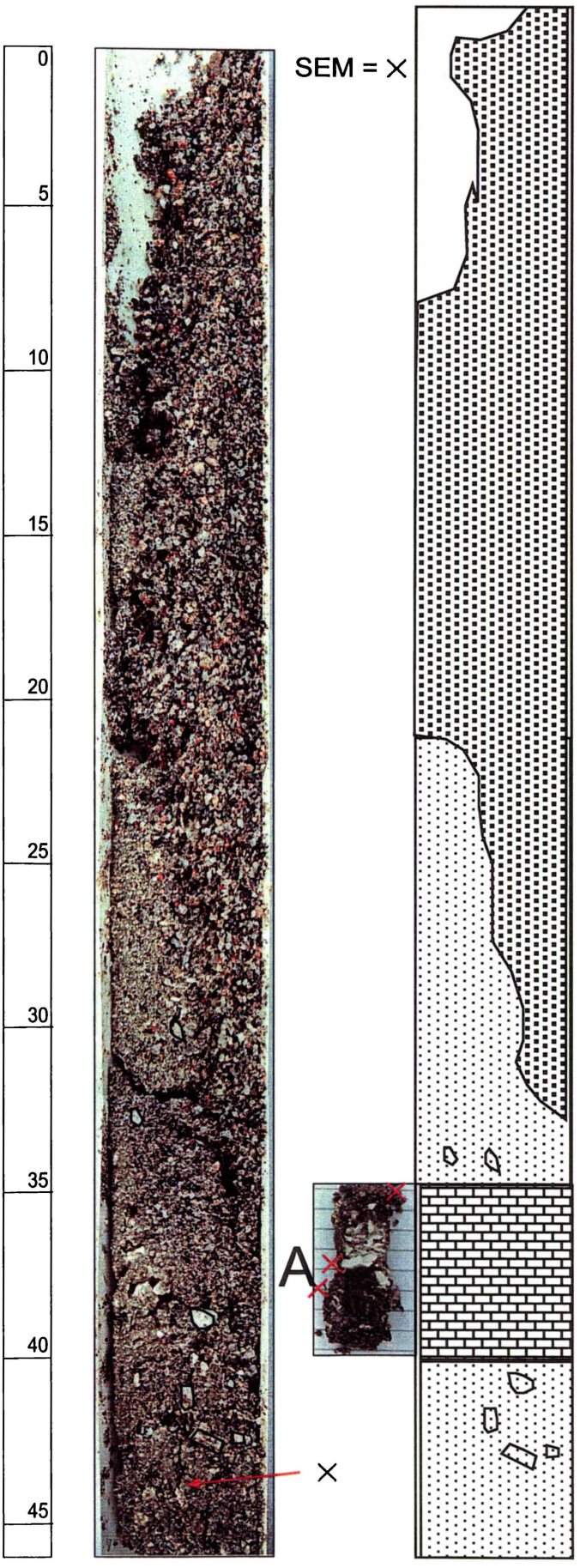

Figure 28: B3T3. East Lobe, core stratigraphy and description

4.3.3 B3T3 Unit A; Scanning Electron Microscope studies.

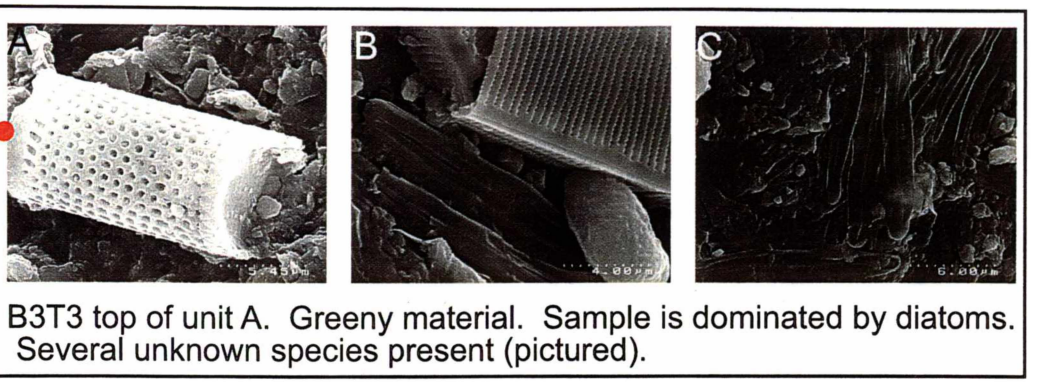

B3T3 top of unit A. Greeny material. Sample is dominated by diatoms. Several unknown species present (pictured).

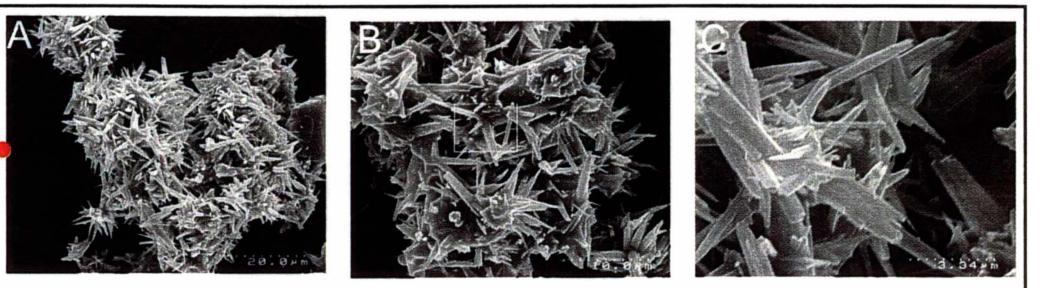

B3T3 37 cm in core. immediately above the unit A. Carbonate needles predominate.

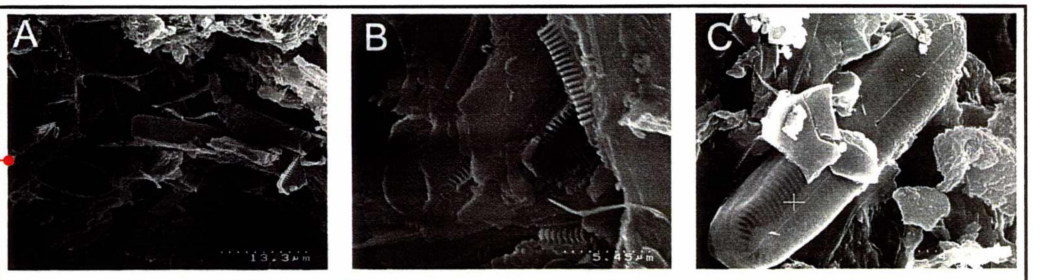

B3T3 4-4.5cm in unit. The Green material contained in the evaporite is dominated by diatoms.

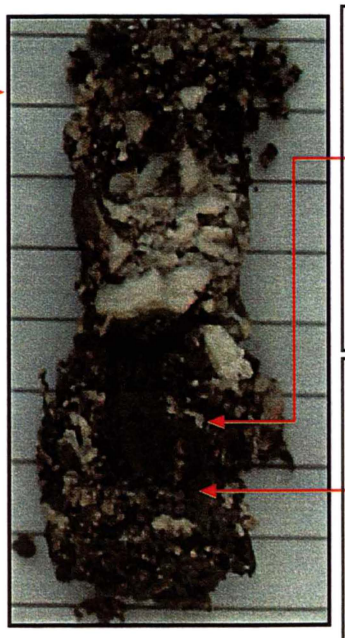

Close up of the B3T3 evaporite sequence before sampling

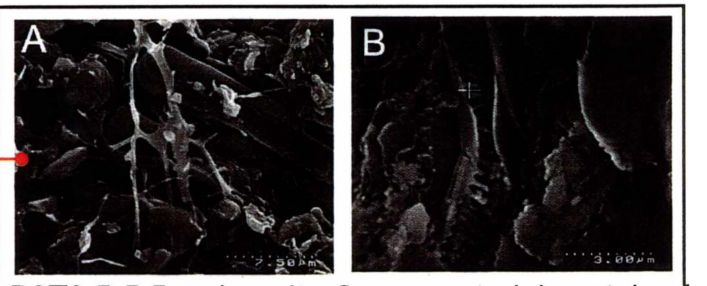

B3T3 5-5.5cm in unit. Green material contained in the evaporite is dominated by diatoms.

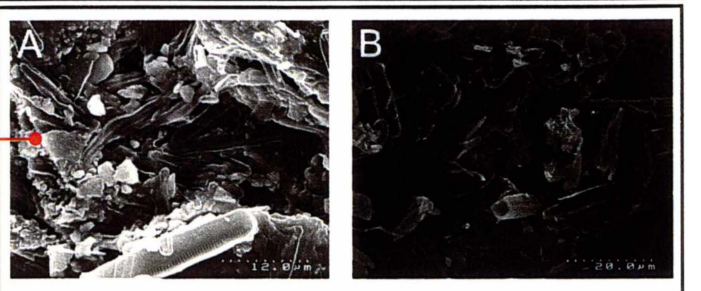

B3T3 43-44cm in core. Green material here is also dominated by diatoms.

B3T3 Hard carbonate from the bottom of the core. The Hard carbonate is dominated by needles, no diatoms are present.

Figure 29: B3T3 scanning electron microscope images of the material found above and below the carbonate unit, identified as unknown during sample processing (previous page), and the Hard carbonate found in the bottom of the core (unit B)

4.3.3 B3T3 chemistry

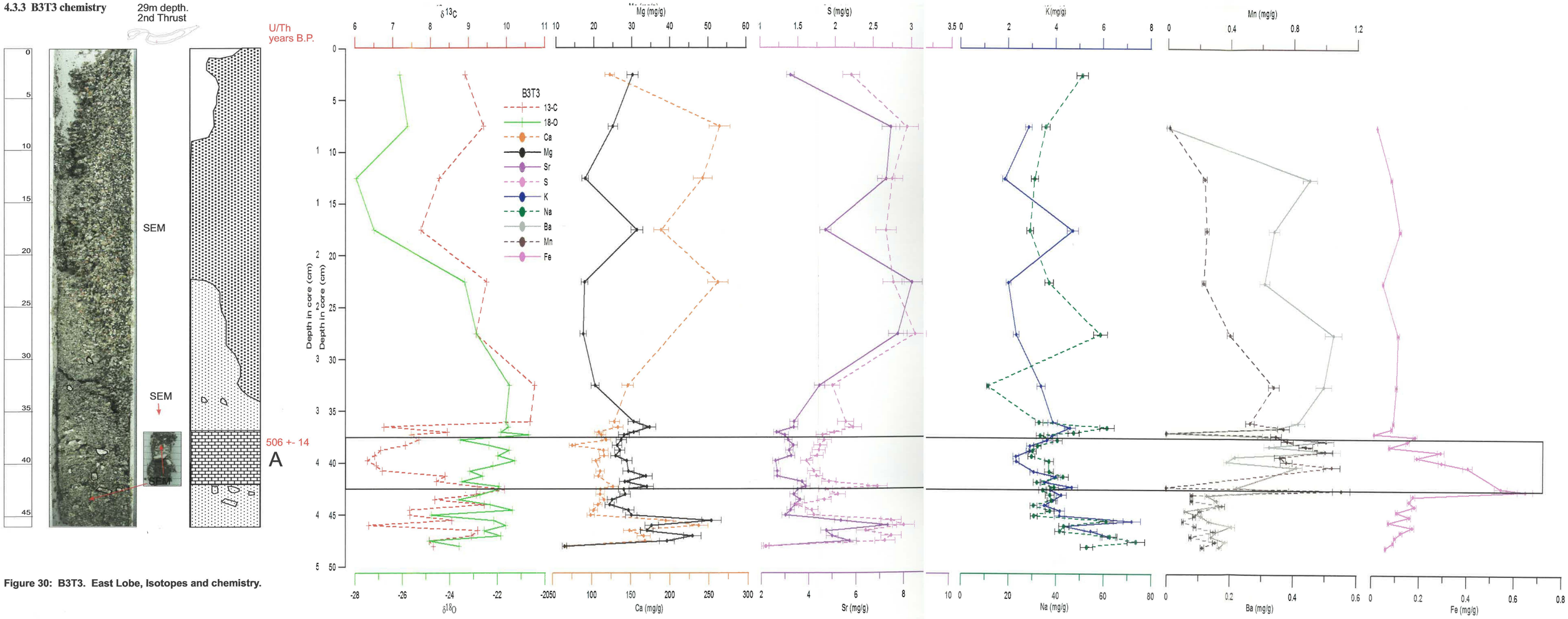

Figure 30: B3T3. East Lobe, Isotopes and chemistry.

4.3.4 B3T4 Core stratigraphy, visual description and SEM studies

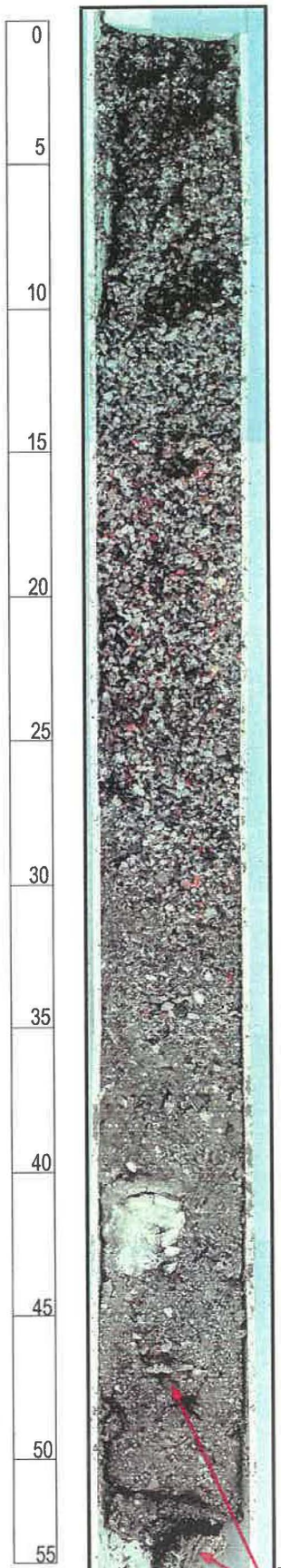

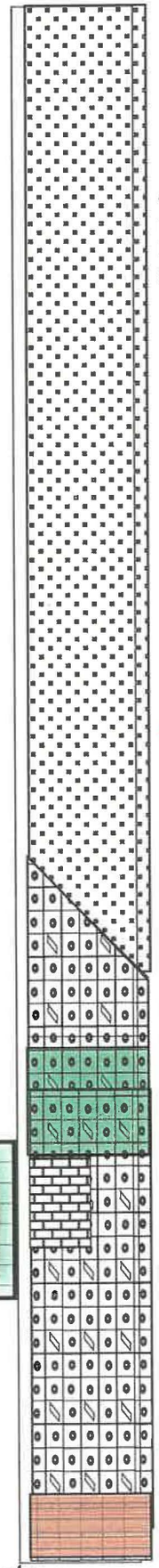

Coarse grained, sub-angular, rounded grains. Acid test reveals carbonate coating on grains.

SEM

SEM

Indistinct (diagonal) boundary to finer, well sorted grains, carbonate plates visible

Carbonate plates becoming more common with depth

Algae present. Noticeable on filter paper after sample prep.

Carbonate lobe (possibly disturbed due to coring).

Sand matrix containing carbonate plates continues to bottom.

Very hard, discoloured carbonate unit at the bottom of core

Hard carbonate

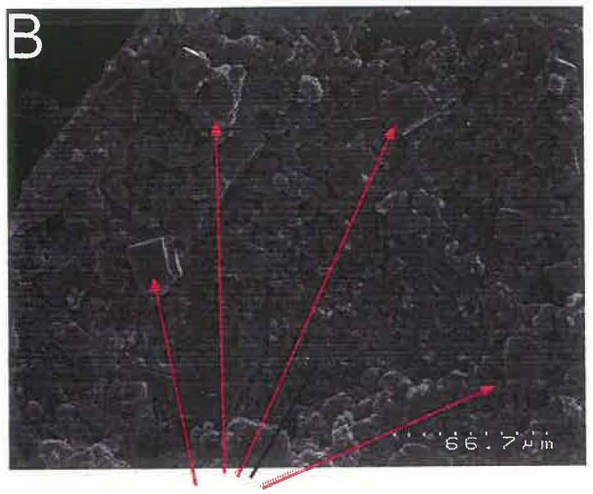

NaCl

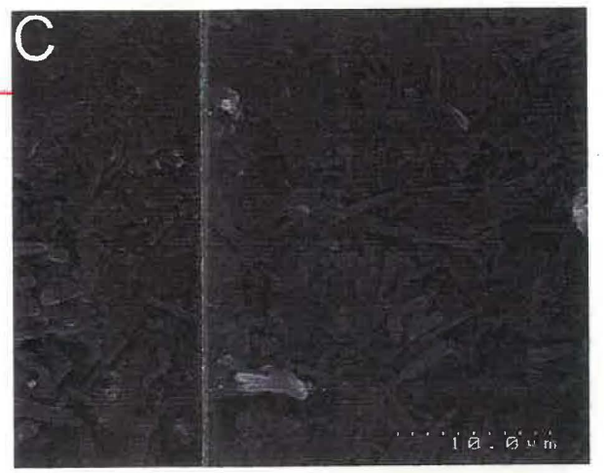

A, B,& C: B3T4 6 (25-30cm) Hard Carbonate Haphazard needle arrangement. NaCl present

D & E: B3T4 23 (47cm) Large (hard) plate. Haphazard needle arraangement

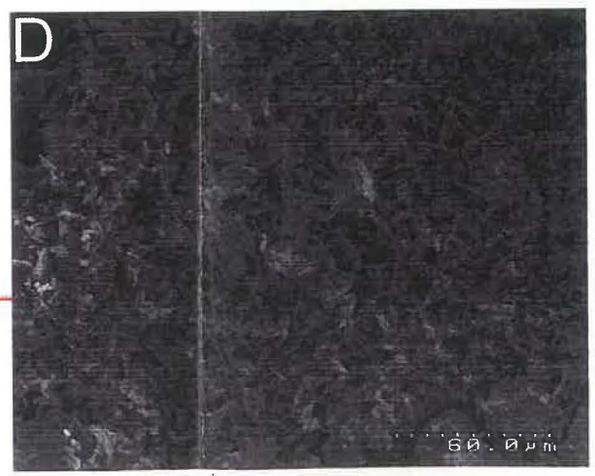

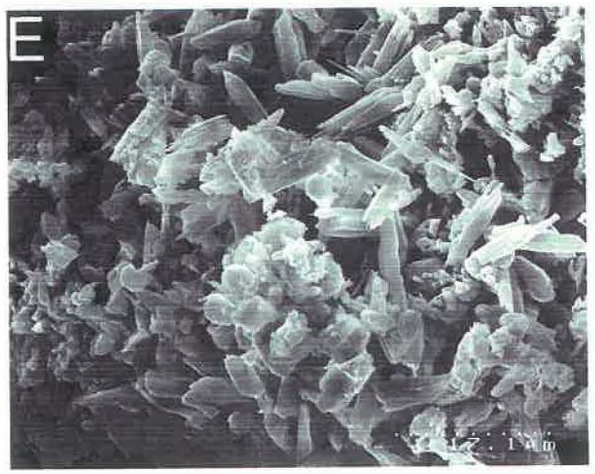

Figure 31: B3T4. East Lobe. Core stratigraphy visual description, and SEM images.

4.3.4 B3T4 Chemistry

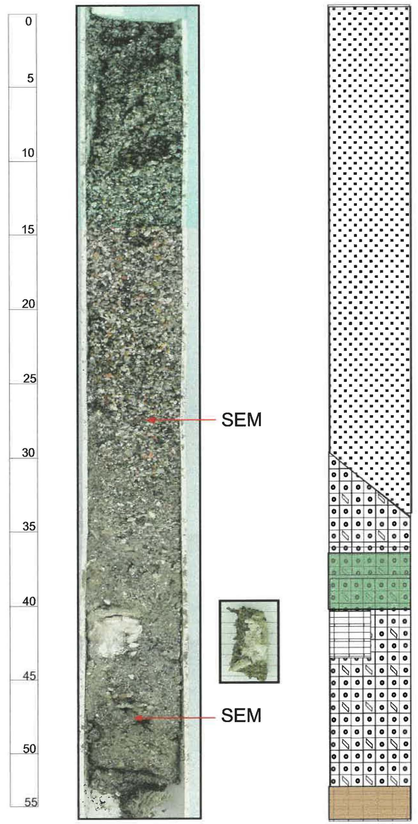

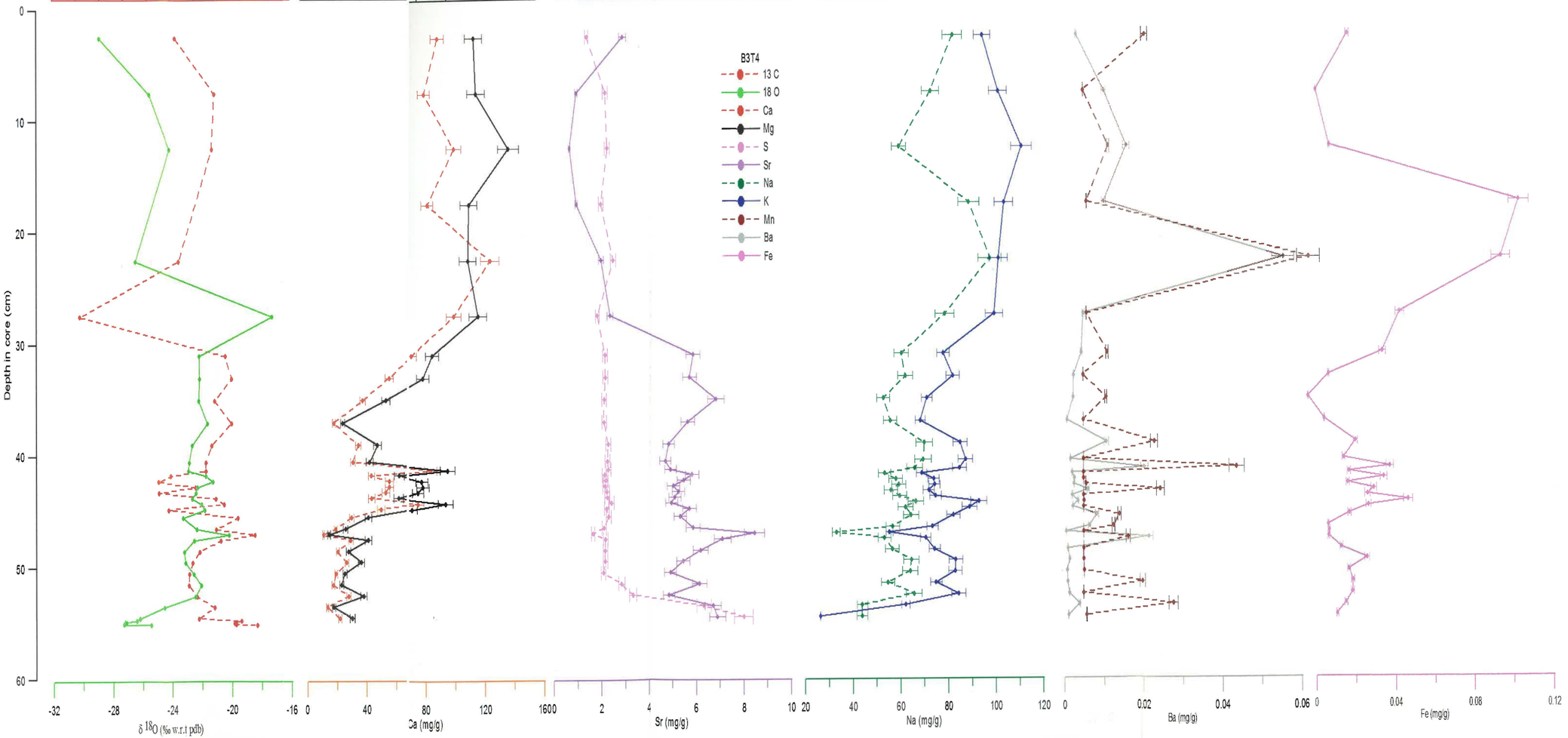

Figure 32: B3T4. East Lobe, isotopes and chemistry.

4.3.3 B3T3 and 4.3.4 B3T4 Summary of characteristics

These cores are both visibly disturbed and will be explained together in the same context. However, B3T3 and 4 still contribute to the development of the thesis as when the cores were processed, I noticed a soft grey material remaining on the filter paper; I noted the samples containing this material and continued processing. Once the sample had been re-weighed I collected this material and took it to the SEM. The material was diatom rich, which was unexpected, and led to a revision of the other cores. The Green layers in the other cores were also sampled, where they could be easily identified by eye, and taken to the SEM for analysis (refer Appendix 8 for further SEM images)

B3T3

B3T3 contains only one carbonate unit, analogous to carbonate A, the core is severely disturbed.

Carbonate A is:

- Located between 37 and 42cm
- Thick ~5cm
- Soft
- U/Th dated at 506± 14[1] years
- Flanked above and below by a diatom rich sediment.
- Severely disturbed

Carbonate A is characterised by:

- High Fe, decreasing through the unit
- Depleted ^{13}C (compared to above and below the unit), and enriched ^{18}O throughout the core.
- Low Mg and Ca
- Very little coherency between elements

[1] The error reported for this date has not been fully calculated.

Above unit A the core is visibly disturbed, likely the result of sediment falling into the hole made during the first core. It is unlikely the sediment recovered comes from lower in the stratigraphy, but is the result of material falling back into the first hole.

During sample processing, I noticed a soft green material remaining on the filter paper after the carbonate had been dissolved. I collected this material and took it to the SEM, where I discovered it was diatom rich. Subsequent to this discovery, the other cores were inspected for this material (by eye), and samples were taken for SEM analysis.

The photographs were sent to Sarah Spaulding at the University of Colarado for identification, who reported; "This species is not known to be described, and its genus affility is uncertain. It does not fit within Navicula sensu stricto. At this point in time, these are the only documented records of this taxon known to us. SEM images were provided by T. Whittaker and J. Croall".
http://huey.colorado.edu/diatoms/about/index.php

B3T4

B3T4 contains two carbonate units, a severely disturbed carbonate A, and a hard carbonate B.

Carbonate A is:

- Located between 40 and 45cm
- Thick
- Soft
- Flanked by algae
- Severely disturbed

Carbonate A is characterised by:

- Fe peak as unit begins

- Coherency between Mn, Fe, Ba, and Ca and Mg
- Enriched ^{18}O and ^{13}C Very little change of isotope values through unit.
- Very low Ba, Mn and Fe

Above unit A:

- Ca, Mg, Fe, Na and K rise substantially, but Fe decreases at the top of the core

Between unit A an B there are few correlateable features,

Carbonate B is:

- Located at 55cm depth
- ~1cm thick
- Hard
- Laminated

Unit B is characterised by:

- Very enriched $\delta^{13}C$
- Relatively depleted $\delta^{18}O$
- High S

4.3.5 B4T1 Core stratigraphy, description and optical microscope study of unit A.

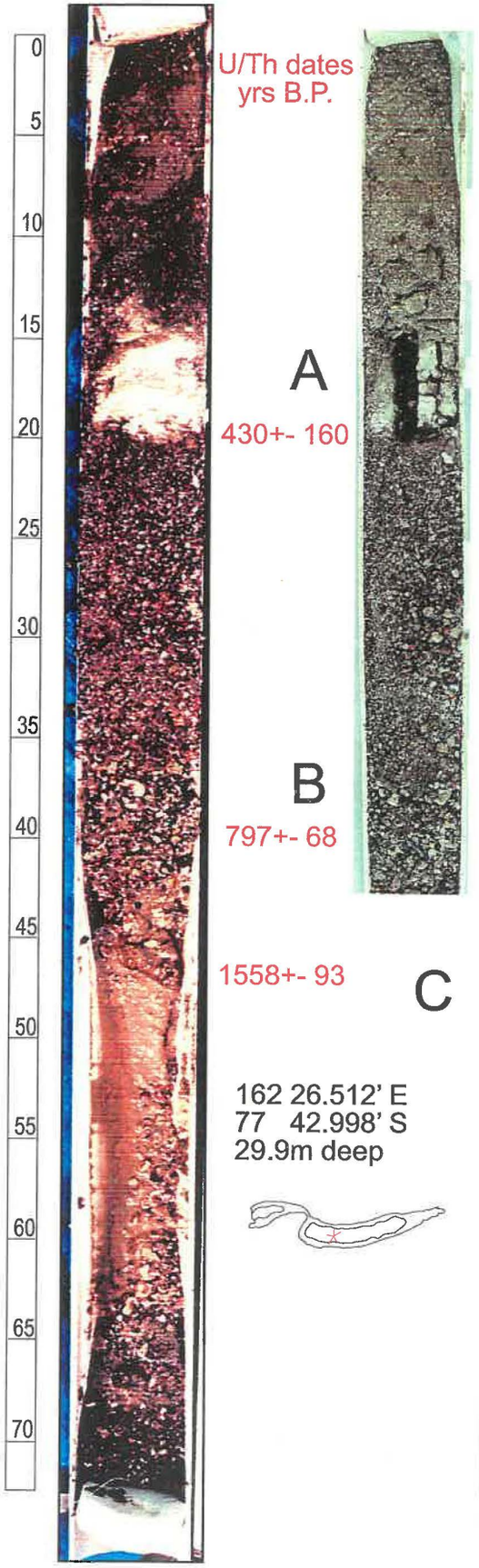

0-6cm Fine sand, black flakes throughout. Carbonate plates (small). Some fine almost silty material, light brown (poorly sorted).

6-14cm Indistinct boundary to a coarser sand, darker brown, containing black flakes and sparse carbonate flakes.

Unit A

19-27cm Distinct boundary to coarse sand, getting coarser with depth. Some small carbonate clasts possibly dragged down by coring and splitting. Some large mineral clasts (4mm) Increasing coarse fraction towards 30cm.

27-39cm Semi distinct change to a finer grain size, lighter brown sand. Small fraction of large mineral clasts (2-3mm). No visible carbonate.

37-44cm Distinct boundary to well sorted. Large mineral clasts with sand matrix. 1 large carbonate biscuit dated.

Hard Carbonate unit (48cm).

44-50cm Distinct boundary, sand matrix continues, large mineral clasts do not. Carbonate plates, medium size and frequent. Greyish brown sand matrix with fine silts.

50-70cm Gap in core, fine silts, poorly sorted sand, large carbonate plates, medium size mineral clasts (2mm).

70-73cm Silt horizon, small <1mm carbonate flakes, grades to a coarse sand.

B4T1 Unit A description.

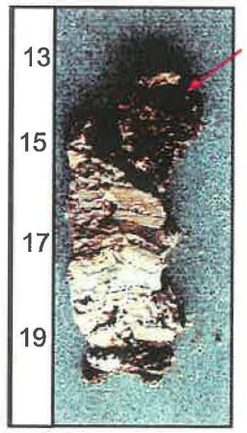

13cm Greeny brown material, hard chunks present interspersed with sand. Possibly biological.

14-16.5cm Carbonate layer, laminated, some very pure (white).

16.5-17cm Greeny material (soft) Biological?

17-19cm Laminated carbonate, biscuity, pure. (dated 430+- 160)

19cm Greeny materail

Light microscope photo: Samples locations

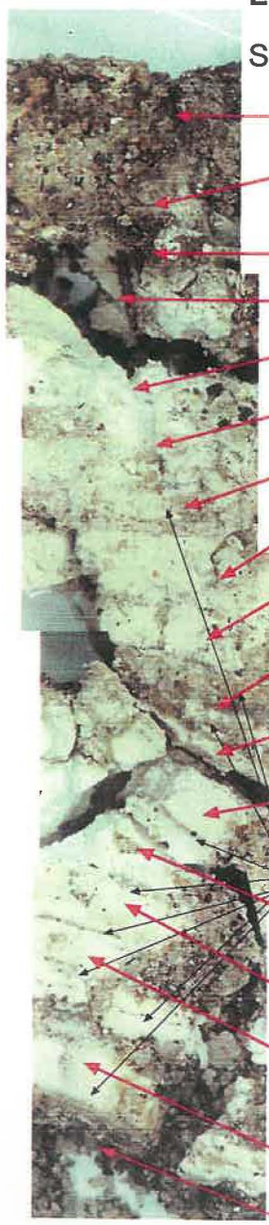

SEM studies on all (Following page)

1. Top, light brown layer.
2. Dark brown layer, razor cut revealed a chunk of carbonate or gypsum?
3. Dark brown, sandy. Greensih material.
4. Sandy carbonate.
5. Sandy carbonate.
6. Sandy carbonate.
7. Browny-grey unit.
8. Browny-grey unit.
9. Browny-grey unit. Sharp contact to greeny material.
10. Green unit, contact to thin white carbonate unit
11. Green and white (very fine laminations).
12. Thick (3mm) hard carbonate layer, reasonably pure. Contact to next unit is sandy.

Varves

13. Soft carbonate layer (4mm think), grey materal at contact to next unit, not a sharp contact.
14. 2mm thick carbonate layer.
15. 3-4mm thick carbonate layer, contact to sandy material (<0.5mm) split along sandy contact easily.
16. 3mm carbonate layer, sharp contact to soft greeny layer.
17. 4mm greeny layer (soft) carbonate flecs (very thin) present.

Figure 33: Visual description of core B4T1, including Light microscope photographs of the evaporite sequence found at 19cm. Sample locations shown.

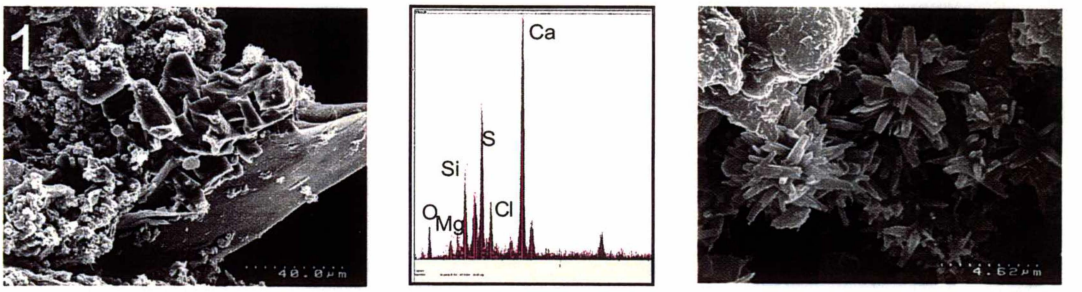

Sample 1; Well defined carbonate needles, massive carbonate (with large amounts of Cl, and gypsum coexisting, suggesting coprecipitation.

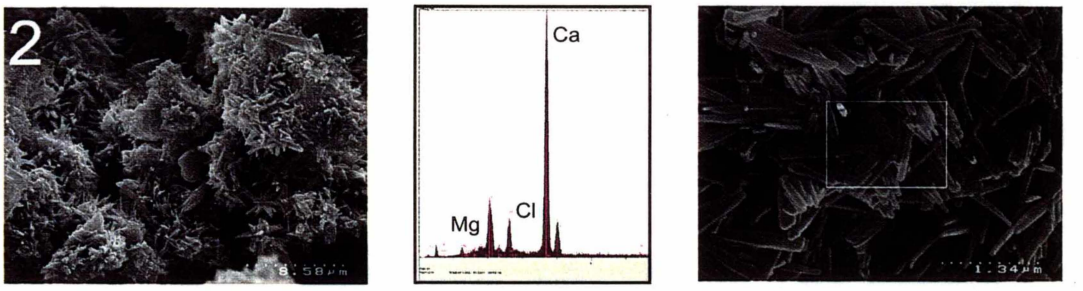

Sample 2; Well defined, radiating carbonate needles. Calcium and Chlorine are dominant, with small amounts of Magnesium.

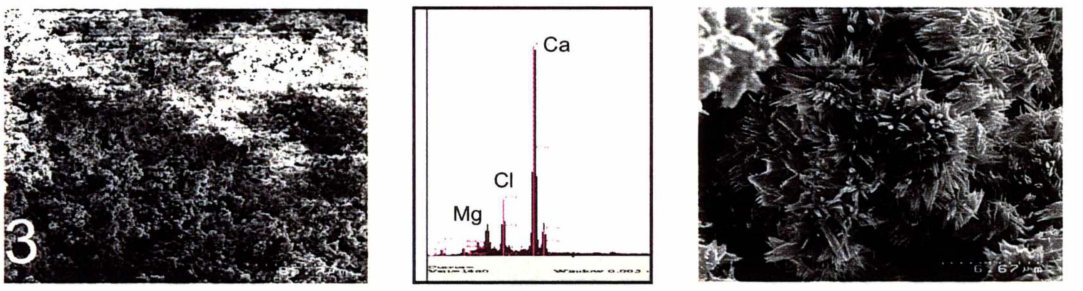

Sample 3; Sample consists entirely of well defined radiating needles. Ca and Cl dominate, with small amounts of Magnesium.

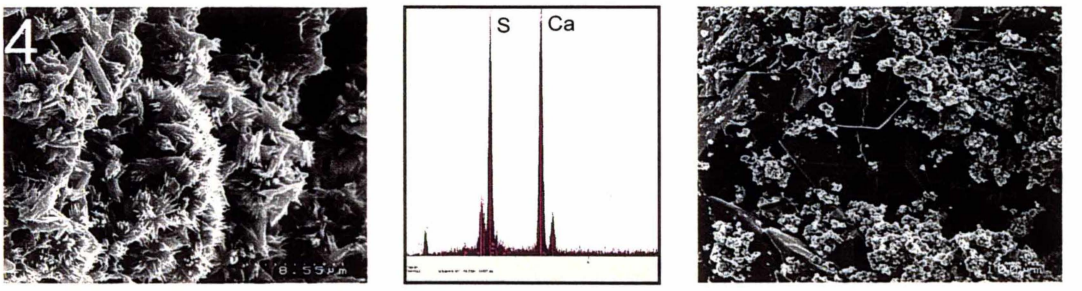

Sample 4; Well defined carbonate needles and gypsum coexisting, suggesting coprecipitation.

Figure 34: SEM studies of B4T1 unit A, showing the changing conditions from top (1) to bottom (15),showing the typical composition of samples analysed for chemistry.

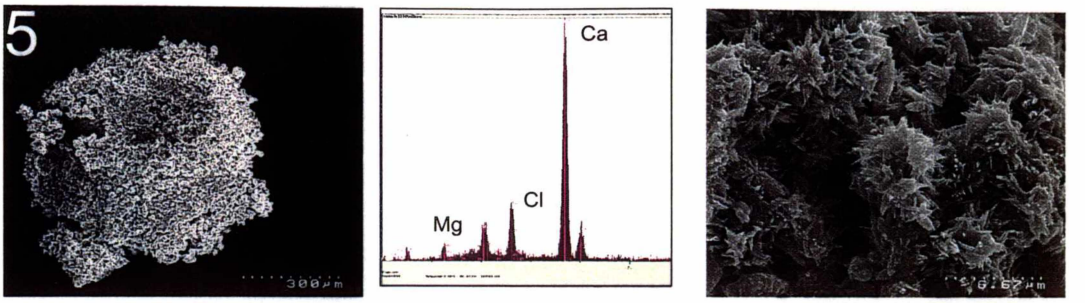

Sample 5; Sample consists entirely of well defined radiating needles. Ca and Cl dominate.

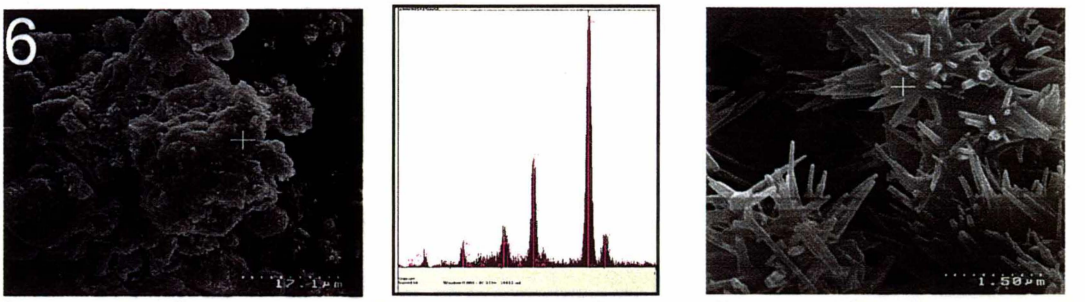

Sample 6; Consists of well defined radiating needles, growing from a cemented centre, the cement is NaCl. A sand grain is usually at the middle of the radiating centre.

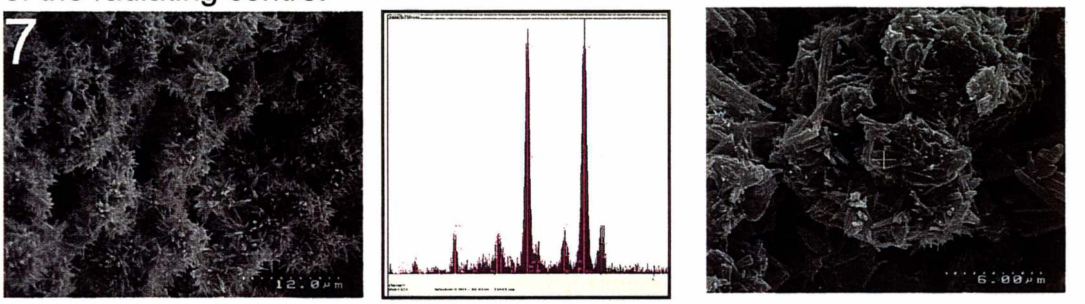

Sample 7; Sample consists of well defined radiating needles. Ca and Cl dominate EDAX trace.

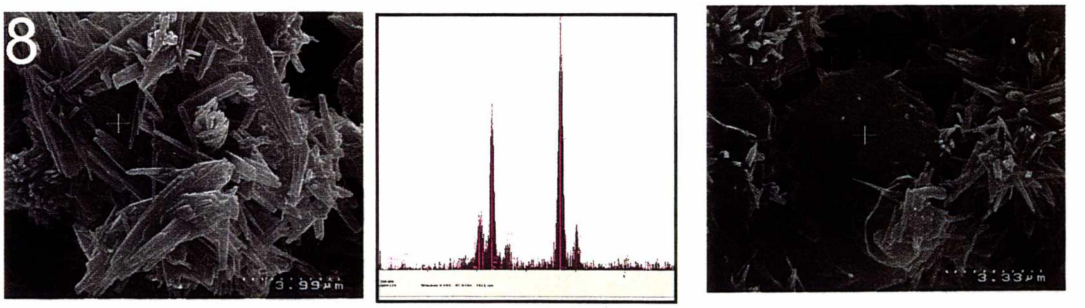

Sample 8; Sample consists of well defined needles (not radiating). Needles surrounded by NaCl.

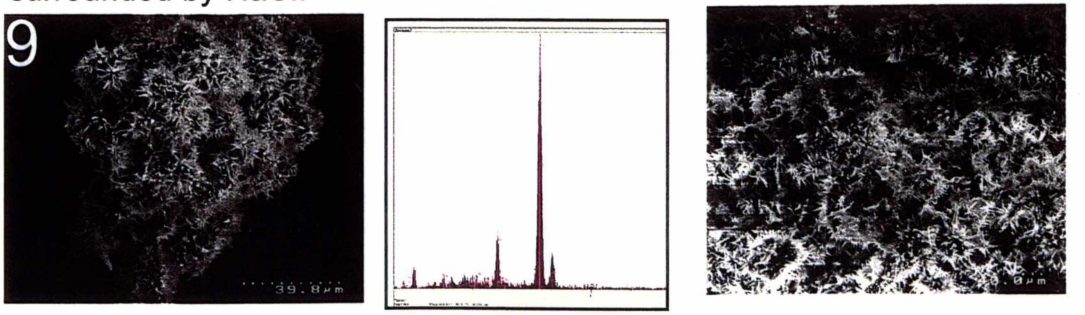

Sample 9; Sample consists entirely of well defined radiating needles. NaCl cement not present in this sample.

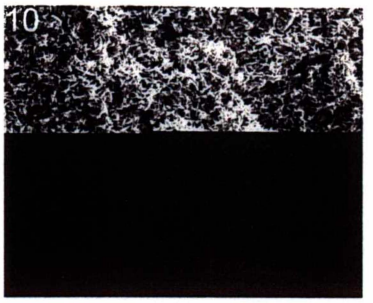

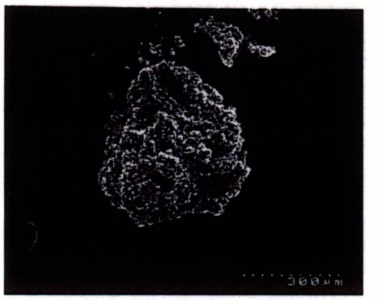

Sample 10; Radiating needles, no NaCl cement present. Pure carbonate sample.

Sample 11; Change of carbonate crystal growth from point growth to a pattern resembling a "hay-stack", needles are haphazardly arranged. No NaCl

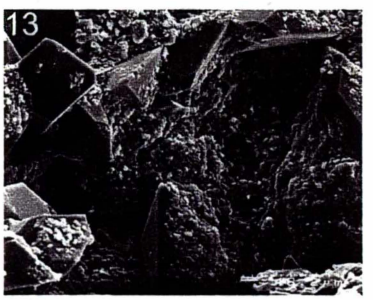

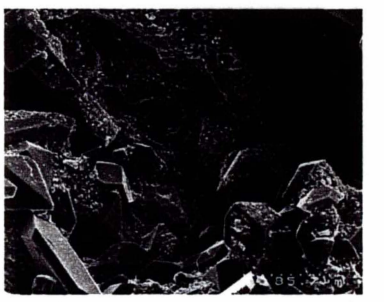

Sample 13; Carbonate is massive again, large amounts of gypsum and NaCl present. Carbonate appears to coat the sample.

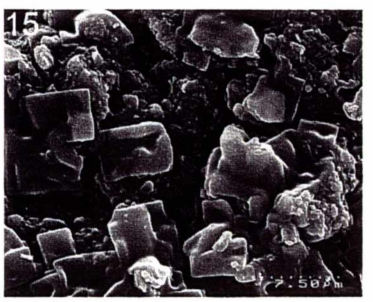

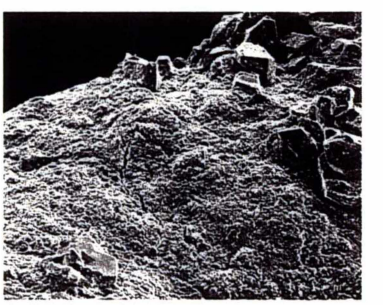

Sample 13; Carbonate coats the sample, large amounts of gypsum and NaCl present.

See Appendix 8 for further photographs

4.3.5 B4T1 Carbonate unit C

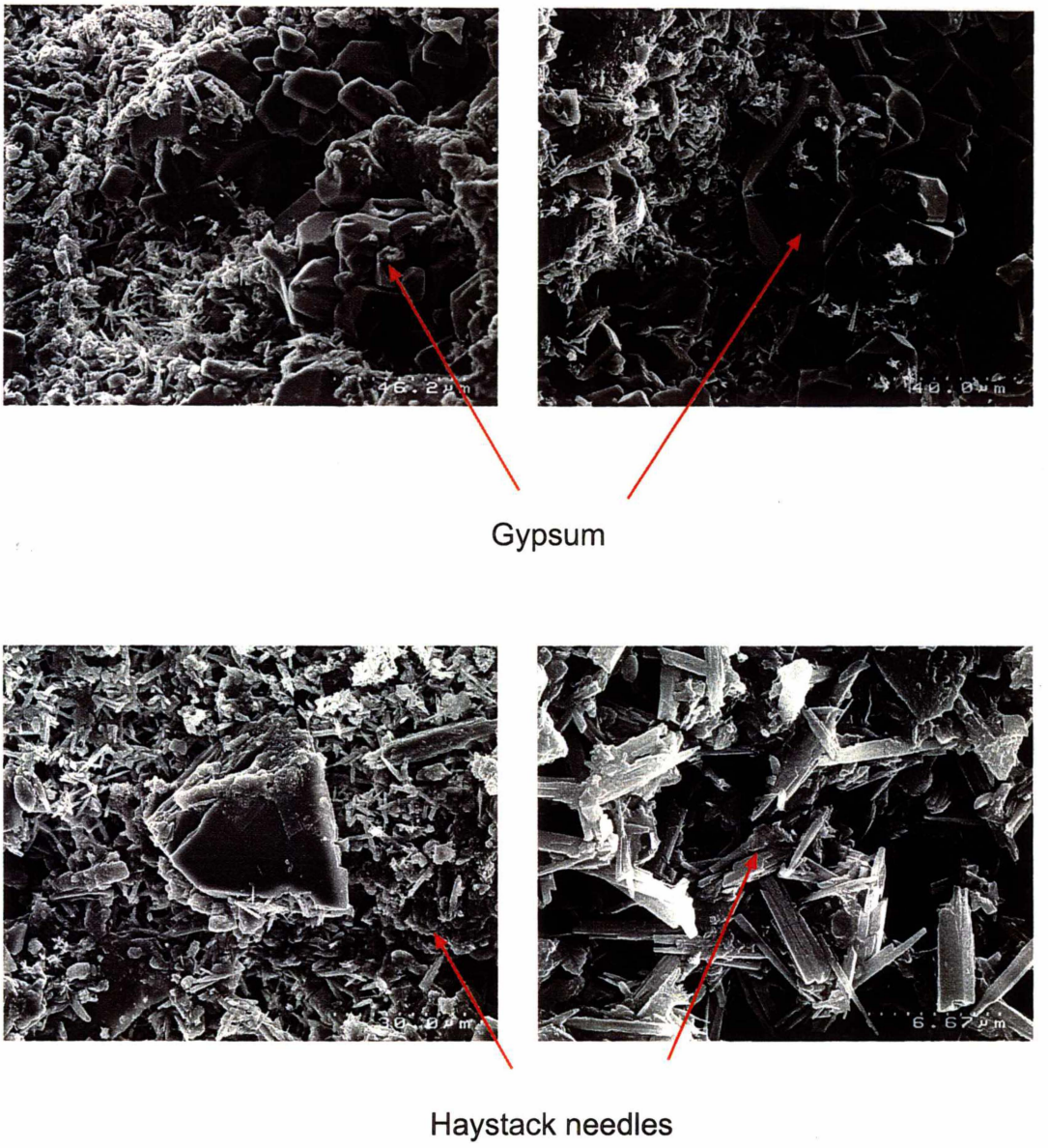

Figure 35: B4T1Unit C SEM images showing gypsum and "haystack" carbonate structure.

4.3.5 B4T1 Isotopes and chemistry

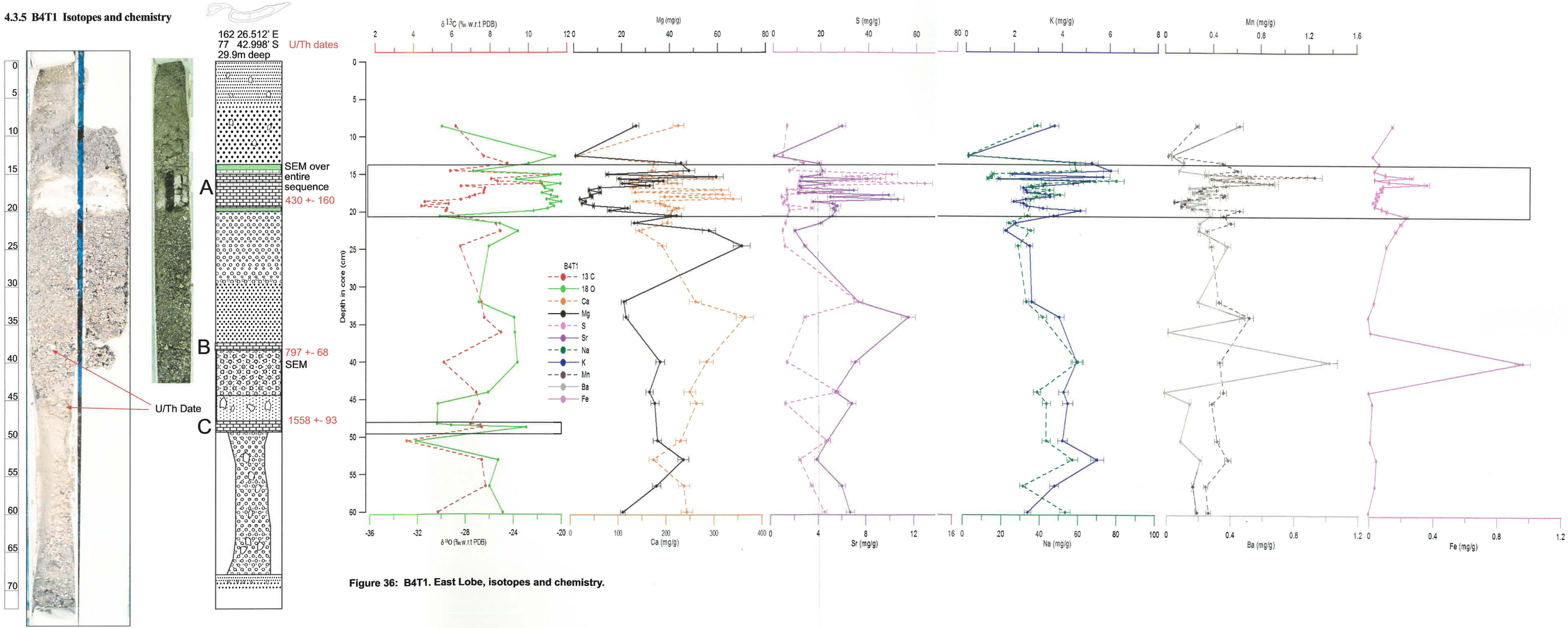

Figure 36: B4T1. East Lobe, isotopes and chemistry.

4.3.5 B4T1 summary of core characteristics

B4T1 has three distinct carbonate units (A, B and C)

Carbonate A is:

- Located between 15 and 20cm
- Thick ~5cm
- Soft
- U/Th dated at 430±160 yr B.P.
- Flanked by biological material
- Has a discoloured layer (biological) in the middle of the unit.

Carbonate A in B4T1 was chosen as representative, and analysed by SEM and optical microscope. Visual (light microscope and SEM studies) characteristics of unit A are described in the following section.

Light Microscopey

The unit is highly laminated, the layers being of different colour and thickness. The layers are separated by thin lamina of very fine clastic material, stained orange (probably iron staining). Approximately 20 of these layers are visible under the light microscope. The lamina are most likely the result of annual / semi-annual ice cover forming on the hypersaline waters during the winter months, and collecting windblown clastic material. When the ice cover is lost in summer, as the temperatures rise enough to allow the ice to melt, the grains settle as a distinct layer to the bottom of the lake. The layers of carbonate have almost no clastic material incorporated, suggesting that the carbonate deposition is primarily during the winter, with the ice cover present.

Scanning Electron Microscopy

Changes in the calcium carbonate structure through the sequence indicate changing conditions of formation. Gypsum, halite and poorly formed carbonate are all present

in large quantities as the sequence begins (sample 15), this is succeeded by well defined needles amongst a NaCl cement. Three samples have the haystack structure, and correspond to ^{13}C enrichment and were therefore most likely formed in the water column due to freezing of the hypersaline water during winter, forming a cryptocrystalline powder, as noted in Clark and lauriol (1992) which also corresponds with the low Mg content of the carbonate to be discussed later. Oxygen and Carbon isotopes co-vary from this point on, suggesting an input of freshwater, the subsequent samples contain gypsum again.

Following unit A, $\delta^{18}O$ and $\delta^{13}C$ co-vary (depleted then enriched), this occurs twice. The second, a greater shift than the first. At most points where the isotopes enrich and co-vary, Ba, Fe and Mn also increase.

Unit A is characterised by:

- Depletion and covariance of $\delta^{18}O$ and $\delta^{13}C$ immediately prior to the unit
- A massive $\delta^{18}O$ shift (~31—20) as the unit begins
- No biological material within the unit
- Progressively enriching $\delta^{13}C$ through the unit
- Increasing Mg prior to the unit, decreasing as the unit begins until approximately half way through, where it rises substantially until the unit ends.
- Na, K and Mg broadly follow the same pattern
- Coherency of Ca and Sr
- S begins low and increases over the unit
- Mn and Ba increase over the unit
- Fe peaks at the start of the unit, then decreases, increasing again in the final stages.

Between Unit A and B Carbonate deposition occurred with some large plates formed. $\delta^{13}C$ and $\delta^{18}O$ show enrichment and co-vary, Mg also increases.

Carbonate B is:

- Located between 37 and 38cm
- Thin ½ - 1 cm
- U/Th dated at 797± 68 years
- Hard
- Laminated

Carbonate B is characterised by:

- A "haystack" type of crystal growth
- High Fe and Ba
- No biological material present

(Isotope studies are pending due to NaCl contamination)

Between carbonate B and C there is a co-variant enrichment of $\delta^{13}C$ and $\delta^{18}O$

Carbonate C is:

- Located between 46 and 47cm
- Hard
- Laminated
- U/Th dated at 1558±93 yr B.P.

Carbonate C is characterised by:

- "haystack" style carbonate structure
- Extremely enriched $\delta^{18}O$ (from ⁻30 - ⁻22)
- Co-variance of $\delta^{13}C$ and $\delta^{18}O$ enriching significantly
- No biological material present

(Isotope studies were lost due to NaCl contamination)

Below carbonate C the sediment is not in-situ, and shows no distinct patterns.

4.3.6 B5T1 Core stratigraphy and description

33m depth
No GPS

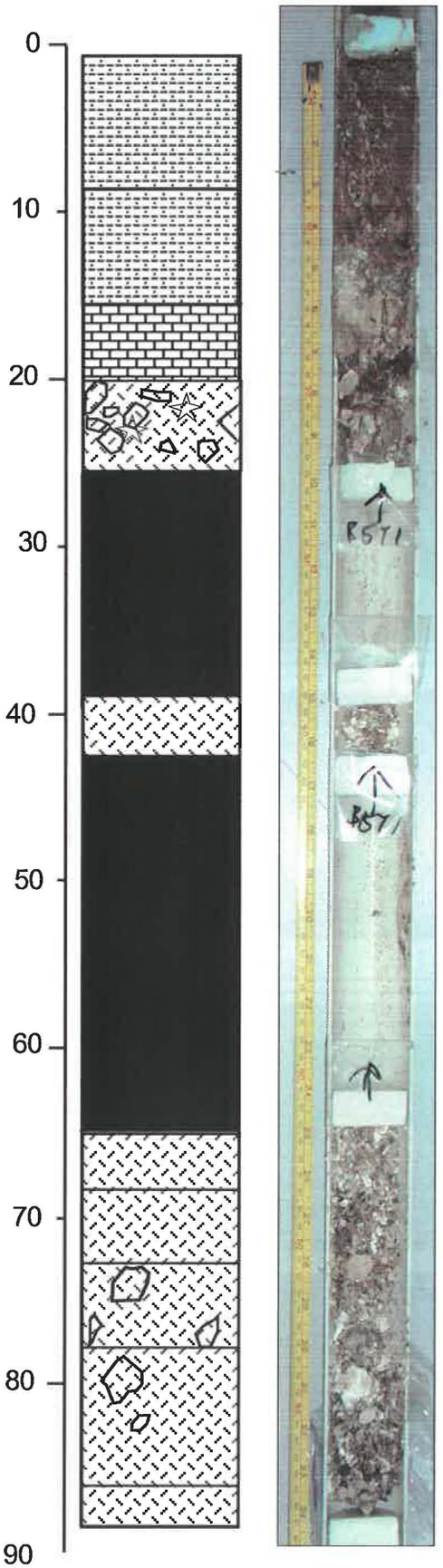

U/Th dates

479+-95 A

809+-88 B

C 920+-420

0-8.5cm	Fine silty sand with sparse black flecs. Carbonate rich, small plates. Carbonate with dominant silty sand matrix.
8.5-14.5cm	Predominantly carbonate, broken into small plates, containing thin laminates (gypsum?) , silty sand matrix throughout.
14.5-19.5cm	Massive carbonate unit. Thin laminae present, intermittent grey-brown material. discoloured carbonate.
19.5-27cm	Thin large laminates of carbonate, containing crystal clasts.
27-37cm	Gap in core
38-41cm	4mm thick layer of very pure (white) carbonate plates. Grading to light olive green. U/Th dated at 809+- 88 Years BP
39-63cm	Gap in core
63-67cm	Large percentage fine yellow silts, black and white sand at top. Packed with thin white/creamy plates, 1-4mm thick 10-20 mm across.
67-72cm	Dominated by larger white/creamy plates, silt (yellow) a little sand.
72-77cm	Chunky laminated plates, largely white with thin darker layers. 20mm thick and 30mm across. U/Th dated at 920+- 420 years BP
77-85cm	Smaller chunks with more darker laminated material, increasingly large clastics towards bottom.
85-88cm	Larger chunks of white cream laminated carbonate. Clasitc gravels 10mm across, has had fines washed out.

Figure 36: B5T1 Visual stratigraphy and description of B5T1, and SEM images of selected samples

4.3.5 SEM studies of carbonate units A and C

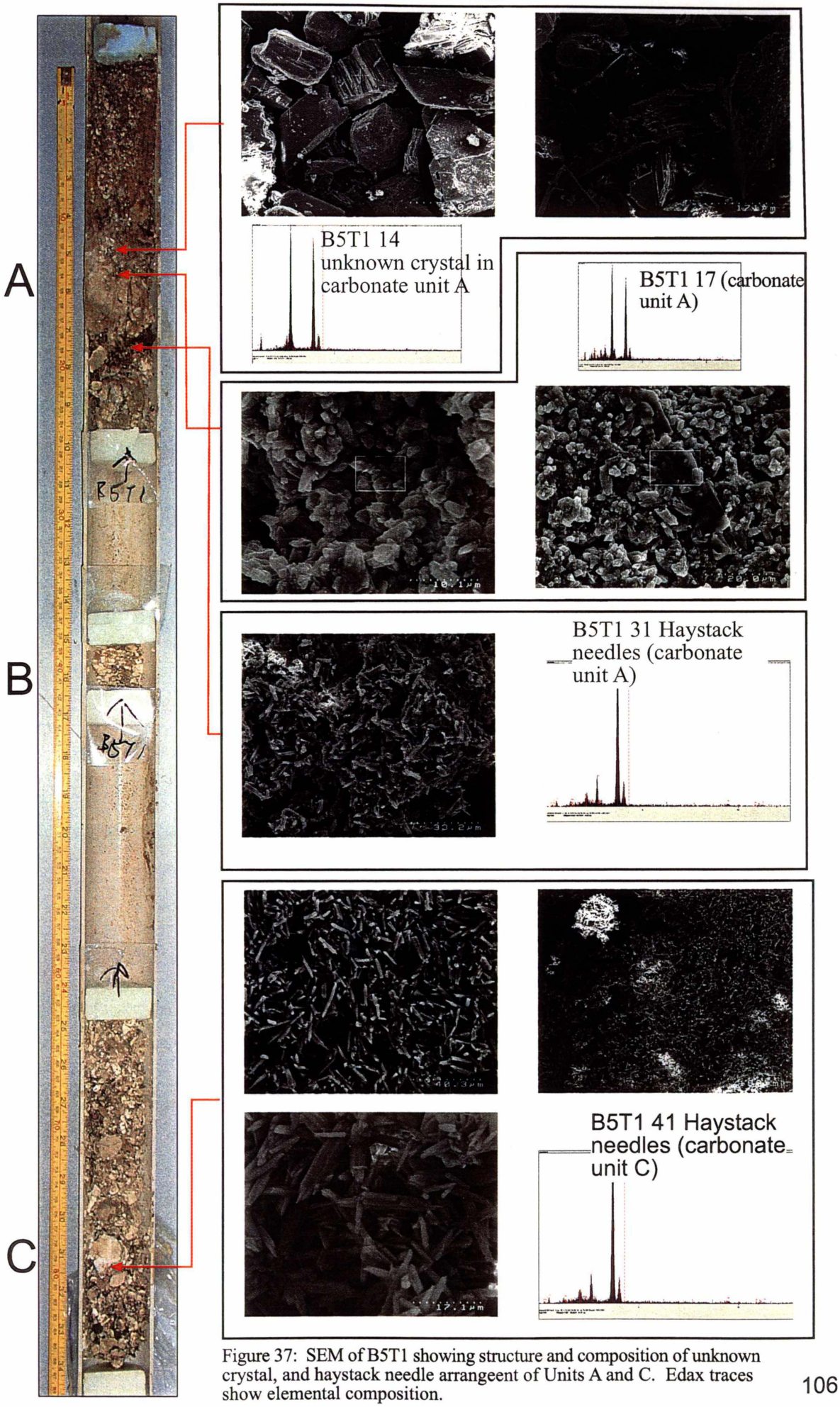

Figure 37: SEM of B5T1 showing structure and composition of unknown crystal, and haystack needle arrangeent of Units A and C. Edax traces show elemental composition.

3.6 B5T1 Isotopes and chemistry

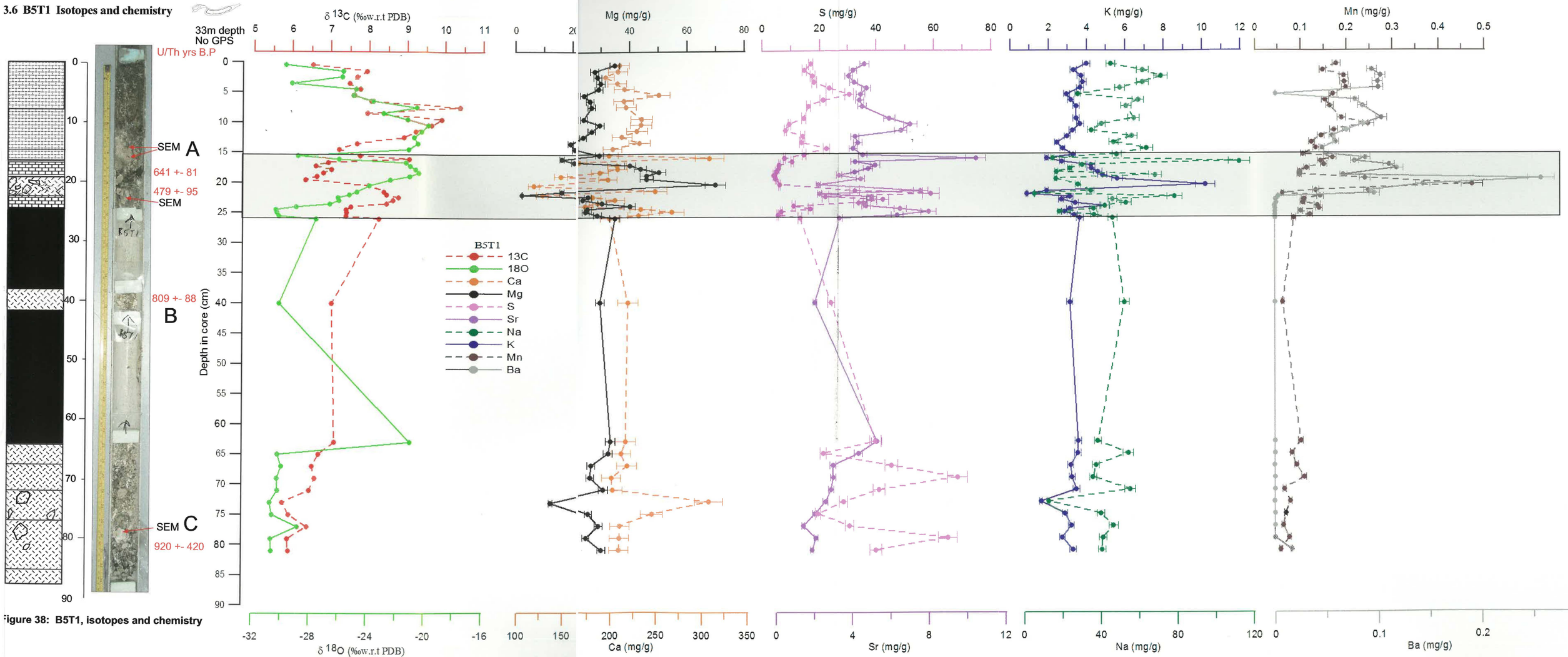

Figure 38: B5T1, isotopes and chemistry

B5T1 summary of characteristics

B5T1 is distinctly different to the other cores; the deepest, it is completely dominated by $CaCO_3$. The stratigraphy has been severely disturbed due to the coring process, and sediment has "run-out" towards the bottom of the core, therefore the distance down-core (sampled from) has been somewhat exaggerated, making identification and interpretation of the carbonate units difficult. However, three distinct carbonate units are identified.

Carbonate A is:

- Located at 15cm-20cm
- Thick (~5cm)
- U/Th dated at 479± 95 yrs B.P.
- No algae appears to flank this deposit

Carbonate A is characterised by:

- Progressive enrichment of $\delta^{18}O$
- Initially enriched $\delta^{13}C$, dropping, then abruptly enriching towards the end of the unit
- The maximum $\delta^{13}C$ value occurs above the unit at 10cm
- Decreasing Mg and Na in the first stages of the unit, followed by a spike and decrease
- Rise in Mn, Ba, Na, and Mg Concurrent with a depletion of $\delta^{13}C$
- Simultaneous Ca, Sr and K changes
- Large oxygen shift at the top

After Unit A, there is a large, co-variant isotope depletion, followed by enrichment.

The isotopes then co-vary, depleting punctuated by small enrichments.

Between unit A and B there is insufficient sample resolution due to the disturbed nature of the core.

Carbonate B is

- Located at approximately 40cm in the core
- Hard
- Dated at 809±88 years
- No algae flanks this unit

Carbonate B is characterised by:

- A probable $\delta^{18}O$ shirt from -31 to -20 (although this occurs below the unit and it is difficult to assess which carbonate comes from where, nevertheless there is a large enrichment immediately beneath the unit, similar to the shift seen prior to other units).

Carbonate C is:

- Located at approximately 78cm
- Thick ~ 3cm
- Laminated
- Hard

Carbonate C is characterised by:

- Co-varying enrichment of $\delta^{18}O$ and $\delta^{13}C$, although this signal is minor, the

unit was severely altered, and I could not sample with the same high resolution as in other units

- High S

Crystal discovery

Unusual crystals were discovered while processing the samples; these were translucent, with clean well formed crystal faces and were very hard. The crystal was within the carbonate and did not dissolve in water or acid.

A sample was initially analysed by X-ray diffraction (thanks to Brian Nicholson) at the University of Waikato, but could not be accurately identified, so it was sent to the x-ray crystallography centre at Auckland University.

The crystal was found to be a perfect example of $CaSO_4.2H_2O$ (Figure 39 and 41) (so good in fact, it may be published to make corrections to the established literature on bond-angles and lengths, full x-ray data are presented in appendix).

The ^{18}O signal does not show the same abrupt shift at the onset of carbonate deposition, as seen in B3T1 and B4T1, instead the shift is gradual, but is of exactly the same magnitude. This being the deepest core, I believe that the waters depositing this material were characteristic of a dense, hypersaline brine, isolated from the waters above by density. Therefore the oxygen enrichment as water evaporated was muted, as it had to diffuse through the brine to the waters above, hence the slower signal.

The $\delta^{13}C$ signal shows the same characteristics as the B4T1 and B3T1 cores, showing a pattern of progressive enrichment through the sequence, reaching a maximum of $^{+}11‰$. It is likely that the lack of correspondence regarding the location of the peak is a result of the core disturbance coupled with the previously discussed density effect of the waters of formation.

location of the peak is a result of the core disturbance coupled with the previously discussed density effect of the waters of formation.

The same features are present in the B5T1 isotope record as the shallower cores; a 2‰ ^{18}O shift at the same sample as the shift to the highest ^{13}C value. The meltwater input signals (co-variance) at the end of, and after the evaporite deposition period are also present in B5T1.

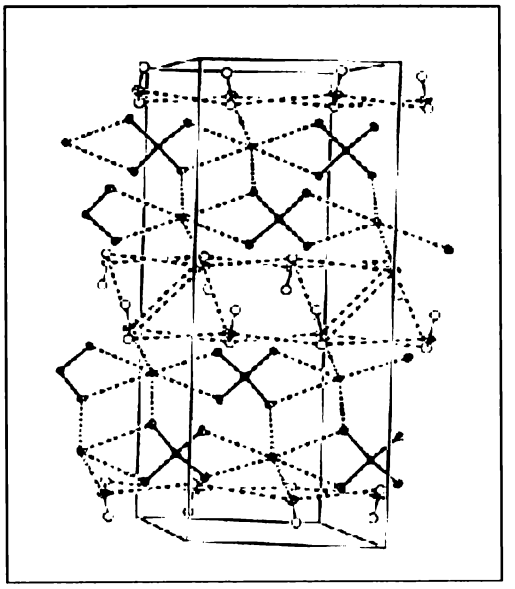

Figure 39: Structure of unknown crystal identified in B5T1. The crystal was found to be $CaSO_4.2H_2O$

4.3.7 B7T1 West Lobe. Core stratigraphy and description

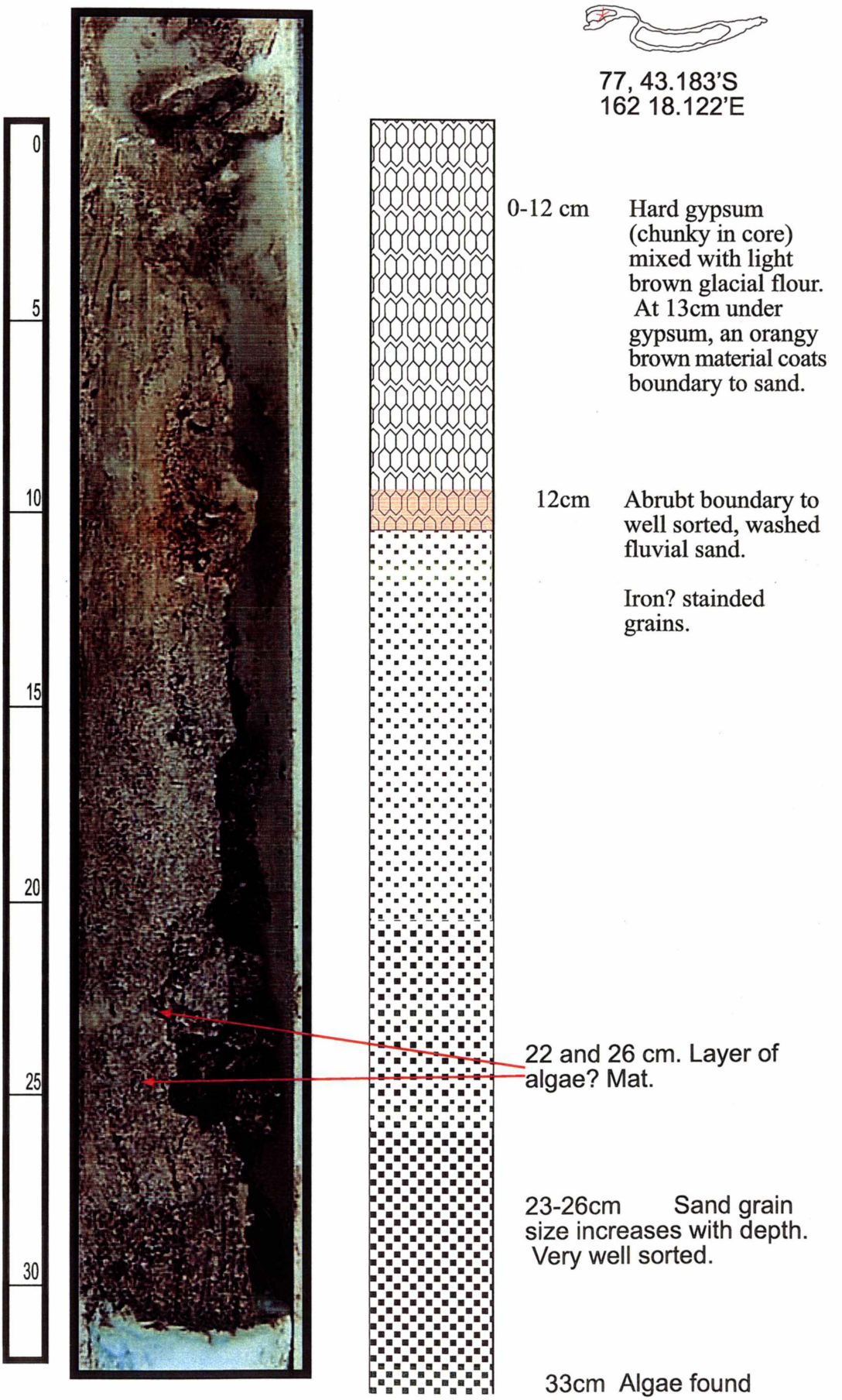

Figure 40: B7T1 West Lobe, visual stratigraphy and description

4.3.7 B7T1 SEM studies

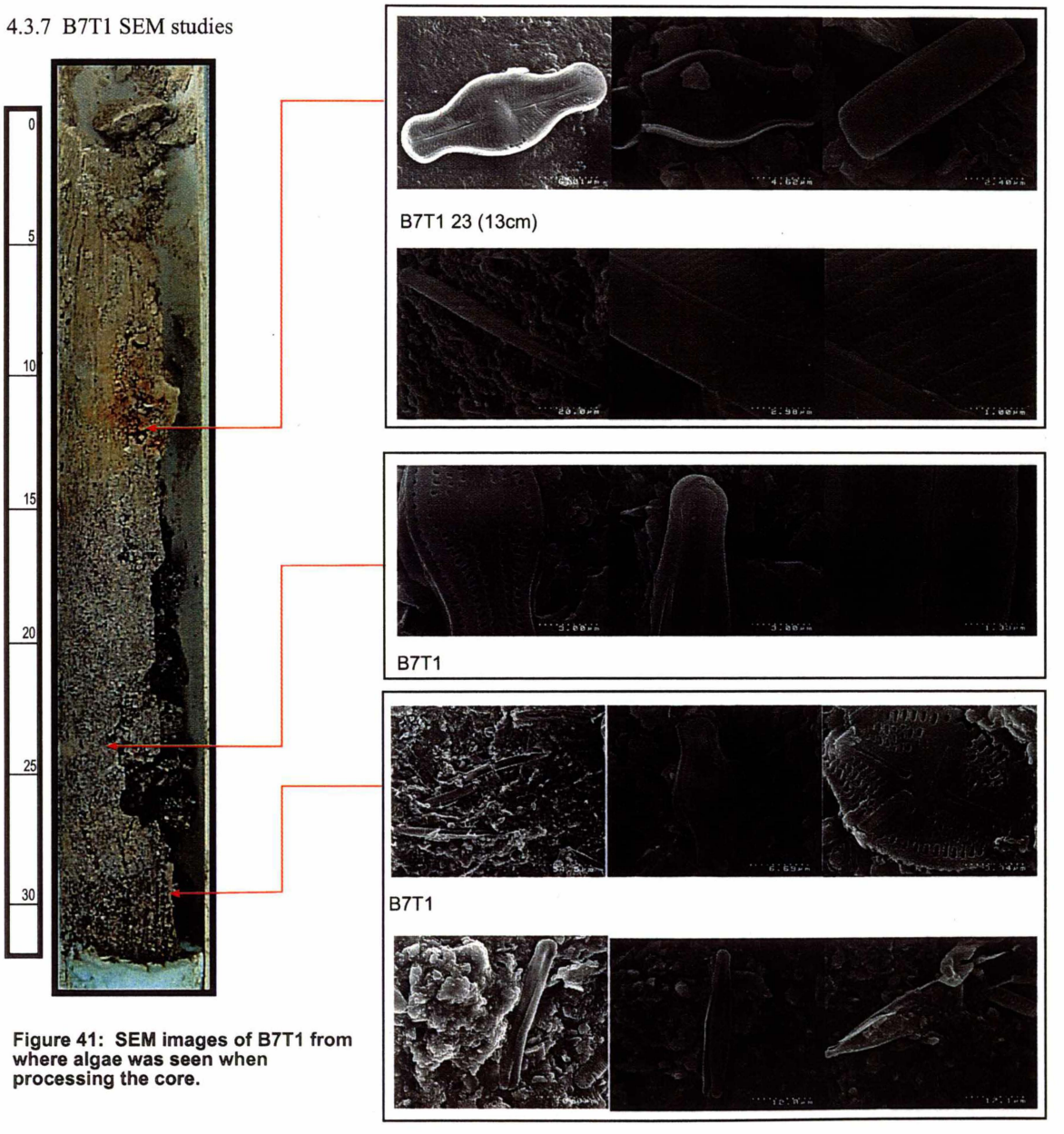

Figure 41: SEM images of B7T1 from where algae was seen when processing the core.

4.3.7 B7T1 West Lobe Isotopes and chemistry

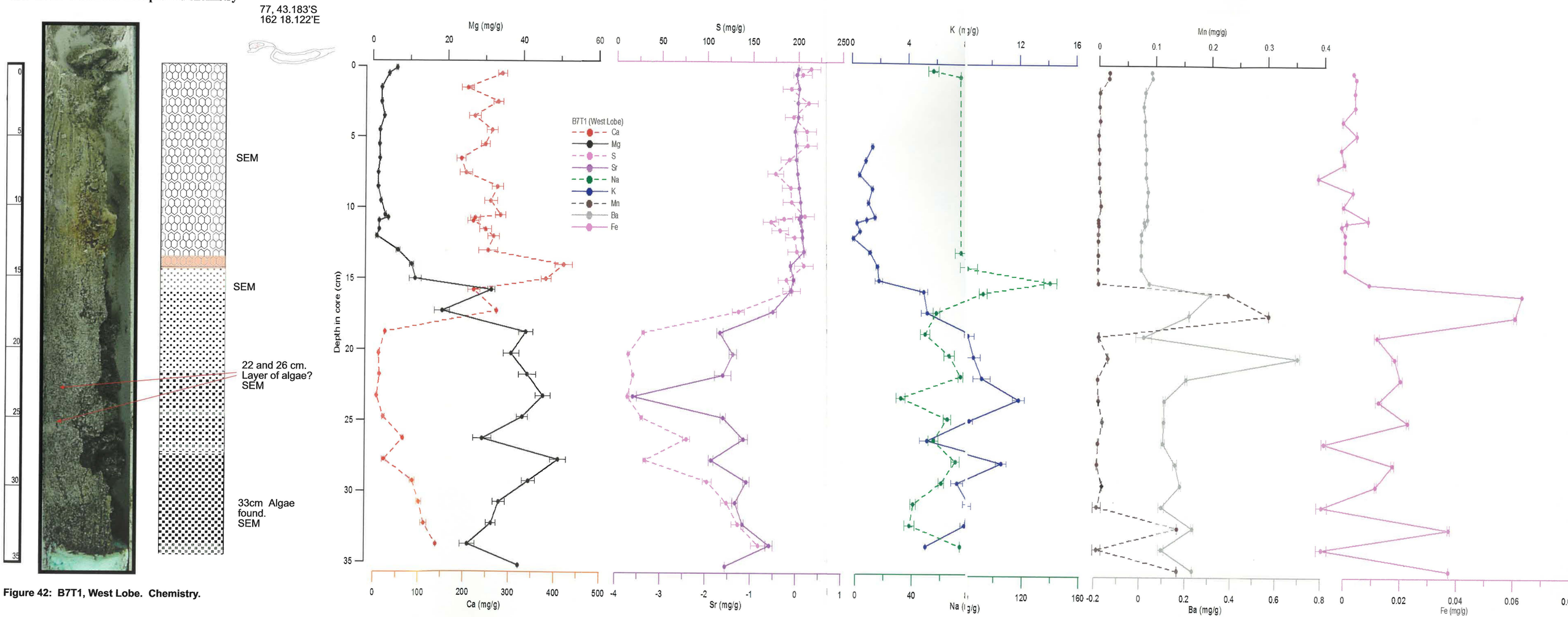

Figure 42: B7T1, West Lobe. Chemistry.

4.3.7 B7T1 Summary of core characteristics

The sediments in West Lobe are dominated by gypsum, no carbonate units are identified in the sediments

B7T1:

- The top sediments are dominated by gypsum (~13cm)
- Iron staining occurs below the gypsum
- Algal layers are obvious in the sediment below the gypsum, isolated diatoms are present within the gypsum

B7T1 is characterised by:

- Ca and S increase as the gypsum begins
- Sr follows Ca, increasing in the gypsum
- K and Mg decrease to almost zero in the gypsum
- Na remains high through the gypsum
- Fe, Ba and Mn peak immediately prior to the gypsum, coincident with the visible orange stained layer, and decrease to zero throughout

The discovery of the diatoms led to the identification of an unknown *Naviculoid* species, found in Lake Fryxell but previously only seen under a light microscope. Several other species found are as yet unidentified. The diatom material was easily seen above and below the major evaporite sequences (400yr B.P) in all cores from East Lobe, and was abundant, occurring as mats in number of locations below the gypsum in the West Lobe, as well as isolated occurrences within the gypsum.

Chapter 5

Interpretation & Discussion

"Blood Falls", at the snout of the Taylor Glacier.

Introduction

This discussion correlates carbonate units A, B and C from B3T1, B4T1 and B5T1, to construct a sediment stratigraphy and history of the East Lobe. B3T3 and 4 were severely disturbed as a result of the coring process, and do not show the same features seen in the other cores, it is unlikely that the material recovered comes from lower in the stratigraphy, but rather is a re-coring of the same evaporite sequence found in the upper section of B3T1, as it was dated at 506± 14[1], and therefore does not add to the data set.

The West Lobe stratigraphy is discussed with respect to B7T1 data.

Sediment stratigraphy (Figure 43)

Lake Bonney East Lobe, is flat bottomed due to a 20cm thick halite playa occurring at / below 38.8m depth (as at 2003), 5cm of hydrohalite lies immediately below the halite followed by platy carbonate, no further material was recovered. Three distinct carbonate units are present in the cores from the East Lobe at locations above the halite playa (Carbonate A, B and C). The presence of unstable hydrohalite below the halite playa made coring of deeper sites very difficult, the hydrohalite re-crystallises to halite and brine, washing out material below it in the core barrel.

Carbonate A: represents the most significant event recorded in the East Lobe sediments, is thick (~5cm), pure, highly laminated and dated at ~450 ±100 yrs B.P (average of U/Th dates).

[1] The error reported for this date has not been fully calculated.

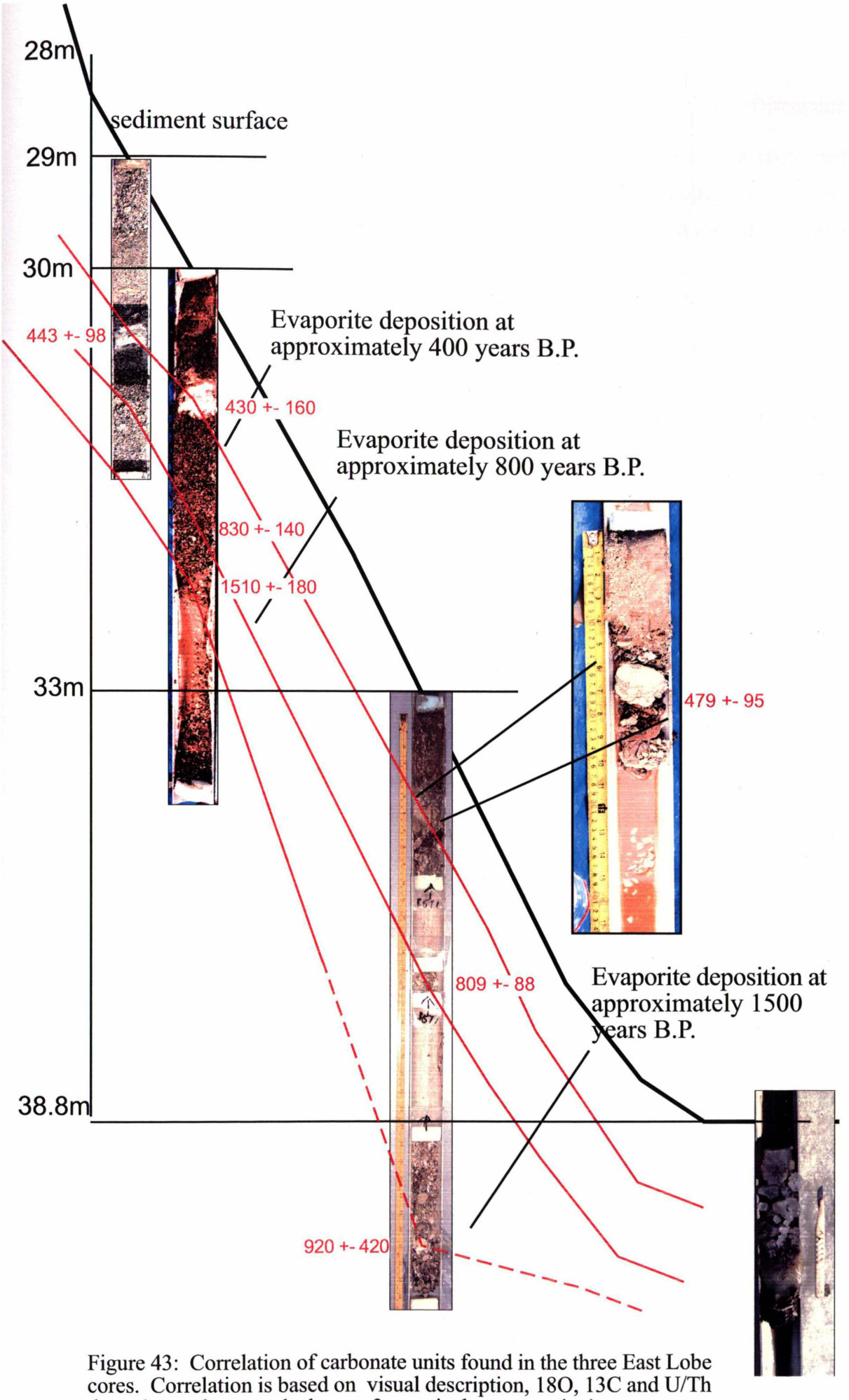

Figure 43: Correlation of carbonate units found in the three East Lobe cores. Correlation is based on visual description, 18O, 13C and U/Th dates (core photographs have a 3x vertical exaggeration).

Immediately prior to its deposition, a meltwater pulse, indicated by a co-variant depletion of $\delta^{18}O$ and $\delta^{13}C$ (Li 1997) from the depleted West Lobe waters (-40‰ $\delta^{18}O$, ~ 0‰ $\delta^{13}C$) inundated the East Lobe, causing a brief algal bloom and mixing of the lake water. Carbonate deposited from these waters has a depleted isotope signature. Immediately following the meltwater pulse, the East Lobe desiccated to low volume, concentrating the solutes causing precipitation of carbonate. Massive $\delta^{18}O$ enrichment (caused by fractionation during evaporation of an open water body) indicates the East Lobe could not maintain an ice cover at this time; this is likely due to extreme salinity of the water.

$\delta^{13}C$ progressively enriches throughout the carbonate deposition (from bottom to top), and was punctuated by three large enrichments, reaching a maximum of +11‰. These enrichments are concurrent with differing carbonate structure seen under the SEM, changing from radiating needles to a haystack style. The only mechanism able to enrich $\delta^{13}C$ to the values seen here is non-equilibrium fractionation, caused by rapid freezing excluding salts fractionating carbon between calcium carbonate and carbon dioxide. The carbonate with the haystack structure is interpreted as having formed in the water column or perhaps the ice cover (rather than growing in-situ from a nucleation point as seen in other carbonates), due to this rapid freezing. (Clark and Lauriol 1992) report the formation of a "cryptocrystalline" powder within the ice as a result of the freezing of a saline brine. It is possible that the haystack structure is analogous to the cryptocrystalline powder, and is released as the ice melts during summer, depositing as a layer.

Carbonate A is highly laminated, the layers being of different colour and thickness, the carbonate lamina are split by distinct, very thin clastic layers, visible under the optical microscope. The clastic lamina are likely the result of seasonal freezing of the lake ice (during the sub -60°C temperatures in the valley in winter), collecting windblown sediment (indicating that the lake was not ice-free year round). As the summer begins the ice cover is lost due to the temperature increase, and the collected sediment settles to the lake bottom as a layer. The lack of clastic material within the

carbonate lamina, likely indicates that the majority of the carbonate is deposited during winter as the ice cover thickens, excluding salts, driving carbonate to saturation. (Neumann *et al.* unpublished) commented on the seasonal changes of carbonate saturation in the Lake Bonney water column, and concluded that supersaturation is reached in winter.

Unit A may have been deposited over a relatively short (~20 potentially seasonal lamina), extremely cold period, with most carbonate precipitation during winter. At least three periods of extreme prolonged cold caused carbonate precipitation within the water column, or within the ice cover (haystack structure carbonate) coincident with non-equilibrium $\delta^{13}C$ enrichment.

Magnesium anomaly

Divalent cations such as Mg and Sr are expected to substitute into the precipitating carbonate lattice in increasing amounts as the concentration of the brine progresses (decreasing ratio Ca : Mg/Sr).

Mg increased prior to the deposition of carbonate A, consistent with a concentrating brine, but decreased to almost zero during the initial stages, then increased in the latter stages. Sr however, behaves as expected, and increases with respect to calcium through the unit (Figure 44), At the point where Mg begins increasing again Sr decreases. The haystack structure also corresponds with the low Mg content of the carbonate.

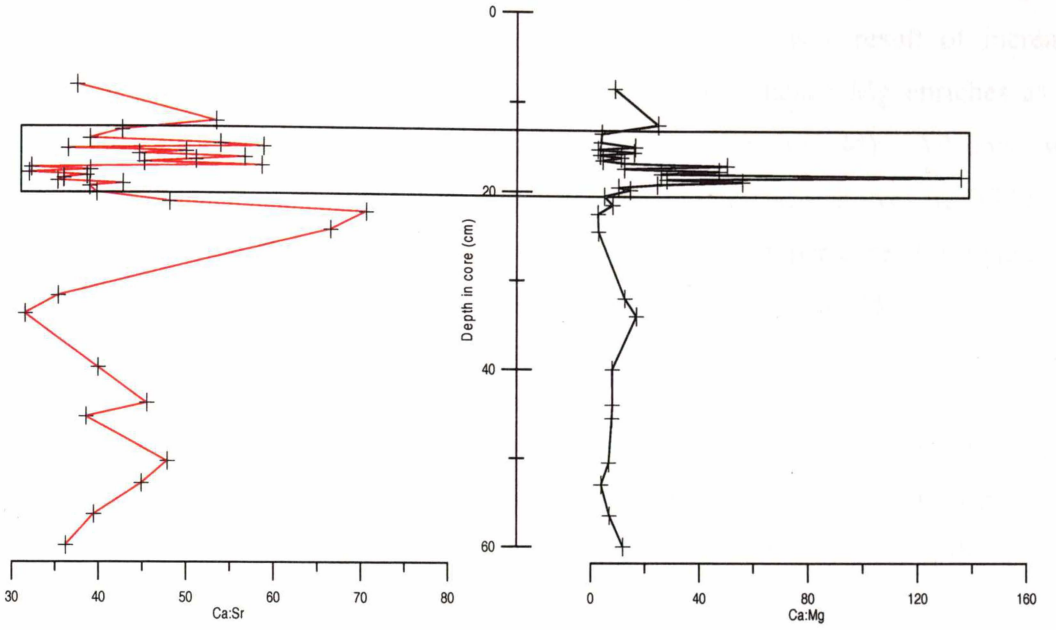

Figure 44: Ca:Mg and Sr ratios of B4T1. The ratio indicates a drreverse op in Mg and a rise in Sr through the initial stages of unit A, followed by the in the latter stages. The location of unit A is indicated by the box.

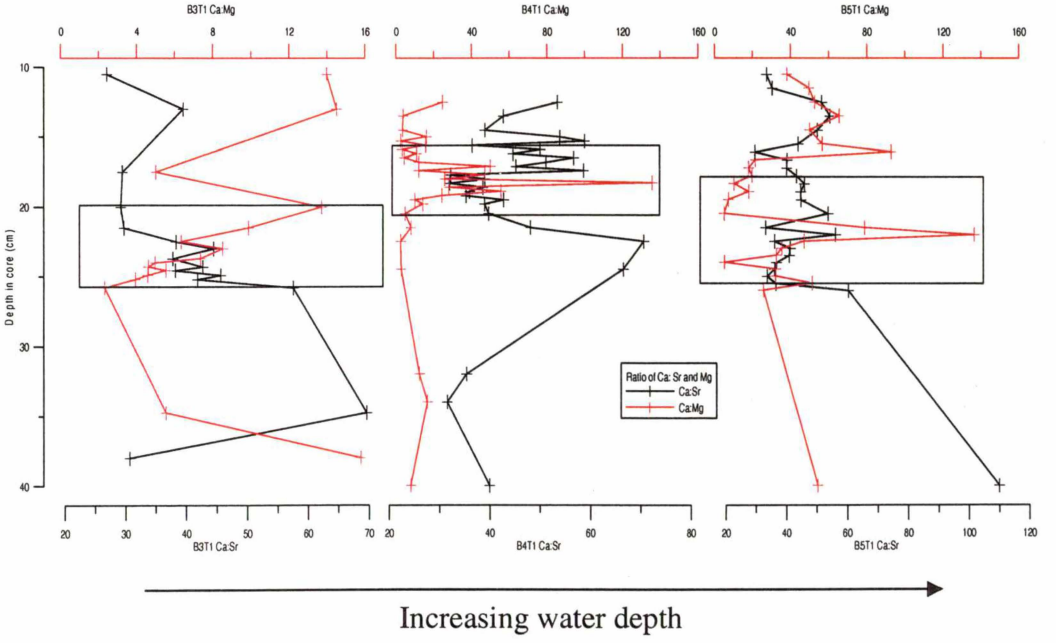

Figure 45: Ca : Mg and Sr, ratios through carbonate A for all East Lobe cores, showing Mg decreasing to almost zero, then increasing, and Sr increasing and decreasing concurrent with the Mg increase. The shallowest core has a much higher Mg content than the deeper cores through the unit.

It is possible that the lake became so concentrated it began to precipitate Mg salts (most likely $MgCl_2$). This $MgCl_2$, was then dissolved as a result of increased meltwater inflow, diluting the lake to below saturation, hence Mg enriches as the sediments dissolve, but Sr decreases due to dilution (Figure 44). All cores with carbonate A show this pattern of Mg depletion (Figure 45), however, B3T1 (the shallowest core) has a much higher Mg content that the deeper cores throughout the unit. B3T1 may have been above the saturated brine precipitating $MgCl_2$.

The unit ends with a two or three phase co-variant depletion of oxygen and carbon isotopes, there is also evidence of an algal bloom, and Ba, Fe and Mn all increase (the likely source of these elements is the dissolution of the valley bedrock.), these are all indicative of a significant meltwater input, Hendy et. al. (1977) record the meltwater input event in the diffusion profile of the water column, and predicted this event took place not less than 250 yr B.P. Hendy et al. (1977) had also predicted that the inundation was not a continuous event, rather several inflows, because the diffusion profile was not uniform, the $\delta^{13}C$ and $\delta^{18}O$ from carbonate formed in the lake at this time agrees with the diffusion profile.

Carbonate B: located at ~34cm depth, is ~ ½ cm thick, laminated and hard, its deposition occurred ~ 800 yr B.P. The structure of this unit is very similar to the structure in parts of unit A, inferred as being the result of extremely cold conditions freeze-concentrating the lake, causing precipitation either in the water column or within the ice.

Carbonate C: located at ~45cm depth, the oldest carbonate unit, is ½ cm thick, discoloured, laminated and hard. Its deposition occurred ~ 1500 yr B.P. Carbonate C also shows similarities in structure to the carbonate formed during parts of unit A. Isotope studies reveal that at this time the lake also lost its ice cover, allowing fractionation of ^{18}O.

A summary of these findings is given in Table 2.

Table 2: Summary of chemistry, visual and isotope character used to make climate inferences

	Above carbonate A	Carbonate A	Below carbonate A	Carbonate B	Carbonate C
Age	>250	450±100	<550	800 ± 100	1500 ± 100
Depth	> 20cm	~ 20 -25cm	< 25cm	~ 35cm	~ 45cm
Algae	Abundant	Absent	abundant	Not detectable	Not detectable
Isotope character	Co-variant depletion	Enrichment, loss of ice cover	Enriched, varying	Enriched	Enrichment, loss of ice cover
Calcium group chemistry (Ca Sr)	Stable	Increasing over unit, purity increases	Increasing	High	Increasing?
Alkali group chemistry Ba Fe Mn	Increase concurrent with isotope depletion (meltwater?)	Increase concurrent with isotope depletion (meltwater?)	Increase concurrent with isotope depletion (meltwater?)	Increase concurrent with isotope depletion (meltwater?)	Low
Na K Mg group chemistry	Diffusing into water column	Increasing, then decreasing as the salts precipitate	Stable	High	Increasing
SEM	radiating needles	Haystack needles covariant with isotope depletion, radiating needles between	radiating needles	Haystack needles	Haystack needles
Interpret-ation	Fluctuating climate, ice covered lake	Cold dry climate, ice free lake	Fluctuating climate, ice covered lake	Cold dry climate ice free lake	Cold dry climate ice free lake

These carbonate units are interpreted as having formed due to evaporative concentration caused by a period of cold arid climate, reducing meltwater inflow to the lake. The time of formation, provided by the U/Th dates can be used to correlate these inferred cold periods, with other proxy recorders of climate, such as the Taylor Dome ice record.

Figure 6 is reproduced here, and the timing of periods of aridity causing precipitation of calcium carbonate, are added for comparison (Figure 46).

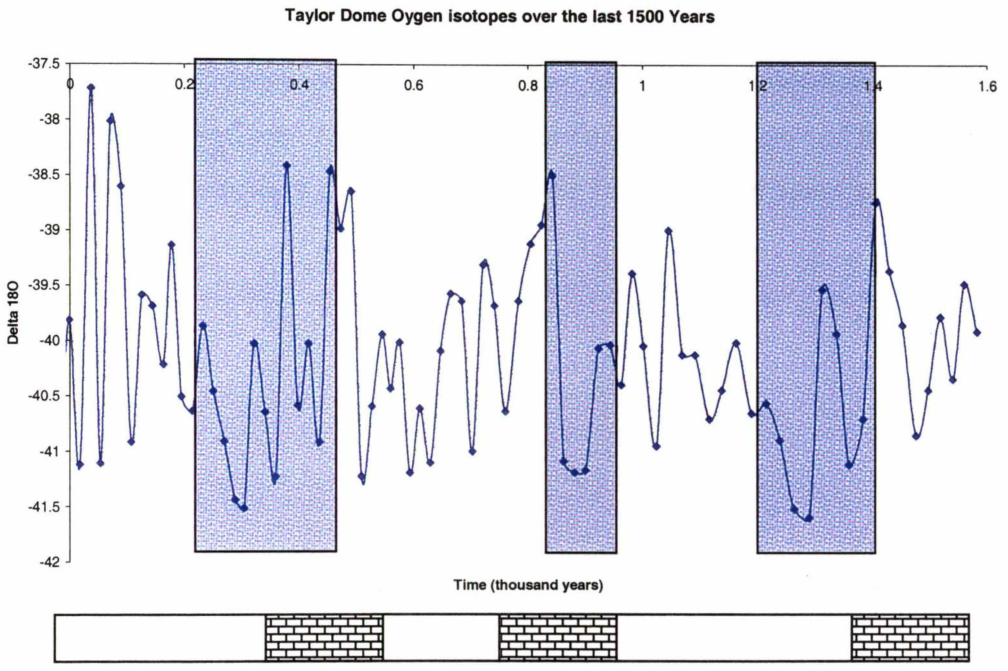

Unit A	Unit B	Unit C
430±160	830±140	1558±93
443±98	809±88	920±420
479±95		

Figure 46: 1600 year oxygen isotope record from Taylor Dome. Three prolonged cold periods are identified, and correlated with the 3 intervals of carbonate deposition in Lake Bonney.

Each carbonate unit can be correlated to a significant cold period recorded at Taylor Dome to within the error limits of the U/Th dates.

West Lobe

Gypsum occurs as debris in the basal ice of the Taylor Glacier, and forms a significant fraction of the "Blood Falls" salts flowing into West Lobe (Black *et al.* 1965; Black 1969; Keys 1979). The lobe is currently saturated in gypsum (Neumann *et al.* unpublished) and its first appearance in the sediments probably indicates the arrival of the Taylor Glacier snout in the lake. Minor occurrences prior to this are likely to be the result of evaporative concentration. Unfortunately gypsum is much more difficult to date using U/Th techniques, although samples have been provided, these have not yet been reported. If successful dates are obtained from West Lobe, they may help to resolve the problem of when Taylor Glacier snout arrived at the lake edge.

Chapter 6

Conclusion

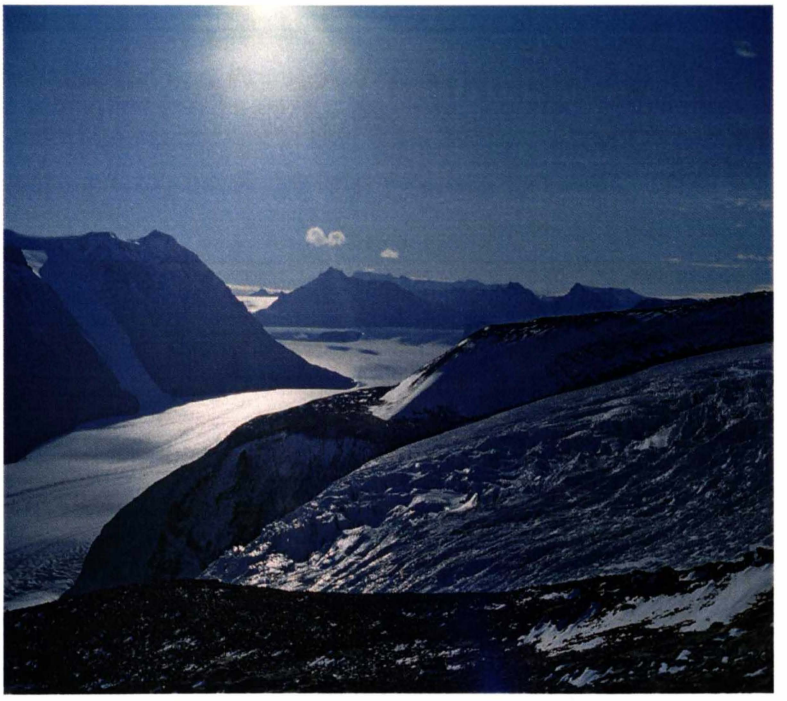

Looking west to Beacon Heights from Mt JJ Thompson

Conclusions

Between 125,000 and 80,000 yr B.P. (at least), Taylor Glacier occupied the whole of the Bonney Basin and was probably responsible for complete removal of any soluble salts. It is unclear what happened between 80,000yr B.P. and 26,000 yr B.P. (oldest date of Glacial Lake Washburn) but the absence of any sufficient fluvial channel from Fryxell Basin into Bonney Basin suggests that ice, or a lake continued to occupy the basin to about the present location of Lake Henderson.

Glacial Lake Washburn occupied Bonney Basin to an altitude of 326m a.s.l., and would have caused collapse and retreat of Taylor Glacier, possibly as far as Cavendish Rocks.

At approximately 14,000 yr B.P., Glacial Lake Washburn drops below the present Lake Bonney level, and the basin appears to desiccate, possibly to a small lake in the 250m below sea level depression near Pearse Valley.

Taylor Glacier begins to expand as the Ross Sea Ice Sheet retreats, first filling the large depression, then expanding down valley until it starts to flood Bonney Basin. As yet we have no dates on this event, but it had to be prior to 6000 yr B.P., when the present West Lobe obtained its diffusion profile.

By 1500, yr B.P., East Lobe had evaporated to low volume, producing a seasonal ice-free brine during a prolonged cold period. Three such events occur and can be identified as carbonate deposition phases in the cores from the East Lobe at 450± 160, 800 ± 100 and 1550± 140 yr B.P., concurrent with sustained cooling recorded at Taylor Dome. The last desiccation was severe enough to cause the precipitation of $MgCl_2$ (and possibly other relatively soluble salts) in the sediment.

Between the desiccation events, overflow from West Lobe into East Lobe causes temporary lake level rise. The last of the flooding events, starting at about 250 yr B.P.,

created a diffusion controlled gradient in the water column, locking the previously exposed brine beneath isotopically depleted Taylor Glacier waters.

This lake level rise continues to the present day.

The prolonged cool climate inferred from East Lobe carbonate sediments, is concurrent with a number of other proxy records from diverse locations around Antarctica, including:

- The Taylor Dome ^{18}O record at all three desiccations
- Lake sediments on James Ross Island at 1200 yr B.P.
- Lake sediments in the Vestfold Hills, 1200 and 450 yr B.P.

It is my contention that Lake Bonney sediments indicate widespread climate change at ~ 250-450 and 1200 - 1500 yr B.P., and local climate at 800 yr B.P.

REFERENCES

Abell, P. I. and I. Plug (2000). "The Pleistocene/Holocene transition in South Africa: evidence for the Younger-Dryas event." Global and Planetary Change 26: 173-179.

Angino, E. E. and K. B. Armitage (1963). "A geochemical study of Lakes Bonney and Vanda, Victoria Land, Antarctica." Journal of Geology 71: 89-95.

Angino, E. E., K. B. Armitage, et al. (1964). "Physiochemical limnology of Lake Bonney, Antarctica." Limnology and Oceanography 9: 207-217.

Ariztegui, D., M. M. Bianchi, et al. (1997). "Interhemispheric synchrony of late-glacial climate instability as recorded in pro-glacial lake Mascardi, Argentina." Journal of Quaternary Science 12: 333-338.

Bird, M. I., A. R. Chivas, et al. (1991). "Sedimentological and stable-isotope evolution of lakes in the Vestfold Hills, Antarctica." Palaeogeography, Palaeoclimatology, Palaeoecology 84(1-4): 109-130.

Bjorck, S., S. Olsson, et al. (1996). "Late Holocene paleoclimatic records from lake sediments on James Ross Island, Antarctica." Palaeogeography Palaeoclimatology Palaeoecology 121: 195-220.

Black, R. F., M. L. Jackson, et al. (1965). "Saline discharge from Taylor Glacier, Victoria Land, Antarctica." Journal of Geology 73(1): 175-181.

Black, R. F. (1969). "Saline discharges from the Taylor Glacier, Victoria Land, Antarctica." Antarctic Journal May-June: 89-90.

Blessing, R. H. (1995). Acta Cryst. **A51**: 33.

Bomblies, A., D. M. McKnight, et al. (2001). "Retrospective simulation of lake-level rise in Lake Bonney based on recent 21-yr record: indication of recent climate change in the McMurdo Dry Valleys, Antarctica." Journal of Paleolimnology 25: 477-492.

Broecker, W. S. (2001). "Was the Medieval Warm Period Global?" Science 291(5508): 1497-1499.

Bromley, A. M. (1985). Weather Observations: Wright Valley, Antarctica. New Zealand Meterological Service. Information Publication 11, New Zealand Meterological Service.

Bronge, C. (1992). "Holocene Climatic Record From Lacustrine Sediments in a Freshwater Lake in the Vestfold Hills, Antarctica." Geografiska Annaler 74a: 47-58.

Chinn, T. J. (1990). The Dry Valleys in Antarctica: The Ross Sea Region, Department of Scientific and Industrial Research.

Chinn, T. J. (1993). Physical hydrology of the Dry Valley Lakes. Physical and biogeochemical process in Antarctic Lakes: Antarctic research series. W. J. Green and E. I. Friedmann, American Geophysical Union. 59: 1-51.

Clark, I. D. and B. Lauriol (1992). "Kinetic enrichment of stable isotopes in cryogenic calcites." Chemical Geology (Isotope Geoscience Section) 102: 217-228.

Clow, G. D., C. P. McKay, et al. (1988). "Climatological Observations and Predicted Sublimation Rates at Lake Hoare, Antarctica." Journal of Climate 1: 715-728.

Cook, E. R., J. G. Palmer, et al. (2002). "Evidence for a 'Medieval Warm Period' in a 1,100 year tree-ring reconstruction of past austral summer temperatures in New Zealand." Geophysical Research Letters 29(14): 12-1 - 12-4.

Coplen, T. B. (1988). "Normalization of oxygen and hydrogen isotope data." Chemical Geology (Isotope Geoscience Section) **72**: 293-297.

Coplen, T. B. (1994). "Reporting of stable hydrogen, carbon, and oxygen isotopic abundances." Pure Applied Chemistry **66**: 273-276.

Craig, J. R., R. D. Fortner, et al. (1974). "Halite and Hydrohalite from Lake Bonney, Taylor valley, Antarctica." Geology 2(8): 389-390.

Denton, G. H., Stuvier, M. and Austin, K.G., 1985: Radiocarbon chronology of the last glaciation in the McMurdo Sound, Antarctica. Antarctic Journal of the United States, 20(5): 15-17.

Denton, G. and C. Hendy (1994). "The Younger-Dryas age advance of Franz Josef Glacier in the Southern Alps of New Zealand." Science 264: 1434-1437.

Denton, G. H., J. G. Bockheim, et al. (1989). "Late Wisconsin and Early Holocene Glacial History, Inner Ross Embayment, Antarctica." Quaternary Research 31(2): 151-182.

Des Marais, D. J. (1995). The biogeochemistry of hypersaline microbial mats, Plenum, New York.

Drewry, D. J., S. R. Jordan, et al. (1982). "Measured Properties of the Antarctic Ice Sheet: Surface Configuration, Ice Thinkness, Volume and Bedrock Characteristics." Annals of Glaciology 3: 83-91.

Eaton, A. P., L. S. Clesceri, et al. (1995). Standard methods for the examination of water and wastewater, Published jointly by; American Public Health Association, American Waterworks Association, WaterEnvironment Federation.

Fountain, A. G., W. B. Lyons, et al. (1999). "Physical controls on the Taylor Valley ecosystem, Antarctica." Bioscience 49(12): 961-971.

Group, U. S. i. c. w. (2003). United States Ice Core Science: recommendations for the future. http://www.nicl-smo.sr.unh.edu/documents/pdf/USICSExSumm.pdf: 1-4.

Gumbley, J. W. (1975): The sedimentology of three Antarctic lakes. (Unpublished M.Sc thesis lodged in the Library). M.Sc. University of Waikato,

Hall, B. (2001). Millennial-Scale Fluctuations of Dry Valley Lakes: Implications of Regional Climate Variability and the Interhemispheric (A)synchrony of Climate Change. Research Proposal

Hall, B., G. Denton, et al. (2000). "Evidence from Taylor Valley for a grounded ice sheet in the Ross Sea, Antarctica." Geografiska Annaler 82 A(2-3): 275-303.

Hall, B. and G. H. Denton (1995). "Late Quaternary lake levels in the Dry Valleys, Antarctica." Antarctic Journal of the United States 30(5): 52-53.

Hall, B. and G. H. Denton (2000). "Radiocarbon chronology of Ross Sea Drift, Eastern Taylor Valley, Antarctica: Evidence for a grounded ice sheet in the Ross Sea at the Last Glacial Maximum." Geografiska Annaler 82A(2-3): 305-335.

Hall, B., G. H. Denton, et al. (2001). "Glacial Lake Wright, a high-level Antarctic lake during the LGM and early Holocene." Antarctic Science 13(1): 53-60.

Hall, B., Denton, G., Hendy, C. (2000). "Evidence from Taylor Valley for a grounded ice sheet in the Ross Sea, Antarctica." Geografiska Annaler 82 A(2-3): 275-303.

Hendy, C. H. (1979). "The late Quaternary chronology of the Taylor Glacier." Memoirs of the National Institute of Polar Research special issue, 13: 204-205.

Hendy, C. H. (2000). "Late Quaternary lakes in the McMurdo Sound region of Antarctica." Geografiska Annaler Series a-Physical Geography 82A(2-3): 411-432.

Hendy, C. H., 2003: Lake level History and climate change in Antarctica. 2003 field season proposal to Antarctica New Zealand.

Hendy, C. H., T. R. Healy, et al. (1979). "Late Pleistocene Glacial chronology of the Taylor Valley, Antarctica, and the Global Climate." Quaternary Research 11(2): 172-184.

Hendy, C. H., 1977., Wilson, A. T., Popplewell, K. B. and House, D. A., 1977: Dating of geochemical events in Lake Bonney, Antarctica, and their relation to glacial and climatic changes. New Zealand journal of geology and geophysics, 20(6): 1103-1122.

Higgins, S. M., G. H. Denton, et al. (2000). "Glacial geomorphology of Bonney drift, Taylor Valley, Antarctica." Geografiska Annaler Series a-Physical Geography 82A(2-3): 365-389.

Higgins, S. M., C. H. Hendy, et al. (2000). "Geochronology of Bonney drift, Taylor Valley, Antarctica: Evidence for interglacial expansions of Taylor Glacier." Geografiska Annaler Series a-Physical Geography 82A(2-3): 391-409.

House, D., R. A. Hoare, et al. (1966). "Chemistry in the Antarctic." Journal of Chemical Education 43: 502-5.

Hughes, M. K. and H. F. Diaz (1994). "Was there a 'Medieval Warm Period', and if so, where and when?" Climate Change 26: 109-142.

Jouzel, J., G. Raisbeck, et al. (1989). "A Comparison of Deep Antarctic Ice Cores and their Impications for Climate Between 65, 000and 15, 000 Years Ago." Quaternary Research 31: 135-150.

Judd, F. M. (1986): The Chronology of the Ross Sea II Glaciation, a Glaciation of Illinoian Age. MSc Thesis. University of Waikato, Hamilton, New Zealand.

Keys, J. R. (1979). "Saline discharge at the terminus of the Taylor Glacier." Antarctic Journal of the United States 14: 82–85.

Keys, J. R., Williams, K. (1981). "Origin of crystalline, cold desert salts in the McMurdo region, Antarctica." Geochimica et Cosmochimica Acta 45(12): 2299-2309.

Lawrence, M. J. F. and C. H. Hendy (1985). "Water Column and Sediment Characteristics of Lake Fryxell, Taylor Valley, Antarctica." New Zealand Journal of Geology and Geophysics 28: 543-552.

Leng, M. J. and J. D. Marshall (2004). "Paleoclimate interpretation of stable isotope data from lake sediment archives." Quaternary Science Reviews **23**: 811-831.

Li, H.-C. and T.-L. Ku (1997). "d13C-d18O covariance as a paleohydrological indicator for closed-basin lakes." Palaeogeography Palaeoclimatology Palaeoecology 133: 69-80.

Livingston, D. (1965). "The use of filiment tape in raising long cores from soft sediment." Limnology and Oceanography **12**: 346-348.

Lowell, T. V., C. J. Heusser, et al. (1995). "Interhemispheric correlation of late Pleistocene glacial events." Science 269: 1541-1549.

Lyons, W. B., A. Fountain, et al. (2000). "Importance of landscape position and legacy: the evolution of the lakes in Taylor Valley, Antarctica." Freshwater Biology 43(3): 355-367.

LTER: http://huey.colorado.edu/LTER/images/maps/ap.html)

Lynde, S. R.

(Figure from http://ewr.cee.vt.edu/environmental/teach/smprimer/ise/ise.html#Howdothey).

Lyons, W. B., K. A. Welch, et al. (1998). "Chlorine-36 in the Waters of the McMurdo Dry Valley Lakes, Southern Victoria Land, Antarctica: Revisited." Geochimica et Cosmochimica Acta 62(2): 185-191.

Masson, V., F. Vimeux, et al. (2000). "Holocene climate variability in Antarctica based on 11 ice-core isotopic records." Quaternary Research 54: 348-358.

Matsubaya, O., H. Sakai, et al. (1979). "Antarctic saline lakes--stable isotopic ratios, chemical compositions and evolution." Geochimica et Cosmochimica Acta 43(1): 7-25.

Mayewski, P. A., W. B. Lyons, et al. (1995). "An ice-core based, Late Holocene history for the Transantarctic Mountains, Antarctica." Contributions to Antarctic research IV: Antarctic research series 67: 33-45.

Meyerhoff, ME and WN Opdycke. 1986. "Ion Selective Electrodes." Advances in Clinical Chemistry. 25:1-47

Moreno, P. I. and A. L. León (2003). "Abrupt vegetation changes during the last glacial to Holocene transition in mid-latitude South America." Journal of Quaternary Science 18: 787-800.

Nakai, N. (1974). Stable isotope studies of the salts, water and ice from Ross Island core and Lake Vanda. Dry Valleys Drilling Project Bulletin: 4: 46-47.

Neumann, K., W. B. Lyons, et al. (unpublished). "Biogeochemical cycling of calcium and carbon in streams and lakes of Taylor Valley, Antarctica."

Newnham, R. M. and D. J. Lowe (2000). "Fine-resolution pollen record of late-glacial climate reversal from New Zealand." Geology v. 28(8): 759-762.

Newnham, R. M., D. J. Lowe, et al. (1998). "A late Holocene and prehistoric record of environmental change from Lake Waikaremoana, New Zealand." The Holocene 8(4): 443-454.

Péwé, T. L. (1960). "Multiple glaciation in the McMurdo Sound region, Antarctica - A progress report." Journal of Geology 68: 498-514.

Poreda, R. J., A. G. Hunt, et al. (2004). "The Helium Isotopic chemistry of Lake Bonney, Taylor Valley, Antarctica: Timing of late Holocene climate change in Antarctica." Aquatic Geochemistry 10: 353-371.

Powell, R. D. (1981). "Sedimentation conditions in Taylor Valley, Antarctica, inferred from textural analysis of DVDP cores." Dry Valley Drilling Project, Antarctic research series 33(331-349).

Quay, P. D., S. R. Emerson, et al. (1986). "The carbon cycle of Lake Washington - A stable isotope study." Limnol. Oceanog 31: 596-611.

Schreiber, B. C. and M. El Tabakh (2000). "Deposition and early alteration of evaporites." Sedimentology 47: 215-238.

Sadler, A. J., 1989: Sedimentation in Antarctic proglacial lakes. University of Waikato Masters thesis.

Scott, R. F. (1905). The voyage of discovery, Smith Elder, London.

Sheldrick, G. M. (1997). SHELX97 programs for the solution and refinement of crystal structures,, University of Göttingen, Germany.

Smart and Saint (1996). Software Reference Manuals Version 4.0, Siemens Energy & Automation Inc., Madison, WI,.

Steig, E. J., D. L. Morse, et al. (2000). "Wisconsinan and Holocene climate history from an ice core at Taylor Dome, Western Ross Embayment, Antarctica." Geografiska Annaler 82a: 213-236.

Steig EJ, Hart CP, White JWC, Cunningham WL, Davis MD & Saltzman ES. Changes in climate, ocean and ice sheet conditions in the Ross Embayment at 6 ka. Annals of Glaciology 27, 305-310 (1998).

Steig EJ, Morse DL, Waddington ED, Stuiver M, Grootes PM. Wisconsinan Holocene climate history from an ice core at Taylor Dome, western Ross Embayment, Antarctica. Geografiska Annaler 82A: 213-235 (2000).

Stuvier, M., G. H. Denton, et al. (1981). History of the Marine ice Sheet in West Antarctica During the Last Glaciation: A Working Hypothesis. The Last Great Ice Sheets. G. H. Denton and T. J. Hughes, New York: Wiley Interscience.

Takamatsu, N., N. Kato, et al. (1998). "The origin of salts in water bodies of the McMurdo Dry Valleys." Antarctic Science 10(4): 439-448.

Thermo (2003). Orion Bromide / Chloride electrode instruction manual: 49.

Wright, H. E. J. (1967). "A square rod piston sampler for lake sediments." Journal of sedimentary petrology **37**: 975-976.

Thompson, D.C., 1973: Climate of the Dry Valleys area of South Victoria Land. New Zealand Geographical Society Conference series, 7: 259-265.

Weand, B. L., R. D. Fortner, et al. (1975). "Subterranean flow into Lake Bonney." Antarctic Journal of the United States 10(1): 15-19.

Webster, J., I. Hawes, et al. (1996). "Evidence for regional climate change in the recent evolution of a hight latitude pro-glacial lake." Antarctic Science 8(1): 49-59.

Whittaker, T. (2004): Lake level fluctuations in the Fryxell basin, Eastern Taylor Valley, Antarctica. University of Maine,

Wilson, A. T. (1964). "Evidence from Chemical Diffusion of a Climatic Change in the McMurdo Dry Valleys 1,200 Years Ago." Nature 201(4915): 176-177.

Wilson, A. T., C. H. Hendy, et al. (1974). "Dry valley lake sediments: a record of Cenozoic climatic events." Antarctic Journal July-August: 134-135.

APPENDIX 1

Location and details of all cores

B1T1	GPS unavailable	38.8m	Piston and core catcher
B1T2	"	"	"
B1T3	"	"	"
B1T4	"	"	"
B2T1	GPS unavailable	38.8m	Unsuccessful core
B3T1	GPS unavailable	29m	core catcher only
B3T2	"	"	core catcher only
B3T3	"	"	core catcher only
B3T4	"	"	core catcher only
B4T1	162° 26.512E 77° 42.998S	29.9m	Piston and core catcher
B4T2	Unsuccessful core		Piston and core catcher
B5T1	GPS unavailable	33m	Piston and core catcher
B6T1	77° 43.201S 162° 177E	41.1m	Core catcher
B7T1	77° 43.183S 162° 18.122E	21m	Core catcher
B8T1	Same as B7	21m	Core Catcher
B9T1	77° 43.169S 162° 18.355E		Core catcher
B10T2	No GPS		Core catcher

APPENDIX 2

Description of all cores not analysed

B6T1

0-38cm	Sloppy mixture of silt, sand and chunks of gypsum.
22cm	1cm lens of medium sand
32cm	1cm lens of medium sand
24-26cm	Band of yellow chunky material
31-32cm	Band of yellow chunky material
37-40cm	Compact gypsum, at its base it appears oxidized
40-43cm	Abrupt contact with well sorted, well washed sand.

B8T1

0-5cm fine	Medium fine sand, small (1-2mm) chunks of gypsum and brown silt.
5-30cm chunks of matrix.	Grading into matrix dominated by fine silt with large gypsum, and occasional coarse sand. Fine silt
30-35cm	Gypsum dominates, large chunks.
35-39cm well	Sharp contact to bright orange lamina, overlying 2cm of sorted medium sand. No silt present.

39-54cm approx	Grades down to a fine sand quickly, looks featureless, 10% silt in matrix.

B9T1

0-11.5cm Smell	Browny grey silt matrix, sloppy. Gypsum chunks 0.5-1cm. like the ocean. 5% sand in matrix.
11.5-19cm	Solid gypsum, pasty outside. 5% sand in matrix.
19-20cm	Very thin layer, slightly rolled over because of disturbance. Abrupt boundary at top, to well sorted medium grey sand.
20-28.5cm gravel	Semi abrupt boundary to poorly sorted coarse sand and (10%). Dark orange stain throughout this unit gradually weakening down core.
28.5-31.5 cm	Gradational boundary to finer sand, slight orange tarnish.
31.5- 32.5cm	Abrupt boundary to grey sandy silt.
32.5-36.5cm	Coarse sand, very slight orange tarnish.
36.5-37cm top.	Abrupt boundary to grey silt, 1mm thick orange layer at the
37-41cm	Abrupt boundary to coarse, poorly sorted grey sand.
41cm	Change to finer sand, to bottom of core.

B10T1

0-5cm 2.5cm.	Coarse gypsum, broken. Possible layer of coarse sand at Silty sand, grey pasty matrix.
5-9cm silt ½	Layer of medium sand 2-3mm, abrupt boundary to dry fine cm thick, with internal oxidation.
9-14.5cm well- layers	Very sharp contact to coarse sand, possible sorting gradient, poor, containing gypsum layers of 1-2mm thickness. 3 in upper part of unit.
14.5-15.5cm	thick diffuse layer of gypsum.
15.5-23.5cm contact	Well defined contact to well sorted medium-fine sand containing a 1cm layer of orange brown tinge, diffuse at either side.
23.5-45cm layer of 7-8mm. with lamina	Greenish grey silt 7-8mm, sharp contact, followed by a sand ½ cm thick. Another layer of greenish grey silt Very sharp contact to very fine sand, well sorted, of greenish brown tinge.

B10T2

5cm reworked material, gypsum and sand.

0-5cm	Medium fine sand, well sorted.
5cm	Disrupted sandy silt, ½ cm.
5-18cm sand 4-	Well sorted, medium grey sand. At 9cm, a brown tinge to 5mm. At 11cm, smaller, less pronounced colour.

18-22cm	Sharp contact to coarser grained, less well sorted.
22-29cm sand.	Grading down to coarse, sorted sand, from medium-fine
29-36cm	Greenish, silty sand, diffusely laminated throughout.
36cm describe	Coarser sand (disturbed by core catcher, difficult to further).

Appendix 3

Samples sent for U/Th dating.

0203 B4T1

Top - Run out from top of core.

15cm - Top of carbonate layer.

17cm - Middle of carbonate layer.

19.5cm - Bottom of carbonate layer..... 430± 160

40 cm -Carbonate block.....797± 68

47cm - Bottom of core before material flowed out, *ie* the last in situ carbonate, sample is hard and laminated.....1510± 180

0203 B3T1

15.5cm - Small carbonate biscuits.

19 cm - Small carbonate biscuits.....443± 98

34.5 cm - Poorly formed carbonate layer.

40 cm - Chunky carbonate layer.

0203 B3T3

22 cm - Small carbonate biscuits.....320± 480

24.5 cm

33 – 39 cm - Carbonate flakes in this range.....506± 14

46 cm - Carbonate plate.

0203 B5T1

15 cm -Fine white plates.

19 cm -Thin lamina present in large carbonate plates. Evaporite sequence present here, visible translucent crystal clasts.....641± 81

22 cm - Same unit as previous sample. 479± 95

26 cm - Same unit as previous sample.

40.5 cm - 40mm thick layer of very pure carbonate.....809± 88

63 cm - Large amount of thin white plates 1-4 mm thick.

73 cm - Chunky laminated plates, with thin dark layers, 20mm thick, 30mm wide.....920± 420

Samples analysed for isotopes and chemistry

B3T1

1. 1-6cm. Carbonate biscuit, grayish brown of irregular shape, very hard. No other similar biscuits in vicinity.
2. 8.5-9cm. Small white carbonate biscuits interspersed in sand matrix.
3. 10.5cm. Large hard carbonate biscuit, just after contact from large clasts to fine sand.
4. 13cm. Carbonate, white, thin, midway through sand unit.
5. 16cm. Small carbonate plate, in-situ, just prior to a layer of plates with a different matrix.
6. 17.5cm. Softer greeny material with lamina of what appears to be carbonate. This is a layer.
7. 20cm. Carbonate after greeny layer, but before evaporite sequence.

8. 21.5cm. Top of evaporite sequence, large chunks of carbonate, not a continuous layer, after is a sand matrix again.
9. 22.5cm. Half way through a very white layer.
10. second half of very white layer.
11. Grey green material, 0.3cm width.
12. 0.2cm green layer with fine lamina, green –white-green- white.
13. 0.2cm sample taken to bottom of grey/green layer.
14. 0.2cm sandy material in this part of the core.
15. 0.2cm very sandy, almost a layer.
16. 0.2cm last of evaporite sequence.
17. Green material, soft, at bottom of evaporite sequence.
18. 34.5-36cm. very small pure carbonate flakes, large grain size in matrix.
19. 38cm. A very large plate, grey/green in colour.
20. 43.5cm. A very large plate at 43.5cm, hard, obviously laminated.

B3T3

1. 0-5cm. Small carbonate plates
2. 5-10cm. Small carbonate plates
3. 10-15cm. Small carbonate plates
4. 15-20cm. Small carbonate plates, some larger.
5. 20-25cm. Small carbonate plates

This core appears to have a disturbed section, possibly slumped from previous coring attempts.

6. 25-30cm Small carbonate plates
7. 30-35. Carbonate becoming soft. Biological material obvious.
8. 35-37.
9. 37cm. Start of disturbed evaporite sequence.

10.
11.
12.
13.
14.
15. Evaporite deposit.
16. Samples evenly spaced over 5cm.
17.
18.
19.
20.
21.

22. 42-42.5cm.
23. 42.5-43cm.
24. 43-43.5cm.
25. 43.5-44cm.
26. 44-44.5cm
27. 44.5-45cm.

Fine grained sand containing soft carbonate throughout. Samples taken at even intervals across this unit.

B3T4

Sample #	Depth (cm)	Notes	Sample #	Depth (cm)	Notes
1	0-5		**17**	43-43.5	
2	5-10		**18**	43.5-44	algae
3	10-15		**19**	44-44.5	
4	15-20		**20**	44.5-45	
5	20-25		**21**	45-46	
6	25-30		**22**	46-47	
7	30-32		**23**	47	Large plate at 47cm very hard carbonate, added 2ml more acid
8	32-34		**24**	47-48	
9	34-36		**25**	48-49	
10	36-38	algae	**26**	49-50	
11	38-40	a lot of algae	**27**	50-51	
12	40-42	a lot of algae	**28**	51-52	
13	41-41.5		**29**	52-53	
14	41.5-42		30	53-54	
15	42-42.5		31	54-55	
16	42.5-43				

Hard laminated CO_3 at the bottom of this core was split along the lamina. 5 samples in total.

B4T1

A= Carbonate plate sampled

B= Sand matrix containing carbonate sampled

The sand was found to have a carbonate coating, therefore the sand was sampled

1. 0-1cm	B	Top Sand containing carbonate.
2. 2-3cm	B	small carbonate flecs
3. 3-4cm	B	
4. 4-5	B	
5. 5-6	B	
6. 6-7	B	
7. 7-8	B	A change from fine to coarse sand
8. 8-9	A&B	
9. 9-10	B	
10. 10-11	B	
11. 11-12	B	
12. 12-13	A&B	
13. 13-14	A&B	
14. 14-15	A&B	Top of evaporite seq.
15. 20-21	B	
16. 21-22	A&B	
17. 22-23	A&B	
18. 23-24	B	
19. 24-25	A&B	
20. 25-27	B	
21. 27-29	B	very coarse sand
22. 29-31	B	
23. 31-33	A	some large carbonate plates
24. 33-35	A	
25. 35-37	A&B	a very large stone present 1.5cm

26. 37-39	B	very coarse sand, no visible carbonate
27. 39-41	A	a very large stone present 1.5cm
28. 41-43	B	
29. 43-45	A&B	
30. 45-46	A	
31. 46-47	A	
32. a – f in middle each	A	soft carbonate, greenish coating, pure white laminated evap seq found here, sampled each lamina. 6 samples in total
33. 49	A	Fine sticky clay here also
34. 50	A&B	
35. 51-55	A&B	Material has "run out" of core
36. 55-58	A&B	
37. 58-62	A&B	
38. 62-66	A	
39. 67	B	large lump of sticky silty material
40. 66-70	A	

B5T1

This core consisted almost entirely of carbonate, the first 10cm a matrix including some sand. Evaporite sequences were found at 18cm and 23cm, although the 23cm sample could be a continuation of the previous sequence.

#	Depth (cm)			#	Dept (cm)		
1	1-2			24	evap	7	Broken carbonate
2	2-3			25	20-21		
3	3-4			26	21-22		
4	4-5			27	22-23		
5	5-6			28	evap	1	
6	6-7		Sandy	29	evap	2	
7	7-8			30	evap	3	
8	8-9			31	evap	4	
9	9-10			32	evap	5	
10	10-11			33	evap	6	
11	11-12			34	evap	7	
12	12-13			35	evap	8	Broken carbonate
13	13-14			36	evap	9	
14	14-15			37	39-41		
15	15-16			38	62-64		
16	16-17	Broken carbonate		39	64-66		
17	17-18			40	66-68		

18	evap	1	Hard block, re-oriented	41	68-70
19	evap	2	Due to disturbance	42	70-74
20	evap	3		43	74-76
21	evap	4		44	76-78
22	evap	5		45	78-80
23	evap	6			

B7T1

West Lobe

# (cm)	Run out from top of core	# (cm)	Orange stained
1. 0-1	sand	17. 16-17	
2. 1-2		18. 17-18	
3. 2-3		19. 18-19	
4. 3-4		20. 19-20	Sand
5. 4-5		21. 20-21	
6. 5-6		22. 21-22	
7. 6-7		23. 22-23	
8. 7-8		34. 23-24	
9. 8-9	Gypsum	25. 24-25	
10. 9-10		26. 25-26	
11. 10-11		27. 26-27	
12. 11-12		28. 27-28	
13. 12-13		29. 28-29	
14. 13-14	Hard	30. 29-30	
15. 14-15	Gypsum Block	31. 30-31	
		32. 31-32	
			Algae

APPENDIX 4

Table 4a: AAs reproducibility and external standards

Quality control

AAS reproducibility and external standards.

El	Sample	Conc.	Conc.	%error	Na independent calibration standards			
						Measured	Diff	
Na	B4T1 2-7	121.49	120.24	1.03	actual	(mg/l)	mg/l	%diff
	B4T1 2-9	104.32	105.52	1.14	std 25	25.395	0.395	1.58
	B4T1 1	545.03	537.52	1.38	std 25	25.971	0.971	3.884
	B4T1 3	229.31	240.23	4.55	std 25	25.769	0.769	3.076
	B4T1 9A	85.85	89.48	4.06	std 25	26.069	1.069	4.276
	B4T1 13A	320.26	354.44	9.64	std 25	26.426	1.426	5.704
	B4T1 16B	72.55	73.12	0.77	std 50	52.944	2.944	5.888
	B4T1 23A	69.79	71.27	2.09	std 50	52.685	2.685	5.37
	61	66.16	67.79	2.40	std 50	51.762	1.762	3.524
	62	37.73	36.26	3.91	std 50	53.379	3.379	6.758
	63	81.75	83.75	2.38	std 50	52.075	2.075	4.15
	65	144.93	143.55	0.96	std 50	52.652	2.652	5.304
	68	269.34	270.07	0.27	std 100	102.587	2.587	2.587
	70	390.92	394.17	0.82	std 100	101.307	1.307	1.307
	71	430.73	431.49	0.18	std 100	99.46	-0.54	-0.54
	72	153.59	156.12	1.62	std 100	101.249	1.249	1.249
	73	235.45	236.60	0.49	std 100	102.29	2.29	2.29
	74	202.11	203.02	0.45	std 100	105.724	5.724	5.724
			%					
			error	2.12		average	1.92	3.65
Ca	12	4.03	3.86	4.27				
	23	9.23	9.71	4.99				
	41	5.46	5.31	2.75				
	45	7.12	7.01	1.57				
			%					
			error	3.39				
					K independent calibration standards			
K	B4T1 2-1	3.36	3.50	3.89	9.78	10.00	2.18	2.18
	B4T1 2-2	4.56	4.63	1.53	10.40	10.00	-3.99	3.99
	B4T1 2-3	2.48	2.36	4.73	10.25	10.00	-2.45	2.45
	B4T1 2-4	6.58	6.41	2.60	10.06	10.00	-0.58	0.58
	B4T1 2-5	2.93	2.82	3.96	9.93	10.00	0.75	0.75
	B4T1 2-6	5.32	4.87	8.58	9.79	10.00	2.06	2.06
	B4T1 2-7	9.01	8.23	8.64	10.16	10.00	-1.55	1.55
	B4T1 2-8	4.17	3.84	8.10	20.27	20.00	-1.36	1.36
	9	6.31	6.90	8.62	20.05	20.00	-0.23	0.23
	7	6.36	6.36	0.03	19.94	20.00	0.32	0.32
	5	5.29	5.19	1.98	19.87	20.00	0.66	0.66
	12	12.44	11.61	6.65	20.69	20.00	-3.42	3.42
	B4T1 41A	6.23	6.38	2.35	20.28	20.00	-1.41	1.41
	B3T3 33	24.16	24.30	0.58	20.47	20.00	-2.36	2.36
	B3T3 35	15.75	15.14	3.87			% error	1.67

B3T3 43	29.50	31.88	7.47
		% error	4.60

Table 4b: ICP-OES quality control

ICP-OES Quality control.

External reference standard diluted to 25, 50 and 100 ppm.

	Ba	Ca	Fe	Mg	Mn	Sr	U * not used
blank	-1.07	-0.89	-0.61	-1.27	-0.53	-1.35	-0.02
blank 1	-0.60	-0.65	-0.51	-1.20	-0.53	-1.34	0.13
blank 2	-0.63	-0.65	-0.59	-1.30	-0.53	-1.35	0.05
blank 3	-0.66	-0.59	-0.59	-1.28	-0.53	-1.34	0.01
blank 4	-0.65	-0.53	-0.60	-1.29	-0.53	-1.35	-0.04
std 25 1	25.80	24.76	26.22	25.84	26.65	25.98	1.89
std 25 2	25.78	25.24	26.66	25.19	26.18	26.12	2.00
std 25 3	26.19	25.38	26.53	25.63	26.37	26.23	2.10
std 25 4	25.76	25.11	25.52	24.85	26.29	26.05	2.00
std 25 5	25.67	25.47	25.41	25.11	25.98	25.64	2.06
std 25 6	25.62	24.67	25.23	25.16	25.39	25.53	2.13
std 25 7	25.60	25.97	25.78	25.24	26.01	25.77	1.95
std 25 8	26.64	26.14	26.66	26.48	26.32	27.27	2.12
std 25 9	26.27	25.98	26.68	26.34	26.94	26.70	2.05
std 50 1	51.12	49.74	49.07	50.28	50.62	51.96	3.75
std 50 2	51.42	49.76	48.84	49.29	51.11	50.34	3.62
std 50 3	50.51	50.16	49.12	50.17	50.22	51.29	3.71
std 50 4	49.88	49.58	49.00	48.29	49.46	49.65	3.68
std 50 5	49.76	50.06	48.35	49.69	50.29	51.15	3.78
std 50 6	50.24	48.41	48.73	49.37	48.91	50.49	3.86
std 50 7	51.19	50.91	49.09	50.73	49.90	51.75	3.87
std 50 8	51.95	50.68	49.35	53.26	52.28	53.51	4.11
std 50 9	51.55	50.97	49.20	52.09	52.08	53.21	3.84
std 100 1	99.68	98.09	48.94	97.51	97.87	100.29	7.33
std 100 2	99.20	97.96	49.04	97.72	97.32	100.41	7.16
std 100 3	100.43	99.56	49.13	96.86	99.08	101.78	6.79
std 100 4	97.61	98.55	49.17	94.47	95.91	97.54	6.95
std 100 5	99.31	98.00	49.17	98.25	97.44	99.87	7.60
std 100 6	98.87	97.83	49.17	97.28	96.27	97.53	7.11
std 100 7	99.35	98.19	49.16	98.19	99.12	101.75	7.28
std 100 8	103.70	99.11	49.11	101.65	102.14	103.90	7.93
std 100 9	101.12	100.28	49.11	101.54	99.97	103.97	7.84

Table 4c: AAS ICP comparison for Ca

AAS / ICP comparison for Ca (mg/l)

Sample	ICP-OES	AAS (dil 100x)	% Diff
B3T3 10-15	474.60	492.06	3.55

B3T3 37	701.90	710.94	1.27
B3T3 EVAP 0-0.5	453.60	463.76	2.19
B3T3 EVAP 0.5-1.0	607.10	571.70	-6.19
B3T3 EVAP 1.5-2.0	1053.10	1038.8	-1.37
B3T3 EVAP 2.0-2.5	970.90	979.37	0.86
B3T3 EVAP 2.5-3.0	1210.80*	1244.77	*-7.09*
B3T3 42-42.5	638.10	651.95	2.12

* Outside of calibration range of ICP-OES

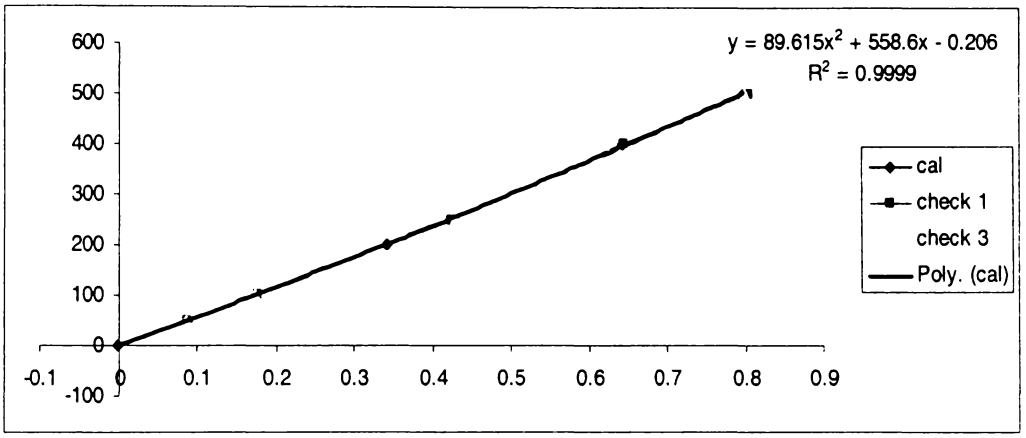

Calibration check example graph.

APPENDIX 5

INTRUCTIONS FOR THE USE OF THE VACUUM LINE

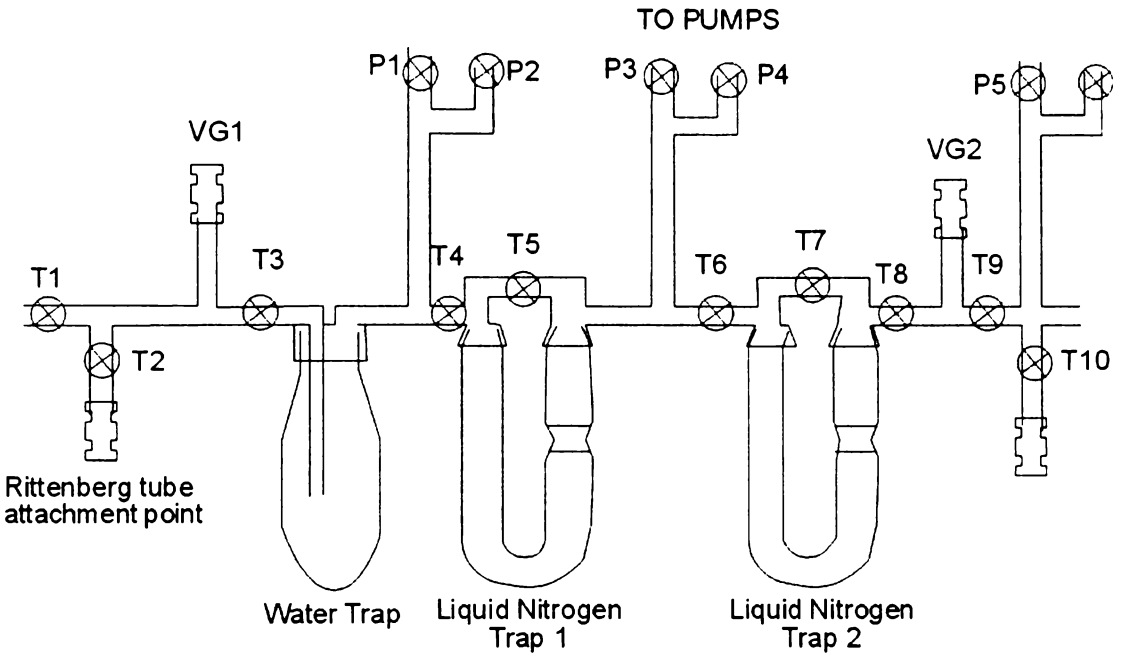

Figure : Vacuum system used in the extraction of CO_2 from carbonate samples.

1. Prepare two dewers with a 50/50 mixture of isopropanol and ethanol, chill these with liquid nitrogen; - one to –80 °C to –110 °C and the other to a temperature of –50 °C.

2. Fill another three dewers with liquid nitrogen.

3. Place liquid nitrogen on the two vacuum line manifold traps. Ensure that the rotary and vacuum pumps are operating.

4. Place the –50 °C isopropanol/ethanol mixture on to T2 and the three liquid nitrogen dewers on to T1 T3 and T4.

5. Close taps T10, T7, T3, T5, P2, P3, P4 and P5.

6. Open taps T9, T8, T4, T3, P1 and P6.

7. Allow the system to come under vacuum.

8. Close P1,and open T2 and T4. When the system returns to vacuum, the sample gas is frozen in Liquid Nitrogen trap 1.

9. Close T2, T4 and T9. Open P1 and T6. Place sample collection vial on swage-lock 3, open T10.

10. Replace Liquid nitrogen dewar with slush dewar on liquid nitrogen trap 1. The gas is now freezing in liquid nitrogen trap 2. Observe VG2, when system returns to vacuum, sample is frozen.

11. Close T6, T8 and P1. Open T9 and P3. Observe VG2, if vacuum is reached, sample vial is ready for sample, if not, wait until vacuum is reached. Place a liquid nitrogen dewar on sample vial.

12. Close P6. Open T8. Replace liquid nitrogen dewar on liquid nitrogen trap 2 with a slush dewar. The sample is now being frozen into the sample vial. When VG2 returns to vacuum, all sample is frozen.

13. Close T10. Open P5.

14. Open the tap to both of the pumps, and working back from the right hand side, open all the taps to allow any gas remaining in the line to be pumped away.

15. Start again at step 5 for the next sample ensuring that the temperatures of the two Isopropanol/ethanol mixtures have not changed.

APPENDIX 6

Instrument conditions

AAS

Fuel flow	2.01 l/min
Air flow	10.0 l/min
Lamp current	5mA
Slit width	0.5
Slit height	normal
Read time	5s
Replicates	3
Ca	239.9nm
Mg	202.6nm
Na	330.2nm
K	769.9nm

ICP-OES

Aux gas flow	0.87
Nebuliser gas flow	0.30
Plasma gas flow	12.05
Mg	383.826nm
Ca	643.907nm
Fe	238.204nm
S	182.625nm
Mn	294.920nm
Ba	614.172nm
Sr	216.596nm
U	367.007nm

APPENDIX 7

Raw data

B3T1

This was the first core processed

These samples are all CO3 biscuits taken in situ in the core	depth in core (cm)	weight (g)	Ca (mg/g)	Mg mg/g	S mg/g	Sr mg/g	K mg/g	Mn mg/g	Ba mg/g	Fe mg/g	Na mg/g	d13Cv pdb	d18O vpdb
B3T1 1	6	0.0967	303.40	14.92	0.39	10.96	1.90	0.04	0.06	0.01	21.04	7.63	-23.3
	9			BROKEN								5.81	
B3T1 3	10.5	0.0792	251.24	17.98	0.40	9.36	2.62	0.04	0.09	0.08	24.05	7.38	-26.35
B3T1 4	13	0.0231	227.42	15.68	0.51	5.77	2.63	0.02	0.41	0.08	25.26	8.26	-22.33
	16			BROKEN								7.32	
B3T1 6	17.5	0.0655	170.10	33.89	0.59	5.78	4.73	0.08	0.13	0.14	49.10	9.7	-20.17
B3T1 7	20	0.045	246.14	17.93	0.47	8.44	2.47	0.03	0.25	0.03	26.09	10.61	-20.65
B3T1 8 evap	21.5	0.1852	237.23	24.00	0.35	7.98	2.80	0.05	0.08	0.05	32.11	10.58	-19.49
B3T1 9 evap	22.5	0.0496	186.86	29.41	0.46	4.88	3.41	0.03	0.25	0.05	37.60	10.63	-19.46
B3T1 10 evap	23	0.0762	220.37	25.84	0.48	4.96	2.68	0.04	0.10	0.02	33.77	7.23	-21.69
B3T1 11 evap	23.7	0.0633	194.30	26.34	0.40	5.15	2.77	0.00	0.12	0.01	32.66	7.19	-21.53
B3T1 12 evap	24	0.042	150.35	30.21			4.07	0.06	0.22	0.01	36.47	7.44	-21.89
B3T1 13 evap	24.3	0.0247	145.30	31.44	0.53	3.40	3.62	0.04	0.32	0.03	38.29	7.31	-21.72
B3T1 14 evap	24.55	0.082	172.67	31.10	0.32	4.52	2.96	0.01	0.10	0.00	32.47	7.1	-21.61
B3T1 15 evap	24.9	0.0476	136.76	29.81	0.33	3.00	3.12	0.00	0.21	0.02	42.57		
B3T1 16 evap	25.2	0.0524	144.08	36.55	0.34	3.44	3.66				35.82		
B3T1 17	25.8	0.0337	103.25	44.42	0.48	1.80	6.78	0.02	0.23	0.04	47.73	NaCl	
B3T1 18	34.75	0.0191	146.69	26.43	0.65	2.11	4.76	0.09	0.40	0.17	30.34	contamination	
B3T1 19	38	0.133	271.17	17.18	0.34	8.85	2.38	0.01	0.05	0.00	22.33		
B3T1 20	43.5	0.1001	319.23	15.02	0.41	10.83	1.94	0.07	0.07	0.01	18.69		

B3T3

Sample name	depth in core (cm)	Weight (g)	Ca mg/g	Mg mg/ g	Mn mg/g	S mg/g	Sr mg/g	K mg/g	Na mg/g	d13Cvpdb	d18Ovpdb
B3T3 0-5	2.5	0.09	123.31	30.16	-0.14	0.22	3.24		49.59	8.91	-26.12
B3T3 5-10	7.5	0.09	263.64	24.97	-0.13	0.29	7.49	2.88	34.30	9.39	-25.79
B3T3 10-15	12.5	0.10	242.14	17.63	-0.14	0.27	7.29	1.89	29.78	8.23	-27.96
B3T3 15-20	17.5	0.07	188.93	31.29	-0.19	0.27	4.73	4.77	28.01	7.74	-27.21
B3T3 20-25	22.5	0.08	261.48	17.49	-0.16	0.28	8.37	2.08	36.12	9.47	-23.37
B3T3 25-30	27.5	0.14		17.10	-0.02	0.30	7.77	2.42	57.93	9.19	-22.87
B3T3 30-35	32.5	0.22	146.04	20.25	0.05	0.20	4.46	3.48	10.72	10.73	-21.5
B3T3 35-37	36	0.16	129.05	30.44	0.02	0.21	3.37	3.98	32.47	10.61	-21.65
B3T3 37	36.5	0.26	133.64	34.54	0.06	0.22	3.36	4.72	61.01	6.76	-21.54
B3T3 sand	37	0.08	108.88	30.41	-0.11	0.20	2.64		47.05	8.44	-21.86
B3T3 EVAP 0-0.5	37.25	0.20	112.22	27.86	0.07	0.18	2.99	3.98	32.91	7.48	-20.69
B3T3 EVAP 0.5-1.0	37.75	0.26	118.39	27.15	0.07	0.18	3.13	3.75	40.25	7.69	-23.57
B3T3 EVAP 1.0-1.5	38.25	0.47	74.92	26.03	0.04	0.18	3.35	3.04	31.86	7.33	-22.36
B3T3 EVAP 1.5-2.0	38.75	0.46	114.97	26.75	0.07	0.18	3.17	3.03	29.79	6.68	-21.51
B3T3 EVAP 2.0-2.5	39.25	0.42	115.69	25.61	0.04	0.17	3.25	2.45	29.33	6.52	-21.98
B3T3 EVAP 2.5-3.0	39.75	0.58	105.23	28.59	0.03	0.16	2.60	2.46	36.77	5.79	-21.28
B3T3 EVAP 3.0-3.5	40.25	0.01			2.81					6.02	-22.2
B3T3 EVAP 3.5-4.0	40.75	0.32	110.90	29.02	0.18	0.17	2.67	3.21	36.80	6.18	-23.17
B3T3 EVAP 4.0-4.5	41.25	0.34	108.57	33.63	0.19	0.17	2.67	4.13	42.74	7.84	-22.63
B3T3 EVAP 4.5-5.0	41.75	0.33		28.10	0.09	0.19	3.71	3.65	31.79	7.61	-23.5
B3T3 EVAP 5.0-5.5	42.25	0.16	127.39	33.91	0.08	0.25	3.86	4.82	38.96	8.69	-21.93
B3T3 42-42.5	42.5	0.29	111.21	27.83	0.12	0.19	3.53	3.91	34.22	9.4	-21.99
B3T3 42.5-43	43	0.19	110.90	28.14	0.10	0.20	3.36	4.37	37.22	8.66	-22.73
B3T3 43-43.5	43.5	0.23	115.87	24.69	0.11	0.18	3.63	4.01	37.86	7.57	-23.63
B3T3 43.5-44	44	0.44	107.72	24.10	0.11	0.15	3.40	3.66	30.40	8.87	-22.3

B3T3 44-44.5	44.5	0.35	102.24	29.02	0.16	0.17	3.23	4.31	37.23	6.9	-21.38
B3T3 44.5-45	45	0.30	98.71	29.77	0.11	0.17	3.02	4.30	30.53	6.91	-24.78
B3T3 45-45.5	45.5	0.25	194.66	50.85	0.26	0.27	5.37	7.34	61.07	8.02	-22.15
B3T3 45.5-46	46	0.28	236.96	35.13	0.17	0.29	7.34	4.51	43.16	5.82	-21.66
B3T3 46-46.5	46.5	0.25	148.15	33.88	0.15	0.24	4.75	5.61	41.41	8.7	-22.56
B3T3 46.5-47	47	0.18	166.37	45.86	0.12	0.27	5.00	6.36	62.53	8.53	-21.86
B3T3 47-47.5	47.5	0.31	168.29	39.15	0.14	0.26	5.73		73.56	7.43	-24.87
B3T3 47.5-48	48	0.50	67.54	12.19	0.03	0.11	2.19		52.87	7.53	-23.61

B3T4

	distance down core cm	weight (g)	Ca (mg/g)	Mg (mg/g)	Mn (mg/g)	S (mg/g)	Sr (mg/g)	K (mg/g)	Na (mg/g)	d13Cvpdb	d18Ovpdb
B3T4 1	2.50	0.11	89.56	59.02	-0.04	0.25	3.01	8.27	82.71	7.13	-28.94
B3T4 2	7.50	0.05	80.43	59.77	-0.36	0.40	1.06	9.06	73.36	8.75	-25.57
B3T4 3	12.50	0.03	100.43	70.63	-0.45	0.42	0.76	10.23	60.02	8.6	-24.23
B3T4 4	17.50	0.05	82.30	57.19	-0.15	0.36	1.04	9.33	89.28		
B3T4 5	22.50	0.04	124.51	56.79	-0.21	0.47	2.07	9.04	98.07	7.18	-26.52
B3T4 6	27.50	0.09	99.85	60.11	0.05	0.33	2.43	8.82	78.94		
B3T4 7	31.00	0.14	71.00	44.62	0.11	0.39	5.93	6.22	60.66	9.11	-22.22
B3T4 8	33.00	0.18	55.13	41.40	0.13	0.40	5.77	6.71	62.36		
B3T4 9	35.00	0.25	37.17	28.51	0.16	0.38	6.87	5.40	53.04	8.62	-22.25
B3T4 10	37.00	0.51	17.78	13.84	0.14	0.38	5.68	5.06	55.89	9.31	-21.66
B3T4 11	39.00	0.28	34.19	25.64	0.25	0.42	4.88	7.07	70.11	8.44	-22.7
B3T4 12	40.50	0.31	30.65	23.00	0.24	0.41	4.74	7.33	69.59	8.17	-22.89
B3T4 13	41.25	0.12	83.78	49.63	0.15	0.42	4.95	7.02	66.03	8.13	-22.95
B3T4 14	41.75	0.22	43.01	32.94	0.03	0.38	5.86	5.12	53.41	6.63	-21.78
B3T4 15	42.25	0.17	55.07	40.88	0.06	0.39	5.51	5.72	58.04	6.08	-21.29
B3T4 16	42.75	0.17	55.10	41.30	0.10	0.39	5.07	5.76	59.30	7.61	-22.32
B3T4 17	43.25	0.18	52.71	39.64	0.04	0.40	5.28	5.47	56.08	6.04	-22.43
B3T4 18	43.75	0.22	43.16	32.75	0.12	0.40	5.13	5.82	59.68	8.35	-22.69
B3T4 19	44.25	0.13	75.29	48.92	0.32	0.44	4.99	7.99	66.50	8.75	-22.06
B3T4 20	44.75	0.19	49.55	37.48	0.51	0.40	5.73	7.53	62.17	6.4	-21.86
B3T4 21	45.50	0.32	29.69	22.51	0.32	0.42	5.35	6.71	64.43		
B3T4 22	46.50	0.48	19.01	14.84	0.22	0.38	5.89	5.65	56.81	8.36	-22.39
B3T4 23	47.00	0.77	10.78	9.25	0.18	0.28	8.47	3.49	33.10	10.49	-20.21
B3T4 24	47.50	0.32	29.11	22.56	0.22	0.39	7.13	5.31	53.35	9.04	-22.54
B3T4 25	48.50	0.45	20.33	15.82	0.27	0.39	6.20	5.76	56.49	8.12	-23.22
B3T4 26	49.50	0.35	26.36	20.09	0.42	0.39	5.47	6.82	64.46	7.79	-23.13
B3T4 27	50.50	0.48	19.14	14.58	0.37	0.37	4.92	6.79	63.96	7.63	-22.57

B3T4 28	51.50	0.52	17.23	13.50	0.35	0.52	6.16	5.82	54.63	7.58	-22.08
B3T4 29	52.50	0.34	27.70	20.94	0.27	0.62	4.86	6.96	65.61	7.89	-22.47
B3T4 30	53.50	0.65	13.46	10.89	0.24	1.22	6.71	4.29	43.94	8.59	-24.56
B3T4 31	54.50	0.42	21.73	17.09	0.34	1.55	6.90	0.00	43.89	7.9	-26.21

Hard carbonate from the bottom of the core, suspected as carbonate unit B

34-1-1	JC207	9.67	-26.43
34-1-2	JC208	9.41	-27.22
34-1-3	JC209	9.31	-27.1
34-1-4	JC210	9.34	-27.3
34-1-5	JC211	10.2	-25.47
34-2-1	JC212	9.08	-27.41
34-2-2	JC213	9.22	-27.09
34-2-3	JC214	9.38	-26.62

B4T1 A's (Carbonate)

ID	label	down core	weights	Ca mg/g	Mg mg/g	Mn mg/g	S mg/g	Sr mg/g	K mg/g	Na mg/g	13 C	18-O
B4T1 08 A	8-9	8.5	0.06	225.33	25.88	0.27	0.57	6.01	3.69	37.43	5.65	-29.97
B4T1 12 A	12-13	12.5	1.06	15.46	0.63	0.03	0.39	0.29	0.14	1.60	7.12	-20.57
B4T1 13 A	13-14	13.5	0.31	174.38	44.76	0.48	1.24	4.09	5.27	57.19	8.34	-22.75
B4T1 14 A	14-15	14.5	0.47	170.23	48.06	0.61	0.67	4.37	6.06	57.89	5.37	-27.36
B4T1 2 01	evap 1	15.0	0.09	224.64	13.85	0.35	4.96	4.17	1.94	14.46	10.76	-20.47
B4T1 2 02	evap 2	15.3	0.04	150.33	59.40	1.25	3.05	2.56	5.75	13.64		
B4T1 2 03	evap 3	15.6	0.08	296.80	18.82	0.39	4.49	8.14	1.39	11.81	10.44	-20.74
B4T1 2 04	evap 4	15.9	0.06	123.11	37.30	0.68	2.37	2.46	5.18	78.99	7.67	-21.22
B4T1 2 05	evap 5	16.2	0.03	223.25	20.24	0.87	6.33	5.01	4.49	41.78	10.7	-20.11
B4T1 2 06	evap 6	16.5	0.08	135.35	31.60	0.51	2.15	2.39	3.24	34.55	6.47	-21.51
B4T1 2 07	evap 7	16.8	0.17	130.99	10.78	0.33	1.82	2.56	2.41	35.18	6.38	-20.99
B4T1 2 08	evap 8	17.1	0.08	314.80	6.30	0.30	0.55	6.97	2.53	44.09	7.67	-20.78
B4T1 2 09	evap 9	17.4	0.14	135.14	11.12	0.24	2.83	2.31	2.57	36.35	7.65	-20.79
B4T1 2 10	evap 10	17.7	0.09	318.46	6.77	0.50	0.57	9.88	3.51	49.60	7.2	-20.88
B4T1 2 11	evap 11	18.0	0.12	196.85	7.64	0.49	0.34	5.05	3.53	37.21	6.92	-20.36
B4T1 2 12	evap 12	18.3	0.13	340.01	2.51	0.20	0.57	10.63	2.51	34.30	3.93	-20.12
B4T1 2 13	evap 13	18.6	0.29	137.77	4.94	0.08	0.46	3.57	2.02		4.58	-20.04
B4T1 2 14	evap 14	18.9	0.09	186.63	3.35	0.17	0.40	5.19	2.42		4.72	-20.3
B4T1 2 15	evap 15	19.2	0.18	197.79	8.12	0.14	0.62	5.61	2.56		4.41	-20.63
B4T1 2 16	evap 16	19.5	0.14	225.64	22.41	0.23	1.61	5.28	3.24		4.11	-21.23
B4T1 2 17	evap 17	19.8	0.09	212.53	14.80	0.63	0.65	5.46	4.80		4.33	-21.12
B4T1 15 A	20-21	20.5	0.07	207.00	42.88	0.49	0.59	5.21	3.69	32.56	5.83	-30.13
B4T1 16 A	21-22	21.5	0.12	201.92	25.29	0.56	0.50	4.20	2.10	22.95	7.75	-25.15
B4T1 17 A	22-23	22.5	0.10	143.14	56.39	0.35	0.38	2.03	1.68	34.27	7.98	-23.64
B4T1 19 A	24-25	24.5	0.06	191.45	70.05	0.39	0.47	2.88	2.69	27.82	5.89	-26.05
B4T1 23 A	31-33	32	0.11	260.90	20.92	0.46	3.55	7.38	2.79	32.40	7.01	-26.9

B4T1 24 A	33-35	34	0.05	363.84	21.75	0.71	1.32	11.54	3.95	40.92	7.14	-23.94
B4T1 25 A	35-37	36	2.43				Broken				8.01	-23.9
B4T1 27 A	39-41	40	0.05	284.01	36.10	0.47	0.57	7.11	4.69	59.53	5.05	-23.68
B4T1 29 A	43-45	44	0.11	249.33	31.64	0.50	2.71	5.48	4.15	38.37	6.74	-26.1
B4T1 30 A	45-46	45.5	0.19	263.47	33.93	0.40	0.50	6.83	4.33	43.26	6.91	-30.3
B4T1 34 A	50-51	50.5	0.21	230.96	34.94	0.45	2.27	4.82	4.12	43.25	3.09	-32.14
B4T1 35 A	51-55	53.0	0.11	173.51	45.75	0.54	1.10	3.86	5.57	56.95	7.02	-25.27
B4T1 36 A	55-58	56.5	0.16	237.39	34.60	0.36	1.60	6.02	3.79	31.27	7.22	-26
B4T1 37 A	58-62	60.0	0.14	243.20	20.52	0.38	2.16	6.71	2.69	53.35	4.75	-24.89

B4T1 Sand Matrix

ID	Label	down core cm	weights g	Ca mg/g	Mg mg/g	Mn mg/g	S mg/g	Sr mg/g	K mg/g	Na mg/g	13 C	18-O
B4T1 01	0-1	0.50	0.24	130.05	42.17	0.32	1.37	2.57	4.55	115.28	6.98	-27.77
B4T1 02	2-3	2.50	0.09	141.97	62.09	0.57	2.07	2.98	6.97	52.68	6.65	-26.61
B4T1 03	3-4	3.50	0.11	152.89	35.44	0.41	1.65	2.83	4.72	110.60	6.99	-26.48
B4T1 04	4-5	4.50	0.12	153.59	59.82	0.62	2.10	3.21	6.77	51.71	6.98	-28.92
B4T1 05	5-6	5.50	0.13	148.90	58.94	0.68	2.01	3.14	6.71	55.19	7.1	-26.67
B4T1 06	6-7	6.50	0.16	195.91	46.47	0.53	1.51	4.43	5.41	45.74	6.55	-26.32
B4T1 07	7-8	7.50	0.09	155.34	41.62	0.66	2.75	3.18	5.71	73.18	6.08	-28.96
B4T1 08 B	8-9	8.50	0.08	117.54	43.23	0.98	2.12	2.21	6.94	53.85		
B4T1 09	9-10	9.50	0.08	161.96	42.93	0.95	2.88	3.34	6.71	55.10	5.75	-27.58
B4T1 10	10-11	10.50	0.10	149.76	31.80	0.66	2.48	2.98	5.16	50.36	7.48	-25.63
B4T1 11	11-12	11.50	0.07	149.12	32.79	0.95	1.86	3.48	5.89	56.87	6.62	-27.54
B4T1 12 B	12-13	12.50	0.09	142.26	31.96	0.87	2.99	2.79	5.43	47.44		
B4T1 13 B	13-14	13.50	0.15	134.72	45.38	0.71	1.52	3.08	6.29	60.17	7.7	-22.35
B4T1 14 B	14-15	14.50	0.20	156.73	46.63	0.78	1.65	3.60	6.64	71.79	7.3	-23.13
B4T1 2 01	evap 1	15.00	0.09	224.64	13.85	0.35	4.96	4.17	1.94	14.46	10.76	-20.47
B4T1 2 02	evap 2	15.30	0.04	150.33	59.40	1.25	3.05	2.56	5.75	13.64		
B4T1 2 03	evap 3	15.60	0.08	296.80	18.82	0.39	4.49	8.14	1.39	11.81	10.44	-20.74
B4T1 2 04	evap 4	15.90	0.06	123.11	37.30	0.68	2.37	2.46	5.18	78.99	7.67	-21.22
B4T1 2 05	evap 5	16.20	0.03	223.25	20.24	0.87	6.33	5.01	4.49	41.78	10.7	-20.11
B4T1 2 06	evap 6	16.50	0.08	135.35	31.60	0.51	2.15	2.39	3.24	34.55	6.47	-21.51
B4T1 2 07	evap 7	16.80	0.17	130.99	10.78	0.33	1.82	2.56	2.41	35.18	6.38	-20.99
B4T1 2 08	evap 8	17.10	0.08	314.80	6.30	0.30	0.55	6.97	2.53	44.09	7.67	-20.78
B4T1 2 09	evap 9	17.40	0.14	135.14	11.12	0.24	2.83	2.31	2.57	36.35	7.65	-20.79
B4T1 2 10	evap 10	17.70	0.09	318.46	6.77	0.50	0.57	9.88	3.51	49.60	7.2	-20.88
B4T1 2 11	evap 11	18.00	0.12	196.85	7.64	0.49	0.34	5.05	3.53	37.21	6.92	-20.36
B4T1 2 12	evap 12	18.30	0.13	340.01	2.51	0.20	0.57	10.63	2.51	34.30	3.93	-20.12

B4T1 2 13	evap 13	18.60	0.29	137.77	4.94	0.08	0.46	3.57	2.02		4.58	-20.04
B4T1 2 14	evap 14	18.90	0.09	186.63	3.35	0.17	0.40	5.19	2.42		4.72	-20.3
B4T1 2 15	evap 15	19.20	0.18	197.79	8.12	0.14	0.62	5.61	2.56		4.41	-20.63
B4T1 2 16	evap 16	19.50	0.14	225.64	22.41	0.23	1.61	5.28	3.24		4.11	-21.23
B4T1 2 17	evap 17	19.80	0.09	212.53	14.80	0.63	0.65	5.46	4.80		4.33	-21.12
B4T1 15 B	20-21	21.50	0.06	199.50	32.55	1.21	0.52	4.53	6.94	60.06		
B4T1 16 B	21-22	21.50	0.07	231.09	37.94	1.04	0.54	4.32	6.35	53.45		
B4T1 17 B	22-23	22.50	0.06	229.03	27.50	1.34	0.52	3.04	7.44	61.15		
B4T1 18	23-24	23.50	0.05	193.86	91.27	1.33	0.45	2.52	8.04	62.57	5.43	-27.59
B4T1 19 B	24-25	24.50	0.05	183.82	65.57	1.18	0.49	2.97	6.88	56.18		
B4T1 20	25-27	26.00	0.04	130.36	26.74	1.25	1.42	2.65	6.90	85.16	8.18	-24.62
B4T1 21	27-29	28.00	0.04	138.93	41.03	0.83	1.20	2.75	8.17	77.54	7.87	-24.68
B4T1 22	29-31	30.00	0.05	114.26	41.12	0.59	0.76	2.50	6.10	73.59	6.25	-26.79
B4T1 23 B	31-33	32.00	0.07	113.33	26.17	0.43	1.24	2.51	4.70	65.51		
B4T1 26 B	37-39	38.00	0.05	105.79	32.40	0.89	0.47	2.25	6.32	101.66	7.43	-26.06
B4T1 28	41-43	42.00	0.09	167.83	34.09	0.57	0.84	3.37	5.28	97.74	6.42	-28.16
B4T1 29 B	43-45	44.00	0.07	177.62	36.16	0.67	1.18	3.88	6.06	88.19		
B4T1 30 B	45-46	45.50	0.25	217.98	36.27	0.34	0.49	5.18	4.36	60.46	5.7	-30.23
B4T1 31	46-47	46.50	0.08	259.67	28.53	0.41	0.42	6.79	4.24	47.20		
B4T1 33	49-50	49.50	0.12	65.90	73.45	0.55	1.85	1.08	10.72	94.01	4.71	-29.54
B4T1 34 B	50-51	50.50	0.11	162.84	42.71	0.55	1.09	3.49	6.06	66.95		
B4T1 35 B	51-55	53.00	0.07	147.35	42.51	0.62	0.99	3.05	5.87	61.05		
B4T1 36 B	55-58	57.00	0.05	152.96	33.09	0.56	0.62	3.34	5.56	67.74		
B4T1 37 B	58-62	60.00	0.06	120.93	52.14	0.48	0.78	3.48	7.47	65.20		
B4T1 38	62-66	64.00	0.24	218.20	37.08	0.11	0.58	5.89	3.78	39.31	6.44	-30.36
B4T1 39	67.00	67.00	0.24	45.84	90.23	0.08	0.28	0.70	10.04	41.91	7.02	-22.95
B4T1 40 B	66-70	68.00	0.13	252.28	0.00	0.02	0.63	8.00	2.45	47.36		

B5T1

	cm down core	weight	Ca	Mg	Ba reps mg/g	S	Sr	Mn	K	Na	d13C vpdb	d18Ov pdb
B5T1 01	0.50	0.30	211.32	34.70	RAN OUT	16.85	4.65	0.18	3.97	45.25	6.52	-29.72
B5T1 02	1.50	0.27	209.21	27.75	0.09	14.63	4.05	0.15	3.29	61.65	7.92	-25.74
B5T1 03	2.50	0.21	195.59	28.77	0.10	17.47	3.81	0.19	3.68	71.28	7.67	-25.83
B5T1 04	3.50	0.25	208.49	29.91	0.10	18.05	4.09	0.20	3.79	61.82	7.47	-29.32
B5T1 05	4.50	0.23	216.22	29.19	0.10	23.27	4.73	0.20	3.64	49.85	7.75	-24.84
B5T1 06	5.50	0.24	253.60	24.01	0.00	30.48	4.44	0.17	2.94	27.87	7.6	-25.03
B5T1 07	6.50	0.37	215.51	26.04	0.08	21.11	4.39	0.15	3.16	59.42	8.04	-23.64
B5T1 08	7.50	0.32	218.21	26.58	0.08	16.09	4.52	0.16	3.45	53.12	10.37	-20.59
B5T1 09	8.50					**SAMPLE DROPPED**						
B5T1 10	9.50	0.26	234.88	23.92	0.10	14.39	5.93	0.19	3.44	57.13	9.89	-21.22
B5T1 11	10.50	0.24	234.65	29.49	0.09	9.35	7.03	0.25	3.64	40.42	9.63	-19.78
B5T1 12	11.50	0.29	230.10	26.66	0.07	8.07	6.54	0.17	3.24	34.89	9.21	-20.27
B5T1 13	12.50	0.29	213.60	23.58	0.05	14.02	4.15	0.14	2.97	56.14	8.89	-20.8
B5T1 14	13.50	0.27	232.73	19.20	0.06	13.67	4.29	0.12	2.42	46.70	7.67	-20.54
B5T1 15	14.50	0.25	203.25	20.69	0.05	22.28	4.05	0.13	2.72	63.83	7.21	-21.15
B5T1 16	15.50	0.42	199.26	29.36	0.05	14.49	4.56	0.10	3.26	48.29	7.75	-28.84
B5T1 17	16.07	0.24	309.27	16.16	0.09	7.73	10.46	0.17	1.89	14.71	9.03	-26.02
B5T1 18	16.64	0.13	166.69	20.55	0.08	10.38	4.15	0.14	2.69	112.04	6.92	-21.34
B5T1 19	17.21	0.17	207.84	40.07	0.11	5.86	5.20	0.15	4.20	30.38	6.6	-21.04
B5T1 20	17.79	0.21	208.55	43.67	0.12	5.52	4.83	0.11	4.22	23.83	7.01	-20.67
B5T1 21	18.36	0.13	189.51	50.12	RAN OUT	4.80	4.14	0.10	4.55	16.59	6.8	-20.46
B5T1 22	18.93	0.28	146.56	45.85	0.07	3.92	3.28	0.10	4.81	68.16	6.63	-21.08
B5T1 23	19.50	0.08	198.03	45.89	0.26	4.61	4.43	0.24	5.58	16.32	6.33	-22.42
B5T1 24	20.50	0.15	117.47	69.82	0.14	5.91	2.19	0.47	10.15	28.11	7.98	-23.89
B5T1 25	21.50	0.25	249.89	16.13	0.09	32.41	7.57	0.13	1.89	34.62	8.38	-24.75
B5T1 26	22.00	0.12	126.33	2.29	0.10	58.96	2.25	0.06	0.85	5.31	8.44	-25.29

B5T1 27	22.50	0.33	181.23	25.27	0.00	21.97	5.04	0.14	3.11	78.41	8.75	-26.07
B5T1 28	23.00	0.20	205.83	23.45	0.00	42.18	5.00	0.11	2.64	45.92	8.61	-26.01
B5T1 29	23.50	0.26	187.17	30.18	0.00	33.70	4.58	0.10	3.38	53.07	8.44	-26.65
B5T1 30	24.00	0.06	173.02	39.95	0.00	10.83	4.72	0.14	4.93	42.09	7.51	-28.98
B5T1 31	24.50	0.17	233.77	25.24	0.00	16.72	6.49	0.14	3.09	36.01	7.39	-30.38
B5T1 32	25.00	0.15	267.91	24.50	0.00	6.58	7.98	0.10	2.83	18.25	7.41	-30.32
B5T1 33	25.50	0.32	231.38	28.60	0.00	5.35	6.36	0.12	3.32	36.51	7.39	-30.16
B5T1 34	26.00	0.22	200.05	34.64	0.00	13.07	3.32	0.08	3.61	46.08	8.25	-27.57
B5T1 35	40.00	0.36	219.82	29.54	0.00	23.82	2.00	0.06	3.10	52.12	7.03	-30.14
B5T1 36	63.00	0.25	217.07	33.01	0.00	39.43	5.24	0.10	3.52	38.24	7.11	-21.02
B5T1 37	65.00	0.24	211.95	32.27	0.00	21.07	4.29	0.08	3.50	54.08	6.7	-30.21
B5T1 38	67.00	0.20	218.56	26.32	0.00	45.03	2.94	0.09	3.13	37.20	6.53	-29.95
B5T1 39	69.00	0.27	201.40	25.87	0.00	68.00	2.95	0.11	3.20	35.70	6.6	-30.25
B5T1 40	71.00	0.23	203.07	30.50	0.00	40.66	2.82	0.06	3.42	55.07	6.46	-30.2
B5T1 41	73.00	0.20	307.66	12.65	0.00	28.24	2.55	0.08	1.57	12.41	5.75	-30.75
B5T1 42	75.00	0.31	245.38	25.21	0.00	19.36	1.98	0.07	2.82	39.82	5.93	-30.59
B5T1 43	77.00	0.37	210.60	28.77	0.00	30.32	1.39	0.06	3.14	46.36	6.4	-28.83
B5T1 44	79.00	0.23	210.08	24.39	0.00	64.65	2.05	0.07	2.68	40.86	5.9	-30.67
B5T1 45	81.00	0.28	209.25	29.76	0.02	39.56	1.84	0.06	3.24	40.27	5.92	-30.61

B7T1

	depth in core	weight	Ca (mg/g)	Mg (mg/g)	S (mg/g)	Sr (mg/g)	K (mg/g)	Na (mg/g)	Ba (mg/g)	Fe (mg/g)	Mn (mg/g)
B7T1 1	0.1	0.12		6.33	213.46	0.00		53.60	0.04	0.00	0.02
B7T1 2	0.5	0.11	281.55	4.23	204.32	-0.03	Unable to Measure	72.86	0.05	0.00	0.02
B7T1 3	1.5	0.14	205.40	2.25	191.73	0.02			0.01	0.00	0.00
B7T1 4	2.5	0.12	272.92	2.32	210.77	0.00			0.01	0.00	0.00
B7T1 5	3.5	0.13	221.66	3.04	194.57	0.00			0.01	0.00	0.00
B7T1 6	4.5	0.12	259.73	1.83	209.17	-0.06			0.01	0.00	0.00
B7T1 7	5.5	0.11	244.89	1.81	209.98	-0.04	1.47		0.02	0.00	0.00
B7T1 8	6.5	0.14	191.62	1.90	190.28	-0.03	0.98		0.02	0.00	0.00
B7T1 9	7.5	0.15	202.22	1.46	174.85	0.00	0.55		0.02	-0.01	0.00
B7T1 10	8.5	0.14	272.05	1.44	191.74	0.03	1.45		0.03	0.00	0.00
B7T1 11	9.5	0.13	257.35	2.23	192.65	0.07	1.19		0.02	0.00	0.00
B7T1 12	10.5	0.12	278.39	3.36	207.45	0.08	1.66		0.03	0.01	0.00
B7T1 13	10.7	0.14	223.16	4.14	184.62	0.04	1.06		0.01	0.00	0.00
B7T1 14	10.9	0.15	218.94	1.73	170.03	0.07	0.38		0.02	0.00	0.00
B7T1 15	11.5	0.14	245.53	1.74	180.03	0.10	0.60		0.00	0.00	0.00
B7T1 16	12.0	0.13	263.77	1.12	196.06	0.11	0.14		0.00	0.00	0.00
B7T1 17	13.0	0.13	251.61	6.79	198.86	0.14	1.31	73.56	0.00	0.00	0.00
B7T1 18	14.0	0.07	418.32	10.40	206.66	-0.15	1.85	80.13	0.00	0.00	0.00
B7T1 19	15.0	0.08	379.59	11.40	187.69	-0.09	1.95	138.43	0.04	0.01	0.00
B7T1 20	15.8	0.07	220.57	31.67	193.43	-0.15	5.12	91.08	0.31	0.06	0.23
B7T1 21	17.3	0.06	270.67	18.60	134.81	-0.54	5.39	56.48	0.21	0.06	0.30
B7T1 22	18.8	0.02	23.80	40.86	29.89	-1.70	8.44	48.57	0.01	0.01	0.00
B7T1 23	20.3	0.03	10.10	36.98	13.31	-1.41	8.85	65.61	0.69	0.02	0.02
B7T1 24	21.8	0.03	11.96	41.24	18.59	-1.63	9.44	73.60	0.20	0.02	0.00
B7T1 25	23.3	0.01	6.23	45.44	12.53	-3.61	12.05	31.59	0.10	0.01	0.00
B7T1 26	24.8	0.03	21.10	40.04	28.34	-1.62	8.57	64.31	0.10	0.02	0.01
B7T1 27	26.3	0.03	64.41	29.43	78.25	-1.17	5.41	54.66	0.10	-0.01	0.00

B7T1 28	27.8	0.02	22.80	49.50	32.15	-1.88	10.85	70.19	0.15	0.02	0.00
B7T1 29	29.3	0.03	85.61	41.72	101.26	-1.10	7.52	60.26	0.18	0.01	0.01
B7T1 30	30.8	0.03	100.85	33.90	122.71	-1.34	8.35	40.63	0.09	-0.01	0.00
B7T1 31	32.3	0.03	111.56	31.83	135.34	-1.18	8.05	38.07	0.23	0.04	0.14
B7T1 32	33.8	0.05	138.44	25.61	157.98	-0.58	5.31	73.72	0.09	-0.01	0.00
B7T1 33	35.3	0.03		39.03		-1.56			0.23	0.04	0.14

APPENDIX 8

Crystal data: $C_{82}H_{76}B_2F_8P_4S_2Cl_4Pt_3$, M_r 2150.11, monoclinic, space group $P2_1/n$, $Z = 4$, a = 17.5405(2), b = 23.8786(4), c = 20.7314(3) Å, β = 92.044(1)°, V = 8677.7(2) Å^3, D_{calc} = 1.646 g cm^{-3}, μ(Mo-Kα) = 5.127 mm^{-1}, size 0.37 x 0.18 x 0.17 mm^3, $T_{max,min}$ = 0.476, 0.253, F(000) = 4176, T = 200 K. Total data 52786, unique data 18979 (R_{int} = 0.0278), 3° < 2θ < 55°, R_1 ($I > 2\sigma(I)$) = 0.0492, wR_2 (all data) = 0.1107, GoF = 1.104, residual Δe +3.09/-2.02 e Å^{-3}.

Table 1. Crystal data and structure refinement for jakes.

Identification code	jakes
Empirical formula	H4 Ca O6 S
Formula weight	172.17
Temperature	84(2) K
Wavelength	0.71073 A
Crystal system, space group	monoclinic, C2/c
Unit cell dimensions	a = 6.2665(6) A alpha = 90 deg. b = 15.1410(14) A beta = 114.3080(10) deg. c = 5.6812(6) A gamma = 90 deg.
Volume	491.25(8) A^3
Z, Calculated density	4, 2.328 Mg/m^3
Absorption coefficient	1.644 mm^-1
F(000)	352
Crystal size	0.18 x 0.18 x 0.14 mm

Theta range for data collection	2.69 to 26.44 deg.
Limiting indices	-7<=h<=7, 0<=k<=18, 0<=l<=7
Reflections collected / unique	510 / 510 [R(int) = 0.0213]
Completeness to theta = 26.44	99.4 %
Max. and min. transmission	0.8025 and 0.7562
Refinement method	Full-matrix least-squares on F^2
Data / restraints / parameters	510 / 0 / 46
Goodness-of-fit on F^2	1.088
Final R indices [I>2sigma(I)]	R1 = 0.0221, wR2 = 0.0599
R indices (all data)	R1 = 0.0225, wR2 = 0.0601
Largest diff. peak and hole	0.278 and -0.442 e.A^-3

Table 2. Atomic coordinates (x 10^4) and equivalent isotropic displacement parameters (A^2 x 10^3) for jakes.
U(eq) is defined as one third of the trace of the orthogonalized Uij tensor.

	x	y	z	U(eq)
Ca(1)	5000	1699(1)	2500	6(1)
S(2)	0	1727(1)	2500	5(1)
O(4)	2884(2)	679(1)	-782(2)	11(1)
O(3)	845(2)	2281(1)	917(2)	8(1)
O(2)	7989(2)	1175(1)	849(2)	8(1)

Table 3. Bond lengths [A] and angles [deg] for jakes.

Ca(1)-O(4)	2.3633(12)
Ca(1)-O(4)#1	2.3633(12)
Ca(1)-O(3)#2	2.3639(10)
Ca(1)-O(3)#3	2.3639(10)
Ca(1)-O(3)#1	2.5371(11)
Ca(1)-O(3)	2.5371(11)
Ca(1)-O(2)#1	2.5424(10)
Ca(1)-O(2)	2.5424(10)
Ca(1)-S(2)#4	3.1335(3)
Ca(1)-S(2)	3.1335(3)
Ca(1)-Ca(1)#5	4.0544(5)
Ca(1)-Ca(1)#3	4.0544(5)
S(2)-O(3)	1.4778(10)
S(2)-O(3)#6	1.4778(10)
S(2)-O(2)#7	1.4811(10)
S(2)-O(2)#1	1.4811(10)
S(2)-Ca(1)#7	3.1335(3)
O(4)-H(2)	0.87(3)
O(4)-H(1)	0.77(3)
O(3)-Ca(1)#3	2.3639(10)
O(2)-S(2)#4	1.4811(10)
O(4)-Ca(1)-O(4)#1	98.37(6)
O(4)-Ca(1)-O(3)#2	159.74(4)
O(4)#1-Ca(1)-O(3)#2	85.17(4)
O(4)-Ca(1)-O(3)#3	85.17(4)
O(4)#1-Ca(1)-O(3)#3	159.74(4)
O(3)#2-Ca(1)-O(3)#3	98.42(5)
O(4)-Ca(1)-O(3)#1	131.85(4)
O(4)#1-Ca(1)-O(3)#1	77.67(4)
O(3)#2-Ca(1)-O(3)#1	68.41(4)
O(3)#3-Ca(1)-O(3)#1	85.10(3)
O(4)-Ca(1)-O(3)	77.67(4)
O(4)#1-Ca(1)-O(3)	131.85(4)
O(3)#2-Ca(1)-O(3)	85.10(3)
O(3)#3-Ca(1)-O(3)	68.41(4)
O(3)#1-Ca(1)-O(3)	139.39(5)
O(4)-Ca(1)-O(2)#1	80.08(4)
O(4)#1-Ca(1)-O(2)#1	76.36(4)
O(3)#2-Ca(1)-O(2)#1	81.42(3)
O(3)#3-Ca(1)-O(2)#1	123.86(3)
O(3)#1-Ca(1)-O(2)#1	141.45(3)

O(3)-Ca(1)-O(2)#1	55.58(3)
O(4)-Ca(1)-O(2)	76.36(4)
O(4)#1-Ca(1)-O(2)	80.08(4)
O(3)#2-Ca(1)-O(2)	123.86(3)
O(3)#3-Ca(1)-O(2)	81.42(3)
O(3)#1-Ca(1)-O(2)	55.58(3)
O(3)-Ca(1)-O(2)	141.45(3)
O(2)#1-Ca(1)-O(2)	143.61(5)
O(4)-Ca(1)-S(2)#4	104.18(3)
O(4)#1-Ca(1)-S(2)#4	76.84(3)
O(3)#2-Ca(1)-S(2)#4	96.05(3)
O(3)#3-Ca(1)-S(2)#4	82.94(3)
O(3)#1-Ca(1)-S(2)#4	27.75(2)
O(3)-Ca(1)-S(2)#4	151.14(3)
O(2)#1-Ca(1)-S(2)#4	153.20(3)
O(2)-Ca(1)-S(2)#4	27.84(2)
O(4)-Ca(1)-S(2)	76.84(3)
O(4)#1-Ca(1)-S(2)	104.18(3)
O(3)#2-Ca(1)-S(2)	82.94(3)
O(3)#3-Ca(1)-S(2)	96.05(3)
O(3)#1-Ca(1)-S(2)	151.14(3)
O(3)-Ca(1)-S(2)	27.75(2)
O(2)#1-Ca(1)-S(2)	27.84(2)
O(2)-Ca(1)-S(2)	153.20(3)
S(2)#4-Ca(1)-S(2)	178.47(2)
O(4)-Ca(1)-Ca(1)#5	164.68(3)
O(4)#1-Ca(1)-Ca(1)#5	79.48(3)
O(3)#2-Ca(1)-Ca(1)#5	35.58(3)
O(3)#3-Ca(1)-Ca(1)#5	91.83(3)
O(3)#1-Ca(1)-Ca(1)#5	32.83(2)
O(3)-Ca(1)-Ca(1)#5	115.16(3)
O(2)#1-Ca(1)-Ca(1)#5	113.73(2)
O(2)-Ca(1)-Ca(1)#5	88.34(2)
S(2)#4-Ca(1)-Ca(1)#5	60.506(7)
S(2)-Ca(1)-Ca(1)#5	118.449(11)
O(4)-Ca(1)-Ca(1)#3	79.48(3)
O(4)#1-Ca(1)-Ca(1)#3	164.68(3)
O(3)#2-Ca(1)-Ca(1)#3	91.83(3)
O(3)#3-Ca(1)-Ca(1)#3	35.58(3)
O(3)#1-Ca(1)-Ca(1)#3	115.16(3)
O(3)-Ca(1)-Ca(1)#3	32.83(2)
O(2)#1-Ca(1)-Ca(1)#3	88.34(2)
O(2)-Ca(1)-Ca(1)#3	113.73(2)
S(2)#4-Ca(1)-Ca(1)#3	118.449(11)
S(2)-Ca(1)-Ca(1)#3	60.506(7)
Ca(1)#5-Ca(1)-Ca(1)#3	106.539(19)

O(3)-S(2)-O(3)#6	110.84(8)
O(3)-S(2)-O(2)#7	111.07(6)
O(3)#6-S(2)-O(2)#7	106.32(6)
O(3)-S(2)-O(2)#1	106.32(6)
O(3)#6-S(2)-O(2)#1	111.07(6)
O(2)#7-S(2)-O(2)#1	111.30(9)
O(3)-S(2)-Ca(1)	53.06(4)
O(3)#6-S(2)-Ca(1)	128.03(4)
O(2)#7-S(2)-Ca(1)	125.64(4)
O(2)#1-S(2)-Ca(1)	53.29(4)
O(3)-S(2)-Ca(1)#7	128.03(4)
O(3)#6-S(2)-Ca(1)#7	53.06(4)
O(2)#7-S(2)-Ca(1)#7	53.29(4)
O(2)#1-S(2)-Ca(1)#7	125.64(4)
Ca(1)-S(2)-Ca(1)#7	178.47(2)
Ca(1)-O(4)-H(2)	114.4(17)
Ca(1)-O(4)-H(1)	133(2)
H(2)-O(4)-H(1)	112(2)
S(2)-O(3)-Ca(1)#3	148.79(6)
S(2)-O(3)-Ca(1)	99.19(5)
Ca(1)#3-O(3)-Ca(1)	111.59(4)
S(2)#4-O(2)-Ca(1)	98.87(5)

Symmetry transformations used to generate equivalent atoms:
#1 -x+1,y,-z+1/2 #2 x+1/2,-y+1/2,z+1/2
#3 -x+1/2,-y+1/2,-z #4 x+1,y,z #5 -x+3/2,-y+1/2,-z+1
#6 -x,y,-z+1/2 #7 x-1,y,z